

Cylindrical Dielectric Elastomer Actuator for Cardiac Assist Device

Thèse N° 9397

Présentée le 3 mai 2019

à la Faculté des sciences et techniques de l'ingénieur

Laboratoire d'actionneurs intégrés

Programme doctoral en robotique, contrôle et systèmes intelligents

pour l'obtention du grade de Docteur ès Sciences

par

Jonathan André Jean-Marie CHAVANNE

Acceptée sur proposition du jury

Prof. J. A. Schiffmann, président du jury

Prof. Y. Perriard, Dr Y. R. C. Civet, directeurs de thèse

Prof. B. Semail, rapporteuse

Prof. A. Sylvestre, rapporteur

Prof. H. Bleuler, rapporteur

2019

"Faire une thèse, c'est droit comme faire son bus, c'est pas facile et ça prend du temps !"

— *Benz G.*

"J'ai remarqué que même les gens qui affirment que tout est prédestiné et que nous ne pouvons rien y changer regardent avant de traverser la rue."

— *Hawking S.*

Remerciements

Cette thèse représente le travail de quatre ans de recherche. Je n'aurais pas pu la mener à bien sans l'appui et la compréhension d'une série de personnes, que j'aimerais remercier à travers ces quelques lignes, tout en m'excusant d'avance pour celles que je pourrais oublier.

Je remercie tout d'abord le Prof. Bleuler, Semail et Sylvestre, pour avoir accepté de faire partie de mon jury, de relire mon travail et d'y apporter des commentaires, qui ont permis de l'améliorer.

Ensuite, j'aimerais remercier Yves, qui a accepté, autour d'une bière à Montréal, de m'engager comme doctorant sans certitude de financement. Grâce à lui, j'ai pu faire une thèse dans un laboratoire génial, entouré de personnes que seul lui possède le secret de choisir.

J'aimerais remercier infiniment Yoan, ou plutôt m'excuser, je ne sais pas bien. Il a relu mon travail, m'a conseillé et m'a supporté pendant ces quatre ans en tant que co-directeur de thèse. Il a appris à me comprendre, ce qui n'est pas facile, et surtout à me relire. Cette thèse ne serait pas ce qu'elle est s'il ne m'avait pas apporté son aide précieuse.

Le laboratoire est rempli d'autres personnes formidables, que je me dois de remercier aussi. Tout d'abord Morgan, pour m'avoir fait recommencer un bon nombre de mes chapitres et surtout pour m'avoir appris énormément en peu de temps. Paolo, sans qui le laboratoire ne fonctionnerait pas si bien et qui est toujours présent pour discuter et donner un coup de main. Il y a aussi Christian, Toff, Shi Dan, Xinchang, Cécile, Jaska, Florian, Louis, Guillaume, Douglas, Adrien, Pato, Sean le magnifique, Camilo, Alexis, Raphael, Francesco, Valentin et David, qui savent créer une ambiance unique dans un labo. Bien évidemment, il ne faut pas oublier Romain et Daniel, qui ont particulièrement égayé mon séjour et avec qui je garde une belle amitié.

Ensuite, un énorme merci à toute ma famille, à mes grands-parents pour tout ce qu'ils ont fait, et surtout à mes parents, qui me soutiennent depuis toujours et m'ont permis d'en arriver là. Ils m'ont aidé et supporté dans bien des situations, pas toujours des plus drôles.

En tout dernier, j'aimerai remercier Mathilde et en profiter pour m'excuser pour ces quatre ans pas toujours drôle. Elle a su m'accompagner mais aussi supporter mon ordinateur un peu partout là où on allait. Grâce à toi, ces quatre ans ont été énormément facilité surtout quand la thèse me prenait la tête (PS: Promis, je ne remercierai pas les chats).

Abstract

This work has been triggered because of the need for a new way to relieve the heart. Current solutions are based on invasive systems and in many cases involve propeller. The main problems of such assistance are infectious risks and hemolysis. In order to define an alternative, state of the art has allowed highlighting an emerging technology, i.e. the dielectric elastomer actuator (DEA). It consists of a soft silicone membrane sandwiched between two compliant electrodes. When an electric field is applied, the electrostatic forces squeeze the film. Because this technology allows reaching large deformations and is soft, it is adequate for such an application. The less invasive devised solution is to place a rolled DE actuator around the aorta and through the appropriate activation, the heart is relieved.

The influencing parameters which allow increasing the performance such as the energy density, are studied before focusing on the application and the possibility to effectively relieve the heart.

This research proposes an original work which is inspired by the thermodynamic domain to model the DEA, including the phase transition which consists of the main limit often neglected. This limit is carefully explained and allows to define a figure of merit composed of the intrinsic electrical and mechanical parameters of the material.

Then, the definition of different energy densities which depends on the consideration of several parameters is introduced. It is observed that generally, the published values of energy density are between $0.1 \text{ J} \cdot \text{cm}^{-3}$ and $1 \text{ J} \cdot \text{cm}^{-3}$. However, according to the proposed development, a more realistic value is about ten times lower and given by the *specific energy density*. Once the definitions and the model, allowing to study a planar dielectric elastomer actuator are provided, the specific energy density of such actuator is studied in several conditions. An external biasing element such as a constant load and an initial pre-stretch of the membrane are analysed. The results show that tracking the maximum strain does not necessary means that the optimal maximum energy density is reached.

In the literature, another biasing element, presenting a negative force characteristic, has been analysed. It has been demonstrated that such element allows improving the displacement of DEAs. Through the proposed definitions of energy density, this biasing element is also studied. The obtained strains and the specific energy densities are twice bigger than with the constant load.

Due to the application previously introduced, a cylindrical spring, having this characteristic is proposed. After the study of the influence of the geometrical parameters of the spring on its force-displacement characteristic, a prototype is proposed. This prototype is coupled to a DEA for which the global system is analytically modelled. The prototype is validated with measurements and FE analysis. An important observation concerns the specific deformation of the spring. Through an analogy with the stability of the elastomer, an explication is provided concerning the global deformation.

Finally, in order to determine the feasibility to use DEA technology such as cardiac assistance, a cylindrical based DEA is analysed. Through a lumped parameter model which allows simulating the cardiac cycle is performed.

It has been decided to analyse the possibility to use such technology to relieve the left ventricle and not to propose an optimised solution. Thus, the previously designed spring is not considered here.

The results show that two main configurations could be used to unload the left ventricle. The first one decreases the energy provided by the heart. The other one allows increasing the cardiac output which seems an attractive solution according to surgeons.

Key words: Dielectric elastomer actuator (DEA), energy density, negative biasing element, figure of merit, Mullins effect, cardiac assistance

Résumé

Ce travail a été motivé par le besoin de trouver une nouvelle technique pour soulager le cœur. Les solutions actuelles sont basées sur des systèmes invasifs composés d'hélices dont le problème principal est le risque d'infection et d'hémolyse. L'état de l'art a mis en évidence une technologie émergente, à savoir les actionneurs à base d'élastomère diélectrique (DEA). Ces derniers consistent en une membrane souple avec de part et d'autre une électrode déformable. Lorsqu'un champ électrique est appliqué, le film s'écrase sous l'action des forces électrostatiques. Cette technologie semble adéquate pour l'application étudiée grâce à ses possibilités de grande déformation. La solution imaginée consiste à placer autour de l'aorte un tube fait de cet actionneur. En l'activant de manière appropriée, le cœur pourra être soulagé, mais en aucun cas remplacé.

Avant de s'intéresser à l'application et l'aide que cet actionneur pourrait apporter au cœur, la technologie des DEAs est étudiée afin de trouver des solutions qui permettent d'augmenter ses performances, principalement sa densité d'énergie.

La présente thèse propose une solution originale qui permet de modéliser les DEAs en considérant la transition de phase, inspirée du domaine de la thermodynamique. Ce modèle est étudié attentivement et permet de définir un facteur de mérite qui dépend des propriétés électriques et mécaniques du matériel.

Ensuite, la définition de différentes densités d'énergie qui dépendent de la considération de certains paramètres est introduite. Il est observé dans la littérature que des densités d'énergie de $0.1 \text{ J} \cdot \text{cm}^{-3}$ à $1 \text{ J} \cdot \text{cm}^{-3}$ sont atteignables avec les DEAs. Cependant, à l'aide du développement proposé, des valeurs plus réalistes et environ dix fois plus faibles sont obtenues.

Une fois les définitions et le modèle permettant d'étudier des actionneurs uniaxiaux et planaires fournis, la densité d'énergie spécifique est donnée et étudiée sous différentes conditions. Des éléments mécaniques qui influencent le comportement de l'actionneur, comme des charges constantes ou des élongations initiales du film, sont analysés. Les résultats montrent que le souhait d'obtenir un maximum de déformation ne signifie pas forcément obtenir un optimum de densité d'énergie.

Dans la littérature, un autre élément mécanique est analysé, à savoir le ressort à rigidité négative. Il est démontré qu'un tel élément permet d'améliorer les déformations des DEAs. À travers des définitions de la densité d'énergie, cet élément est aussi étudié. Il est montré que les déplacements et les densités d'énergie obtenus sont deux fois plus importants qu'avec une charge constante.

Au vue de l'application étudiée, un actionneur avec une configuration cylindrique ainsi qu'un ressort avec cette même forme spécifique sont proposés. Le ressort possède quant à lui la caractéristique négative. Après une brève étude de l'influence de paramètres géométriques de ce dernier, un prototype est analysé. Les résultats obtenus à l'aide des éléments finis (FEM) et d'un modèle analytique sont validés par des mesures. Durant les mesures, une observation importante a été faite. La déformation semble non symétrique et une explication est proposée, basée sur la stabilité du système.

Finale­ment, afin de détermi­ner la faisabilité d'utiliser un DEA comme assistance cardiaque, un système tubulaire basée sur cette technologie est étudiée. A l'aide d'un modèle basé sur l'analogie entre un circuit électrique et le corps humain, différentes configurations d'activation de l'actionneur sont proposées. Les résultats montrent que deux principales solutions pourraient être utilisées afin de soulager le ventricule gauche du cœur. La première permet de diminuer l'énergie fournie par le ventricule gauche alors que la seconde permet d'augmenter le débit cardiaque, ce qui constitue un avantage important du point de vue des chirurgiens.

Mots clefs : Actionneur basé sur un élastomère diélectrique (DEA), densité d'énergie, élément mécanique avec comportement négatif, facteur de mérite, Mullins effect, assistance cardiaque

Contents

Abstract (English/Français)	iii
1 Introduction	1
1.1 Categories of electroactive polymers	2
1.2 Fundamentals of dielectric elastomer actuator	5
1.2.1 Deformation characteristic of DEAs	5
1.2.2 Mechanical and electrical limits of DEAs	10
1.3 Geometries of DEAs	13
1.3.1 Planar configuration	13
1.3.2 Cylindrical configuration	15
1.4 Conclusion	17
1.5 Content of the thesis	17
2 Energy analysis of dielectric elastomer actuator	19
2.1 Thermodynamic analysis applied to DEAs	20
2.1.1 Definition of the system - equilibrium state	20
2.1.2 Homogeneous and inhomogeneous state - Intrinsic stability	23
2.1.3 Phase transition	24
2.1.4 Metastability	26
2.1.5 Nominal stress - uniaxial actuator	27
2.1.6 Discussion	28
2.2 Global characteristic of an uniaxial DEA	29
2.2.1 Deformation model of DEAs - "0D" analysis	29
2.2.2 Variation of stress conditions	30
2.2.3 Relation between stretches	31
2.2.4 Determination of the phase transition	31
2.3 Graphical criterion of stability: ideal elastomer	32
2.3.1 Criterion of convexity for DEA	33
2.3.2 Study of the ideal elastomer	34
2.3.3 Performance of the ideal elastomer	35
2.3.4 Discussion on the figure of merit	36
2.4 Energy density of DEAs	37
2.4.1 Limits of the DEAs	37

Contents

2.4.2	Definitions of the energy density	38
2.4.3	Influence of external loads	39
2.5	Influence of the Mullins effect	40
2.5.1	Effect on the practical energy density	41
2.5.2	Effect on the specific energy density	42
2.6	Biasing elements	45
2.6.1	Performances of common silicone	45
2.6.2	Influence of constant biasing elements	46
2.6.3	Influence of the pre-stretch in the width direction	47
2.7	Conclusion	48
3	Cylindrical negative biasing system	51
3.1	Negative biasing element	53
3.2	Design of the spring	56
3.2.1	Geometrical specifications	56
3.2.2	Radial displacement and force relationship	58
3.3	Influence of geometrical parameters	62
3.3.1	Displacement characteristic	63
3.3.2	Force characteristic	64
3.4	Characterisation of the spring	65
3.4.1	Fabrication of the prototype	65
3.4.2	Measure of the spring	66
3.5	Conclusion	69
4	Tubular DEA	71
4.1	Simplified Model of a cylindrical DEA	72
4.2	Actuator with specific cylindrical spring	73
4.2.1	Prototype	73
4.2.2	Deformation characteristic	74
4.2.3	Results - 200 μm thick membrane	75
4.2.4	Stability of the system	77
4.2.5	Results - 100 μm thick membrane	79
4.2.6	Discussion	81
4.3	Conclusion	84
5	Cylindrical DEA as cardiac assistance	87
5.1	Ventricular assist device	88
5.2	Cardiac cycle	91
5.2.1	Working principle of the circulatory system	91
5.2.2	Strategy of assistance	93
5.2.3	Energy from the left ventricle	94
5.3	Integration of the DEA in the circulatory system	95
5.3.1	Lumped element model	95

5.3.2	Adaptation of the lumped model	96
5.3.3	Strategy of activation	98
5.3.4	Results and discussion	100
5.3.5	Negative biasing through cardiac cycle	104
5.4	Conclusion	106
6	Conclusions and Perspectives	109
6.1	Original contributions	110
6.2	Outlook	112
A	Effective work of a DEA	115
A.1	Definition of the problem	115
A.2	Effective work for a constant load	115
B	Design of experiment for the proposed spring	119
B.1	Methodology	120
B.2	Model of estimation	120
B.3	Results	121
C	Equivalent model of a radially stretched elastomer	125
C.1	Equivalent model	125
C.2	Link between the radial force and the equivalent pressure	127
D	Model of a uniformly deformed cylindrical DEA	131
D.1	Pressure characteristic of cylindrical DEA	131
E	Data of the lumped model	135
E.1	Parameters of the models	135
E.2	Main results	137
E.2.1	Influence of the phase shift	137
	Nomenclature	139
	Bibliography	153
	Curriculum Vitae	155

1 Introduction

The objective of this chapter is to provide an overview of the behaviour of electroactive polymers. These actuators are represented through several common graphs and equations used in the literature to understand the different features that are related to them.

The two leading families of electroactive polymers, the ionic (IPMC) and the dielectric elastomer actuator (DEA) also known as dielectric electroactive polymer (DEAP) [1] are compared both in terms of electrical and mechanical behaviour. Advantages and inconvenient as well as their typical applications are also discussed. These applications highlight the fact that this technology is principally used in order to create actuators providing low energy.

Because this thesis focuses on DEAs due to its large deformation capability and the difficulty to work under the specific condition for the IPMC, the next sections are devoted to them dealing with their mechanical deformation induced by electrical activation and external loads. The linear model and the one based on the strain energy density function are given to represent the behaviour of the so-called hyperelastic material. Afterwards, the effect of the viscosity is highlighted for a 3MTMVHBTM-tape and a silicone based material in order to understand the positive and negative aspects of such polymers as well as the influence of the Mullins effect. Then, the limits and the instabilities of this technology are explained. One solution used in the literature to cancel or to push further these undesirable effects consists of the pre-stretch of the elastomer which is an unavoidable central thematic.

The geometry of the membrane is fundamental in order to obtain the most suitable actuator for a specific application. Thus, the principal characteristics of the standard configurations such as the planar and the cylindrical shapes are finally presented. Their deformations according to mechanical and electrical stress are given with common hypothesis which allows modelling these geometries.

1.1 Categories of electroactive polymers

Ionic electroactive polymer and dielectric elastomer actuator

In the literature, the two leading technologies which are studied in what concerns the electroactive polymer (EAP), are the ionic polymer-metal composites and the dielectric elastomer actuator. According to the number of publications produced each year, these two types represent the significant part of research in this field. They represent the perfect example of the electromechanical conversion where the electric field causes the deformation. The main difference concerns the physical principle of deformation as well as the range of working voltage in order to activate them. The two types of EAP are represented in Fig.1.1 with the deactivated (voltage is null) and the activated state.

The ionic polymer-metal composites are composed of a polyelectrolyte membrane which is permeable to cations and impermeable to anions. This polymer is sandwiched between two compliant electrodes. The particularity of this technology concerns the need for a solvent to split the polymer into polyanions and polycations. Conventionally, the solvent is a water-based solution. Indeed, the H_2O molecules neutralised the cations which are driven through the polymer when a difference of potential appears between the two electrodes. The diffusion of ions results of an accumulation of charges on the negative electrode. This accumulation tends to expand while a shrinking occurs at the opposite side. These two mechanical deformations result in the bending of the membrane due to the distribution of stresses. Thus, the solution used in order to clamp the system influences the way of deformation, i.e. bending or twisting [2]. The possible angles of deformation range from 0° to 85° [3] if the system is not loaded. The main advantage of the technology is the actuation voltage. A few volts are sufficient to move the ions and thus to deform the polymer. With the water-based solvent, an electrolyse appears from 1.23V [1] for which the current could pass in the water. This limit causes the dehydration of the polymer, and thus the cations are no more free to move.

The second type is the dielectric elastomer actuator. This actuator also consists of a polymer membrane; generally, silicone or acrylic, sandwiched between two compliant electrodes. When an electrical field is applied between the electrodes, the Coulomb's force tends to bring closer the conductors due to the sharing of the positive and negative charges on the two electrodes. Contrary to the conventional capacitance, the polymer is soft, and the electrodes are compliant; thus, the system flattens. The pressure induced by the electric field is proportional to the dielectric constant of the material. Thus, this parameter is one of the most important one in this technology. Contrary to the IPMC, the deformation of this actuator is highlighted by the variation of its area and by the decreasing of the thickness usually considered uniform depending on the boundary conditions. The range of biaxial deformation for this actuator could reach 20% - 50% [4], [5]. However, this deformation depends on the nature of the material and the initial pre-stretch of the polymer (see section 1.2.2). Pelrine [6] has demonstrated the feasibility to obtain more than 100% of deformation, Kollosche 360% [7] and 488% [8] for Huang under dead load conditions (no initial pre-stretch of the membrane).

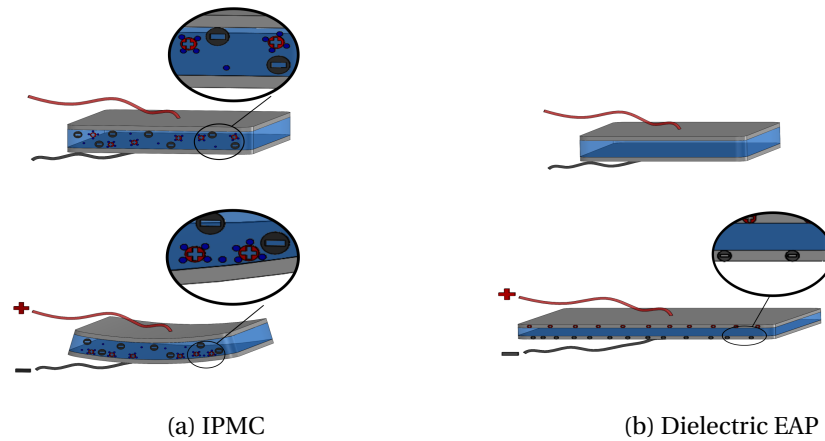


Figure 1.1 – Working principle of the two types of electroactive polymer submitted to an electrical field. The top and the bottom pictures represent respectively the deactivated and the activated state.

These results have been obtained with a polymer, namely VHBTM-tape, which has a high dielectric constant but also a high viscoelasticity. Akbari [9] has obtained 85% of linear strain for small actuator with a silicone based elastomer with a smaller dielectric constant than the one used by Pelrine but with a material for which the viscoelasticity is quasi negligible. Due to these large strains, the electrodes should be compliant enough in order not to influence the deformation of the membrane. Many fabrication and deposition processes exist [10] in order to reach this objective.

To obtain such deformation, several kilo-volts should be applied to the electrodes. The thickness influences the needed voltage, that is why a better parameter to characterise the electrical activation, would be the electric field which is around $50 - 100 \text{ V} \cdot \mu\text{m}^{-1}$ for the values founded in the literature. In order to obtain such high voltage, several power supplies have been proposed. For example, a laboratory from EPFL has developed a home-made power supply for the DEAs [11]. The main advantage of this solution is the cost compared to the commercially available amplifiers. This source can deliver a DC high-voltage or different signals with a frequency ranging from 0.001Hz to 1kHz.

The main advantages and disadvantages of these two families are summarised in the Table 1.1.

Common applications

For these technologies, the primary field of research is robotic with the big advantage to be able to replace the hard and heavy metallic part of current devices. The biomimetism is also well developed. The high reachable deformation with the polymer is adequate with the gestures of humans or animals. Another large field of research is the aerospace sector. The range of forces which could be reached is low (several mili-newton) but this constraint is not a problem in space due to the absence of gravity. Even if this technology is known as *artificial*

Parameters	IPMC	DEA
Deformation	+	++
Electrical activation	++	- -
Time response	- [12]	- [13]/ + [14]
Actuation force	- [15]	+ [16]
Life time	- -	+
Cost	- [17]	+
Fabrication	- [18]	+ [10]

Table 1.1 – Comparison between the IPMC and DEA. ++ and - - corresponds to respectively a favourable or an adverse cases.

muscle, the medical domain is not well developed while the similarity with the organs, the vessels and the muscles seems well established.

For the IPMC, the typical applications are the grippers [19] and the fishtail actuators [20]. Concerning the DEAs, they cover a broader range of applications, and the performances are generally better in comparison to IPMC such as for the grippers [21]. Due to the large deformations and thus the significant variation of the capacitance, it is adequate to use the DEAs such as sensors [22], [23]. Several researches [24], [25], [26] have also focused on the possibilities to harvest energy from the deformation of the membrane (DEG: dielectric elastomer generator). This technology seems adequate for such applications where the origin of the mechanical deformation provides large deformation such as the ocean's waves.

Industrial products are not a lot developed yet. The main elaborated ones are the valves (Fig.1.2a) where several layers of DEA are stacked in order to control the opening. The second application consists of a sensor (Fig.1.2b) based on the dielectric elastomer. It consists of a single layer with integrated electronics. This is principally used in a glove to determine the deformation of the hand. Finally, optical lenses are available on the market (Fig.1.2c) where the focal lens is controllable through the activation and the deactivation of a single layer of DEA.



Figure 1.2 – Industrial applications based on DEA technology

Pumping based on DEAs

Many researches concern the development of micro-pump of few milliwatts based on this technology. The first example [27] in the literature concerns a single layer of elastomer, placed above a tank with valves and pre-strained by a deformable diaphragm. The working principle of this pump is similar to the so-called *diaphragm pump*. The variation of the internal volume of the tank, induced by the DEA, creates a flow rate around $80\mu L \cdot min^{-1}$ when the elastomer is activated at 20 Hz. Based on the same approach, Maffli [28] has proposed to use the electrostatic zipping principle of the membrane to increase the deformation of the actuator.

Concerning "macro-pump" able to drive a higher flow rate (several $mL \cdot min^{-1}$), Goulbourne [29] has proposed an out-of-plane circular membrane able to be deformed in a spherical shape. The internal pressure pre-strains the film, and large deformation is reachable. More recently, a cylindrical system has been studied in order to obtain a higher flow rate with this technology. Carpi [30] and Mao [31] have studied this tubular shape, free in its center, to move the fluid due to the variation of the internal volume. By using several cylindrical actuators in series, they have proposed to develop a peristaltic pump based on the inch-worm movement. The first author has developed the concept and the second one has demonstrated the possibility to use this principle, through a cylindrical prototype composed of a single module.

1.2 Fundamentals of dielectric elastomer actuator

1.2.1 Deformation characteristic of DEAs

When a voltage is applied between the conductors, a pressure tends to bring closer the two electrodes which induces the flattening of the polymer membrane, dependent on the softness of the material. This pressure is called the *Maxwell pressure* and is given by:

$$p_{Maxwell} = \epsilon_0 \epsilon_r E^2 \quad (1.1)$$

where ϵ_0 is the vacuum permittivity, ϵ_r is the dielectric constant of the elastomer, and E is the true or nominal (voltage divided by the initial thickness of the elastomer) electric field between the two conductors. This field is proportional to the applied voltage and inversely proportional to the thickness of the membrane for a planar system. According to the previous equation, the deformation could be increased by choosing the material with the biggest dielectric permittivity, the smallest thickness and by increasing the voltage (Table 1.2 gives typical values of parameters concerning the DEAs, for actuators published in the literature). In this thesis, the dielectric permittivity of the material is assumed to be constant. Some researches have demonstrated a variation of several per cent of this parameter according to the actuation frequency [32], [33], the electric field [34], the pre-stretch of the membrane [35] or the temperature [36].

Generally, the polymers used for the DEA are considered as incompressible, it means that the

Chapter 1. Introduction

Poisson's ratio is $\nu = 0.5$ [37]. In other words, the volume is conserved during the deformation:

$$\lambda_x \lambda_y \lambda_z = 1 \quad (1.2)$$

where λ_x , λ_y and λ_z are the elongations in the principal directions. These two equations represent the basic ones in order to model the dielectric elastomer actuator, and they take place in all the researches.

Deformation models of DEAs

The dielectric elastomer actuators are generally used to transform the electrical energy into a mechanical one. To model such behaviour, the idea is to determine the link between the electrical stress induces by the electric field and the mechanical stress response. In the studied case, the stress in the thickness direction induced by the difference of potential is the only element which deforms the film. Several models exist according to the considered assumptions. The simplest way consists of assimilating the membrane of the DEA to an elastic spring, characterised through a constant stiffness. This parameter depends on the type of material and is proportional to the Young's modulus (Y). In terms of mechanical deformation, the elastic stress of the rubber compressed in the thickness direction is defined through the Hook's law and is given by:

$$\sigma_z = -Y \cdot s_z = -Y \frac{\Delta z}{z_0} \quad (1.3)$$

where s_z is the strain in the thickness direction and z_0 represents the initial thickness of the membrane. The material is supposed incompressible, isotropic and the negative sign is for the compressive state. The previous definition of the strain, which is dependent on the variation of the thickness (Δz), is the common one used for small deformation, i.e. engineering strain. This definition is sometimes given through the logarithmic form and is defined by the true strain. The equivalent force from Eq.1.3 which is needed to squeeze the film is then:

$$F_z = \sigma_z \cdot S = -\frac{YS}{z_0} \cdot \Delta z = -k \cdot \Delta z \quad (1.4)$$

Parameters	Range
Young's modulus	0.5 - 2 [MPa]
Dielectric constant	2.6 - 4.7
Thickness of the polymer	20 - 100 [μm]
Deformation	20 - 200%
Electrical potential	300-5000 [V]
Electrical breakdown	50 - 200 [$\text{V} \cdot \mu^{-1}$]
Mean current	0.1 - 10 [μA]

Table 1.2 – Typical values of DEA parameters

where S is the surface perpendicular to the direction of the deformation and k is the equivalent stiffness of the membrane. From this definition, the link with a common linear spring is highlighted.

When a voltage is applied between the electrodes, the stress in Eq.1.3 is given by the Maxwell pressure (Eq.1.1). For a planar actuator, the electrostatic field is defined as $E = U \cdot z^{-1}$ where U is the applied voltage. From the previous definitions, the strain becomes:

$$s_z = \frac{-\epsilon_0 \epsilon_r U^2}{Y z^2} = \frac{-\epsilon_0 \epsilon_r U^2}{Y z_0^2 (1 + s_z)^2} \quad (1.5)$$

where the thickness z , is replaced by its correspondent strain. Thus, the equation becomes a second order equation. From the Hook's law and by considering that the in-plane deformation is symmetric, the planar strains are given by:

$$s_x = s_y = \frac{-s_z}{2} \quad (1.6)$$

The main advantage of this solution is the need of only one parameter to characterize the deformation, the Young's modulus. The disadvantage consists in the range where the prediction of the deformation is appropriate (less than 20%).

In order to obtain a better model for large deformations (400%) of the DEA, the elastomer is assimilated to a non-linear elastic material. These kinds of models are called hyperelastic. The stress-strain characteristic is not defined by a simple Young's modulus but through the strain energy density function which is principally expressed in terms of the strain in the principal directions and several unknown parameters.

The hyperelastic models are divided into three categories depending on the definition of the strain energy density function which is used. The first one is the model where the unknown parameters are obtained through a phenomenological approach. For this category, the parameters have no physical meaning (Ogden [38], Mooney-Rivlin [39] or Yeoh [40]). The second category is the mechanistic models where the parameters have a physical meaning dependent on the structure of the material (Arruda-Boyce [41] or Neo-Hookean [38]). Finally, the last category consists of the hybrid definition which is a mix between the two previous cases such as the Gent [42]. Its advantage is to provide the information on the maximal strain before that the membrane mechanically breaks. In return, the model does not give a good prediction for large strains.

The stresses in the principal directions are given through the Cauchy stress tensor [38]. They are defined through the derivative of the strain energy density function according to the elongation along the corresponding direction.

Generally, the definition related to the strain energy density function are given in function of the elongation (λ_i) and not according to the strain ($s_i = \lambda_i - 1$) such as in the Hook's law.

Chapter 1. Introduction

Ogden [43] has defined the stresses in each main directions as:

$$\sigma_i = \lambda_i \frac{dW(\lambda_x, \lambda_y, \lambda_z)}{d\lambda_i} - p \quad (1.7)$$

where p is an unknown hydrostatic pressure which is determined according to the boundary conditions. In this thesis, the development of the equations where the strain energy density function (W) is used, are handled through the Yeoh model (Eq.1.8) which gives quite good fitting results for large deformation.

$$W(\lambda_x, \lambda_y, \lambda_z) = \sum_{i=1}^3 C_{i0}(\lambda_x^2 + \lambda_y^2 + \lambda_z^2 - 3)^i \quad (1.8)$$

where the C_{i0} are the unknown parameters obtained through experimental tests (uniaxial, biaxial or pure-shear test) according to the boundary conditions of the actuator. Exactly as for the small deformation theory, when a voltage is applied between the electrodes, the stress in the thickness direction is given by the Maxwell pressure (Eq.1.1). By considering that no external load prevents the displacement in the in-plane direction and that the elongation in the remaining directions are equal, the unknown hydrostatic pressure, p , is determined. Moreover, through Eq.1.2, the strain in the thickness direction is obtained by solving Eq.1.9 which is deduced from Eq.1.1, Eq.1.7 and Eq.1.8.

$$-\epsilon_0 \epsilon_r \frac{U^2}{\lambda_z^2 z_0^2} = \left(2\lambda_z^2 - \frac{2}{\lambda_z} \right) \cdot \left(C_{10} + 2C_{20} \left(\frac{2}{\lambda_z} + \lambda_z^2 \right) + 3C_{30} \left(\frac{2}{\lambda_z} + \lambda_z^2 \right)^2 \right) \quad (1.9)$$

Eq.1.9 consists in a eight degree equation. The strains in the x and y directions are equal and

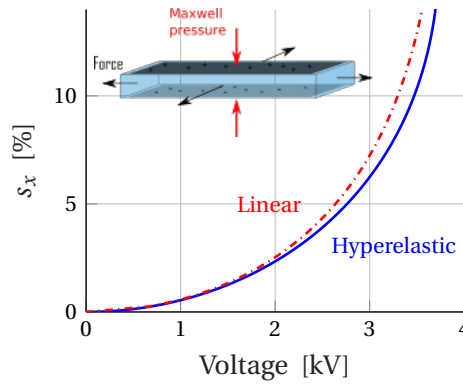


Figure 1.3 – Strain vs voltage, considering linear or hyperelastic model

provided by the incompressibility hypothesis (Eq.1.2). Their definition is given by:

$$s_{x,y} = \frac{1}{\sqrt{1+s_z}} - 1 \quad (1.10)$$

Eq.1.6 consists in the first order term of the Taylor's series of Eq.1.10. Fig.1.3 gives an example of the in-plane elongation of a planar membrane with the linear model (Eq.1.3 - Eq.1.6) and the model based on the strain energy density function (Eq.1.7 - Eq.1.10) according to the applied voltage. In the literature, this curve is generally represented by the voltage in function of the elongation.

Mullins effect

A problem raised by Mullins [44] is the ability of the elastomer to be influenced by its previous deformation in its history. When a mechanical pull-test is performed on rubbers to a final strain, the first characteristic differs from the next one such as on Fig.1.4a (dashed line - virgin path and full line - next paths). Afterwards, when the elastomer is stretched again from the initial state, the characteristic is always similar if the test is performed up to the same final strain. In reality, there is a drift of the force during the first five tests. That is why the fitting of the model should be performed from the fifth tests.

Another studied effect of Mullins is the influence of the maximum strain reached by the rubber. By stretching the silicone up to a more significant strain, the stiffness seems to decrease (Fig.1.4b). Thus, according to the test performed on the rubber and the range where the actuator works, the predictive model is more or less accurate. This effect should be considered in order to obtain a realistic performance of DEAs.

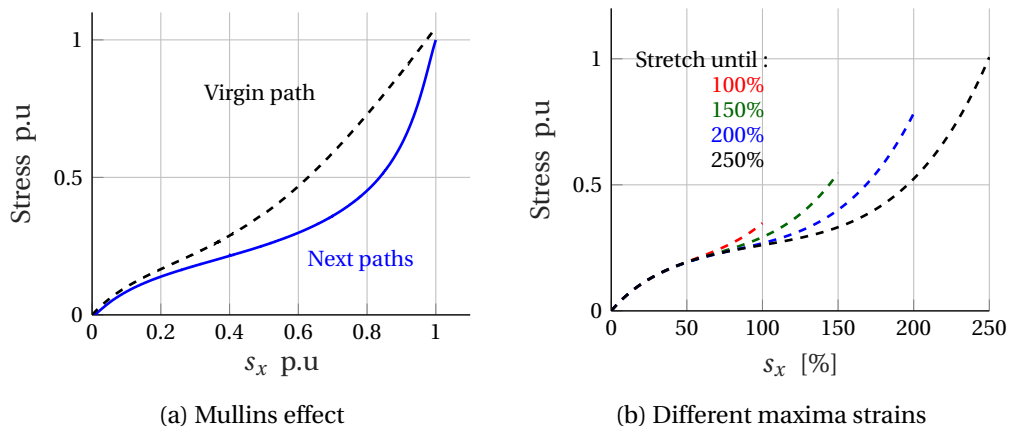


Figure 1.4 – (a) The Mullins effect is highlighted through the strain-stress characteristic. The first stress test is presented by the dashed line and the next one by the full line. (b) The stress characteristic of an elastomer for different maxima strains.

Influence of the viscoelasticity

In order to model the mechanical deformation of a DEA, another parameter should be taken into account, i.e. the viscosity of the rubber. Several studies are focused on this particular behaviour [45], [46] but this effect is often neglected. In order to consider its influence, they used a quasi-static viscoelastic model where the unknown parameters, which are time-varying, are given through a Prony series [47]. According to the material, the effect is more or less critical. The 3MTMVHBTM-tape (acrylic) is often used for the membrane due to its quite high dielectric constant which induces considerable strain and because of its commercial availability and its cost. The problem with this polymer is the high viscoelasticity that is why the study based on this material should be done carefully. Another family of polymer used such as dielectric support is the PDMS (silicone). The viscoelasticity of the material could be neglected for this material [48], but the dielectric constant (around 2.6) is lower than the one of the 3MTMVHBTM-tape (around 4.7). Thus, for the same voltage and the same initial thickness, the deformation is smaller for the PDMS based material.

Fig.1.5 highlights the deformation of a simple planar DEA submitted to a ramp voltage followed by a constant value. For the 3MTMVHBTM-tape, the strain when the voltage becomes constant is more significant than for the PDMS but the elongation continues during the constant voltage. For the PDMS membrane, the maximum strain is much lower, but the viscosity is quasi negligible. When the power supply is switch off, the relaxation time is also important for the VHBTM-tape which prevents from using this elastomer when high frequency is needed (> 1 Hz).

1.2.2 Mechanical and electrical limits of DEAs

The mechanical deformations of the DEA could be significant in terms of elongation, but several limits exist which prevent from obtaining such results. The nature of these limitations is explained in the literature and recalled here. They could be assigned to two domains, i.e. mechanic or electric.

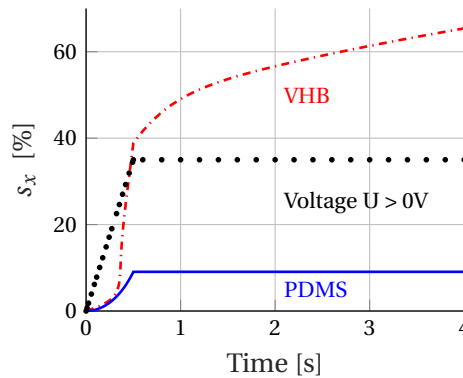


Figure 1.5 – Deformation of a planar 3MTMVHBTM-tape and silicone membrane submitted to a voltage.

The first one is the material strength. Contrary to standard material, the hyperelastic one has no different regimes (e.g. elastic, plastic,...) in the stress-strain characteristic. Even if the elongation could be substantial when the maximum one is reached the membrane breaks. The value of this maximum strain could be different according to the silicone used, the fabrication process and the temperature [49]. This limit also depends on the type of mechanical deformation (uniaxial, biaxial or pure-shear state [50]). Because the material strength is large enough, this limit is not often considered in the research about DEAs.

The actuator consists of a dielectric membrane sandwiched between two electrodes submitted to a high electric field. If this field exceeds the electrical breakdown limit (EB), an electrical arc appears, the current passes through the dielectric, and the silicone is damaged. The value of the electrical breakdown limit depends on the material, the fabrication process (presence of bubbles in the rubber, non-homogeneous thickness of the membrane), the temperature and the humidity. This second limit is also variable during the activation of the actuator. Huang [51] and Gatti [52] have demonstrated that the value of this limit is dependent on the thickness which varies during the activation and the pre-stretch of the membrane. It seems quite difficult to obtain a reliable value for this parameter. Indeed, the way to compute this parameter varies a lot in the literature. The design and the nature of the electrodes is essential too. By considering a planar actuator, if the electrodes are placed beside the edges of the membrane, the electric arc could pass through the air. Indeed, the permittivity of the air is much smaller than the one of the membrane. Thus the preferred path of the electrons becomes the air. In order to avoid the problem near the edges, the electrodes should not cover the elastomer entirely.

The next instability is specific to the deformation characteristic of the rubber induced by the squeezing of the film when the electric field is applied between the electrodes. In the literature, this limit or instability, is called *pull-in*, *electromechanical instability* [53] (EMI) or also known as *snap-through*. The different terms are equivalent but depend on the scientific community. Zhao [54] has classified the DEAs in four categories according to the moment when the pull-in instability occurs. The most common case is represented by the one given in Fig.1.6a. When the voltage is increased, there is a limit value for which the small increase of voltage induced the jump of the strain of the membrane (around 5.5 kV in Fig.1.6a - blue curve). During this jump, the thickness decreases drastically, the electric breakdown limit (Fig.1.6a - dotted line) is generally exceeded which damage the dielectric membrane. This problem is the first limit in order to obtain deformation higher than 5%-10%.

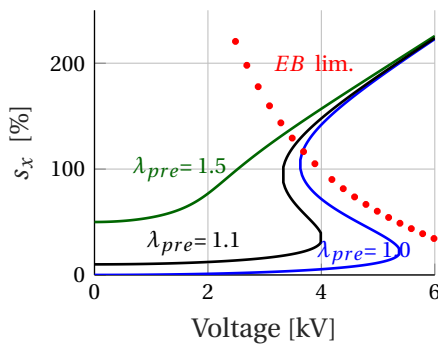
Concerning the electrical breakdown limit, it is classified into three categories. The first one consists of a small leakage current which passes through the dielectric without damaging it. The second is the one which damages the elastomer locally. However, the actuator is still working, even if the damaged zone is no more actuated. Finally, the third one is the electrical breakdown which breaks the film. Holes could appear and be propagated if mechanical stresses are induced to the elastomer.

In order to remove the previously discussed problem, the membrane is pre-stretched [9] and is fixed in this pre-deformed position. Fig.1.6a shows two different characteristics where the

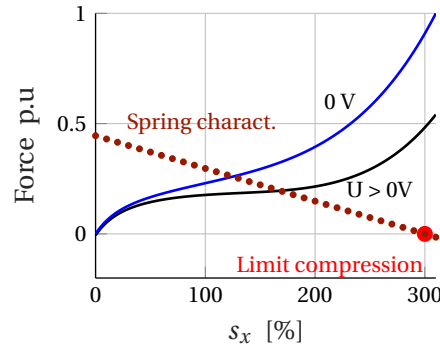
in-plane direction have been pre-stretched. If this mechanical constraint is not sufficient, the problem persists ($\lambda_{pre} = 1.1$ - Fig.1.6a) but if the value is big enough ($\lambda_{pre} = 1.5$ - Fig.1.6a), the limit is pushed further. This particular parameter tends to stabilise the DEA which prevents from the pull-in. Thus, more significant variations of strain are obtained before reaching the electrical breakdown limit.

There are several ways used in the literature to pre-stretch the film. The simplest one is the constant pre-stretch. The film is initially stretched from its initial state and is fixed in this pre-deformed position, i.e. fixed to a frame [55] or by using rigid bars [5]. An indirect advantage to pre-stretch the membrane is related to the needed voltage to activate it. Due to the in-plane pre-stretch and the incompressibility hypothesis of the material, the thickness of the polymer decreases, lowering the voltage needed to squeeze the film in order to obtain the same deformation. The pre-stretch could be applied equi-biaxially or with different magnitudes along the different orientation axis [9]. Another solution to pre-stretch the membrane is to use a mechanical spring. This spring is initially pre-compressed, then it is fixed to the membrane and to a non-deformable anchor and is released. Therefore, the deformation of the actuator is described by the characteristic of this spring (dotted line in Fig.1.6b) where the working positions are established by the stable positions between the membrane and the spring. This solution induces an additional limit. If the other limits are not reached, the maximum possible voltage is when the spring achieved its uncompressed position (circle position in Fig.1.6b). Afterwards, the actuator compensates this load and works to extend this biasing load. It is not precisely a limit, but after this position, the actuator does not provide energy only to the load but also to the spring which decreases the global performances.

The last presented instability is called: *loss of tension* (LT). This instability is directly linked to the fact that the membrane cannot be in compression ($F < 0$). In this situation, the term tension corresponds to stress. The instability represents the moment when the membrane is in compression in one or several directions due to the electrical activation and the particular boundary conditions [5]. By considering the membrane fixed on a rigid frame and activated,



(a) Pull-in instability



(b) Mechanical limit due to the spring

Figure 1.6 – (a) Pull-in instability due to the increasing of the voltage and the pre-stretch solution (b) Limit due to the maximum elongation of the linear spring

the surface of the electrodes would extend. However, this surface is limited by the support and can not increase in the in-plane directions, i.e. the membrane wrinkles [7]. Several researches [56], [57] have studied and have demonstrated the presence of different regions in the rubber where the wrinkling could occur. If the wrinkling induces only the deformation of the rubber in the out-of-plane direction, the material is not damaged. The problem is when this deformation induces the softening of a part of the membrane where can potentially occur an electrical breakdown. A solution consists of the pre-stretch in the problematic direction of the membrane.

1.3 Geometries of DEAs

The linear model based on Young's modulus, used to determine the deformation of a DEA membrane, is limited to small deformations ($< 10\%$). To obtain a better prediction, the model based on the strain energy density function is useful (sec.1.2.1). Generally, this model depends on parameters which should be determined experimentally through strain-stress tests. For one set of parameter of the hyperelastic model, one configuration of the membrane could be described. If another form should be analysed, other parameters of the film should be determined. A simple set of parameter is not sufficient to describe all the possible deformations of the silicone membrane with high accuracy. The deformation of the DEA depends on the design itself (shape of the membrane, way to fix the membrane, type of silicone...) and the conditions of use (load, applied voltage,...). Thus, in order to determine the parameter of the hyperelastic model, the fit of the stress-strain relation should be performed with a system as close as possible of the targeted actuator [58].

Without any assumptions on the stress and the strain of the tested membrane, the system of equations is indefinite. In the previous section, the hypothesis that the equi-biaxial strain is performed has been considered. This assumption allows to provide the information on the relation between the strains and the condition of incompressibility and then to obtain the force characteristic. In most cases, only the uniaxial strain is used in order to obtain the parameters of the rubber.

1.3.1 Planar configuration

A possible way to classify the different solution of planar DEAs is according to their length to width ratio (Fig.1.7), their preferential direction of deformation and the boundary conditions. For each of them and according to the final targeted deformation, two particular configurations are possible, respectively the uniaxial for the low and high ratio and the biaxial stretch. Some hypothesis are possible which permit to solve the equations of deformation in each case according to the principal direction of deformation and if the DEA is activated or not. For all of the previously discussed cases, the stress in the thickness direction being always null when no voltage is applied and equal to the Maxwell pressure when the voltage is supplied, the unknown hydrostatic pressure p (Eq.1.7) is determined. This assumption is valid if no

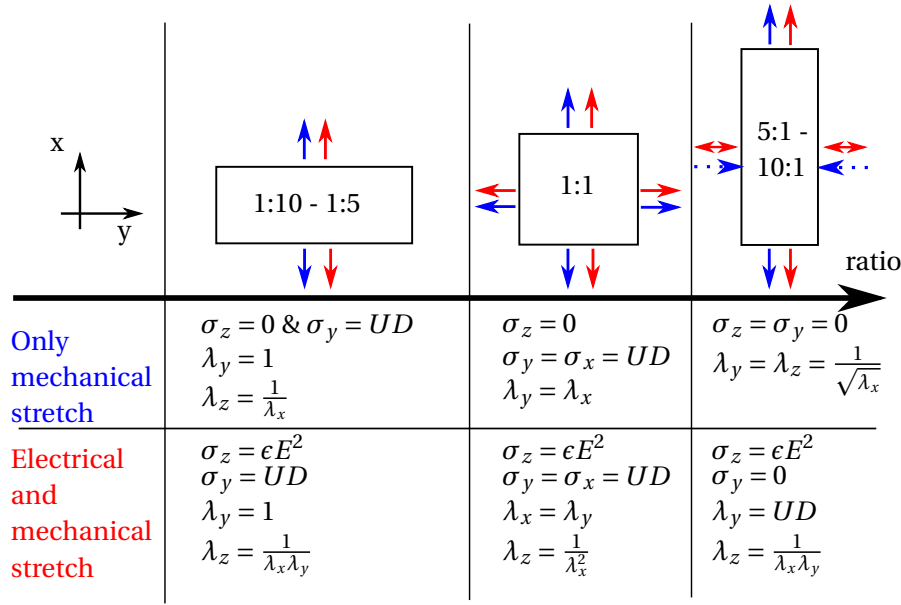


Figure 1.7 – Planar configurations (UD : for undefined situation)

other external load in the thickness direction is provided.

The different possibilities of deformation according to the length to width ratio are summarised in Fig.1.7. For all of them, two states are introduced, i.e. blue and red. The first one (blue) is for the cases when only a mechanical strain is considered according to the arrows. The second one corresponds to the case when a constant voltage is applied between the electrodes and that the membrane is mechanically stretched. Depending on the non-activated or activated state, the stresses and stretches are provided according to the adequate assumptions when it is possible. The different arrows highlight the direction of deformation.

In the literature, the membranes with low ratio (between 1:10 to 1:5) are called *pure-shear* configuration. The particularity of this configuration is the laterally constrained boundary conditions. The specificity of this geometry is the consideration of a fixed strain in the y-direction (no horizontal arrows). Without and with supply voltage, this shape is useful in order to obtain a uniaxial actuator. This configuration is adequate when high forces should be reached.

By contrast, the high ratio configurations (between 5:1 and 10:1) do not have an important difference in assumptions between the activated and non-activated state. When no voltage is applied, and the membrane is stretched vertically (blue arrows), the stress in the opposite direction to the deformation is considered as null. This assumption provides information on the stretch in the y-direction which could be considered as equivalent to the thickness one and decreases (dashed horizontal blue arrows). Only the hypothesis on the stretch in the y-direction is wrong when the membrane is powered and stretched vertically. Indeed, it is difficult to predict the direction of the deformation in the y-axis because the mechanical

stretch (vertical arrows) tends to decrease the width, while the activation pressure tends to increase it (red horizontal arrows). However, for both of them and without external loads in the y -direction, the stress in this direction is considered null.

The last often studied geometry is for square configuration (equal ratios) where a biaxial stretch is performed. When the membrane is activated, the elongation in the in-plane directions (vertical and horizontal arrows) is similar which facilitates the resolution of the system of equations.

1.3.2 Cylindrical configuration

The cylindrical shape is already a studied geometry in the domain of DEAs actuators. The shape of the cylinder is easily reachable due to the elasticity of the elastomer which permits to roll it in this specific configuration. Among all the research in this domain, three main types are highlighted according to their way of deformation, i.e. the axial, the radial and a particular actuator based on the two previous configurations.

Axial deformation

The principle of this configuration is to use the axial elongation of the cylinder in order to obtain a linear actuator able to provide large forces (several newtons). In order to encourage the displacement in the previously mentioned direction, a pre-compressed spring is generally inserted in the tube. This actuator is known as *spring roll* [59]. In order to obtain a quasi-constant thrust of the actuator, Berselli [60] has replaced the positive spring with bistable beams.

The deformation of such axial configuration is characterised by its elongation in the axial direction, encouraged by the spring (Fig.1.8a). When no voltage is supplied, the pre-compressed spring and the tube reach a first equilibrium position by increasing the length of the cylinder (vertical blue arrow) while the radius decreases (horizontal blue arrows). The increase of the hoop stress when power supply actuates the cylinder makes it more difficult to model this geometry. Carpi [61] has proposed a solution by considering the small deformation assumption in order to consider only the linear model of the elastomer. Then, Zhou [62] has developed the model of the axial force for hyperelastic material where the solution is more complex and solve through a numerical way. By considering the tube long enough compared to the radius, the stress in the axial direction is imposed by the spring or the mechanical load while the radial stress is considered as null. All this aspect suggests a similitude with the uniaxial configuration of the planar geometry.

This configuration has been used for applications such as Braille tablet [63], muscles similar to the human arms or dampers when excited at quite low-frequency [64] (several hertz).

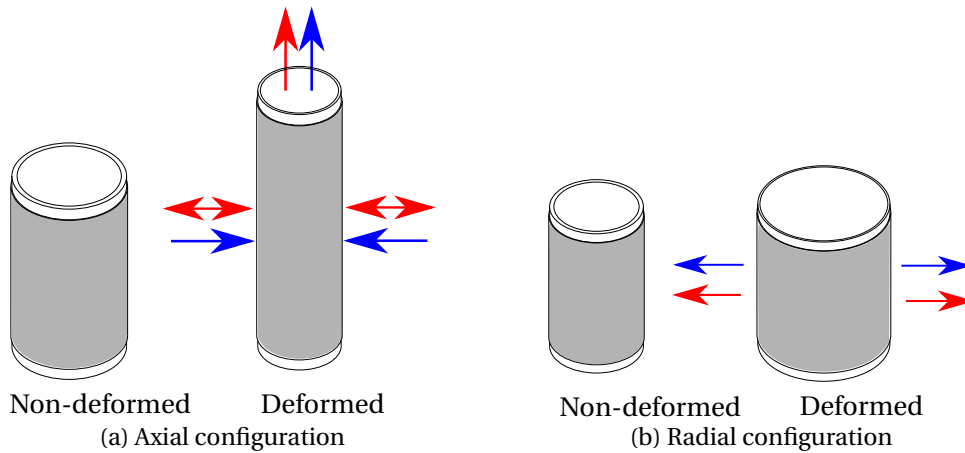


Figure 1.8 – Cylindrical configuration (blue arrows for mechanical stretches and red arrows for stretches induce through electrical activation).

Radial deformation

The second configuration consists in the radial deformation of cylindrical actuators. For this type of geometry, the axial elongation is blocked, and the expansion is concentrated in the radial direction. It is difficult to imagine a radial spring which facilitates and increases the performance of the cylinder in such configuration. Generally, the actuator is only pre-stretched in the axial direction before being fixed on a rigid frame. The pre-stretch allows avoiding loss of tensions in the axial direction when the actuator is activated.

Due to the fixed axial length, the model of the deformation of the tube under pressure is more straightforward. The stress in the axial direction is no more null. However, the length of the tube is considered as constant during the deformation. This particularity on the axial stress and the geometry variation tends to highlight the similitude with the pure-shear configuration. The problem occurs when the stress in the axial direction becomes null due to the electrical activation (loss of tension). In such a situation, the elastomer is in a compressed state which is not tolerated, thus some wrinkling appear. However, a special spring could solve such a problem.

Several authors [30], [31] have imagined to develop a peristaltic pump with this configuration. Another application consists of valves such as McCoul [65] who has developed such actuator in order to control the flow rate.

Particular case

The main disadvantage of the axial actuator is the presence of instability due to the cylindrical geometry submitted to an increase of internal pressure. A well-known observation of this instability is when a cylindrical balloon is inflated, the deformation is split into two distinct parts (two phases) when a certain pressure is reached. The particularity is that a part of

the balloon has a bigger diameter than the other parts. This phenomenon is similar to the two phases present in the thermodynamic analysis. Che [66] has proposed a model which highlights this phenomenon for the balloon. In order to counter this phenomenon, Zhou [62] has demonstrated the possibility to block the radial direction of deformation after letting it free for a short period, in order to increase the axial deformation. The author has also shown the cancellation of the previously discussed instability.

1.4 Conclusion

In this chapter, the main features and purposes of DEA have been explained and highlighted. The model which can describe the deformation of such actuator seems more challenging to obtain, compared to other technology such as piezo or electromagnetic system. A lot of physical phenomena could be highlighted according to the geometry and the boundaries conditions. The primary limits have been recalled which prevent from obtaining large deformation and how these limits could be overcome.

1.5 Content of the thesis

In the next chapter, a model based on the analogy with the thermodynamic field is proposed. It considers the phase transition of the elastomer when activated compared to the aforementioned one. Moreover, contrary to the simple uniaxial or pure-shear models presented in the previous chapter, the proposed model does not consider the hypothesis on the stresses and stretches according to the geometry. A global model able to provide a general behaviour of a linear actuator is thus proposed. Using this model, a study about the definition of energy density will allow characterising this technology and the hoped energy density reachable for a linear actuator. A figure of merit is then introduced in order to explain the different ways to obtain better energy density and variation of stretch. For example, the pre-stretch will be analysed. Finally, the Mullins effect can play a role in order to improve or not the performance of DEA. This effect will also be discussed.

In the third chapter, the design of a special spring with a negative characteristic is proposed. Its particularity is the radial direction of deformation and the particular force-displacement relationship. Indeed, at the beginning of this chapter, it is shown that such negative characteristic coupled to the DEA allows reaching higher displacement and energy density. A solution which allows decreasing the time of simulation through FE analysis is also proposed. Then, the design of experiments is performed to understand the effects of the geometrical parameters on the force-displacement characteristic.

The fourth chapter studies the influences of the proposed radial spring on a cylindrical DEA. A model of the elastomer deformed in this specific shape is proposed and analysed when it is linked to the characteristic of the negative stiffness spring which is obtained via FE analysis. Through a prototype, the model is validated.

Chapter 1. Introduction

The technology of DEA is often assimilated to artificial muscles. Due to this similarity, it has been decided to study a cardiac assist device. The last, but not least chapter analysed how in the cardiac cycle, the DEA based tubular pump could assist the heart. The model of the cardiac cycle, based on a lumped model, is recalled and adapted according to the wish to include the model of the DEA using a tubular shape. Afterwards, the effect of the actuator on the heart is studied, and a conclusion on the proposed approach is provided.

2 Energy analysis of dielectric elastomer actuator

In this chapter, the thermodynamic concept is applied to DEAs' technology. The goal is to define the energy density through the state variables and thermodynamic potentials. This definition is performed on an actuator coupled to an external load. Moreover, the definition of intrinsic stability is presented.

Then, a "0D" model of the DEA is provided, based on the numerical resolution of state equations and which takes into account the fact that the stresses in the in-plane directions of the actuator could change. Indeed, generally, the uniaxial or the pure-shear configuration is used in order to study linear actuators. The primary objective of the "0D" model is to realistically provide the performance (energy density, displacement and stress) of all the elastomers through their mechanical and electrical properties.

Afterwards, an original graphical representation is introduced in order to define rapidly if the elastomer is intrinsically stable, through its true stress characteristic. The study of the stress characteristic of the elastomer and its stability allows defining an ideal material with an equivalent constant Young's modulus. The energy density obtained with such material provides a figure of merit (FOM). This parameter depends on the electrical characteristics of the material but also on the mechanical one. This FOM could also be used to evaluate a non-linear material, i.e. hyperelastic. However, an equivalent Young's modulus should be defined in the latter case.

In the next part, the energy density is defined through different zones, which depends on the consideration of different phenomena. The terminology: maximum, practical and specific are used to classify these energy densities. The goal is to explain the differences and the meaning of these definitions and to highlight which one allows to obtain realistic values targeting effectively an actuator.

Finally, in the last section, the popular Elastosil® film is studied through the proposed models and compared in several situations. For example, the pre-stretch and the constant load are analysed in order to prove their benefits on performance. The Mullins effect is also discussed in order to understand its influence better.

2.1 Thermodynamic analysis applied to DEAs

The domain of thermodynamic was initially developed in order to understand the conversion of heat into mechanical work. Such theoretical domain is particularly convenient to analyse thermal engines. From this field of research, Carnot was able to define an energy cycle, among many possibilities, which optimises the performance of the combustion engine. One of the advantages is the direct access to the energy balance. This definition seems convenient to study the transformation of electrostatic energy into mechanical work like in the domain of the DEA and is used in the next sections.

Suo [67] has been one of the first authors to analyse the elastomer membrane through the thermodynamic domain. His work contains the fundamental equations in order to describe the DEA by considering different thermodynamic potentials. The choice of the adequate parameters allows explaining more or less efficiently, through graphical representations, the different notions like the intrinsic stability and the phase transition. These effects are essential in the thermodynamic analysis.

The primary objective in this section is to provide the theoretical tools able to describe the system. In the first part, the system which is considered is defined through its state equation in order to highlight the external variables as well as the state variables at equilibrium. Then, the hypothesis of incompressibility is recalled in order to define the final proposed equation of the thermodynamic potential able to describe the DEA. From all these proposed definitions, the intrinsic stability is studied as well as the phase transition.

2.1.1 Definition of the system - equilibrium state

The considered system is represented in Fig.2.1. It consists of a thin dielectric film submitted to two forces in the in-plane directions (F_1 , F_2) and a force in the thickness direction (F_3). The dimensions (l_1 , l_2 , l_3) represent the conjugated displacements. The system is connected to a battery u which delivers a quantity of charge $+q$ and $-q$, respectively on the upper and lower surface of the membrane.

The elastomer is assumed to be constituted of a multitude of subsystems ($(F_{1,j}, F_{2,j})$, $(F_{1,k}, F_{2,k})$, ...). The deformation induced by the different external loads is considered homogeneous for all the elastomer, such that the stress and the strain for all the subsystems are equivalent to the one imposed at the boundaries. Moreover, all these subsystems are submitted to the same quantity of electrical charges. Finally, the hypothesis of adiabatic transformation is done, which allows not considering the effect of temperature.

Energy balance

Through the first principle of thermodynamics (conservation of energy), the potential energy could be defined. The mechanical work due to the forces applied in the three main directions

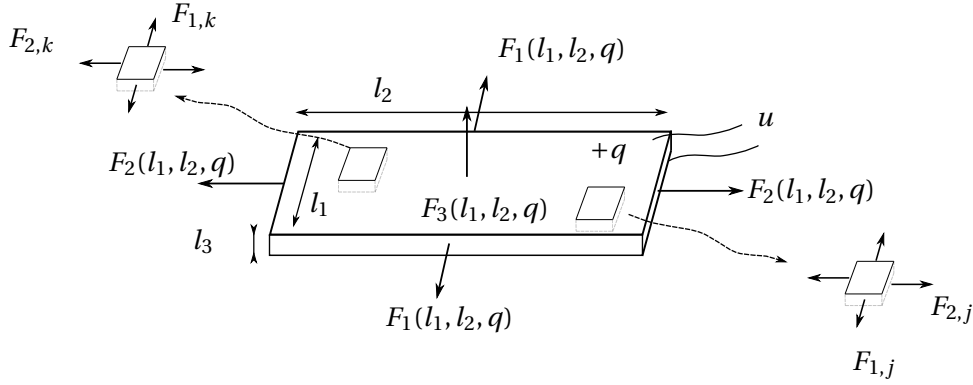


Figure 2.1 – Representation of the system with its state variables. Two subsystems are also represented.

and the electrical work induced by the electrical charges is given by:

$$\delta W_q = F_1 \delta l_1 + F_2 \delta l_2 + F_3 \delta l_3 + u \delta q \quad (2.1)$$

where δl_1 , δl_2 and δl_3 are the variation of the dimensions of the film in its principal directions, δq is the amount of electrical charge provided by the battery and W_q is the internal energy and consists into the first definition of the potential energy. In this study the kinetic energy is ignored; only the static case is analysed. These four variables, l_1 , l_2 , l_3 and q represent the state variables of the considered system and are independent.

In the domain of DEAs, the model of deformation is generally given in terms of the true stress (σ) and the stretch of the film (λ). Through the definition of this stress in the main directions (i), by considering the deformed length of the film equal to its initial length (L_i) multiplied by its stretch ($l_i = L_i \lambda_i$) and by performing the appropriate change of variables, Eq.2.1 becomes:

$$\delta W_q = (L_1 L_2 L_3) \frac{\sigma_1}{\lambda_1} \delta \lambda_1 + (L_1 L_2 L_3) \frac{\sigma_2}{\lambda_2} \delta \lambda_2 + (L_1 L_2 L_3) \frac{\sigma_3}{\lambda_3} \delta \lambda_3 + u \delta q \quad (2.2)$$

Incompressibility

According to the results obtained in [67] about the incompressibility of the material, the stretch in the thickness direction is given in function of the two others.

In order to remove the geometrical parameters of the film in the potential energy (δW_q), it is divided by the initial volume ($L_1 L_2 L_3$). Thus, the potential energy becomes an energy density ($W_{\tilde{D}}$) and is useful in order to compare several technologies.

Suo has adapted the electrical term by introducing the true electric field ($E = u/l_3$) and the true electric displacement ($D = q/(l_1 l_2)$). In order to remove the geometrical parameters of the electrical part in a similar way than Suo, the nominal electric field ($\tilde{E} = u/L_3$) as well as the nominal electrical displacement ($\tilde{D} = q/(L_1 L_2)$), are introduced. These parameters are just

the image of the voltage and electrical load according to the initial geometrical parameters.

Through the proposed changes of variables, the condition of equilibrium associated to small variations $\delta\lambda_1, \delta\lambda_2$ and $\delta\tilde{D}$ becomes:

$$\delta W_{\tilde{D}} = \frac{\sigma_1 - \sigma_3}{\lambda_1} \delta\lambda_1 + \frac{\sigma_2 - \sigma_3}{\lambda_2} \delta\lambda_2 + \tilde{E} \delta\tilde{D} \quad (2.3)$$

By considering the nominal density of Helmholtz free energy $W_{\tilde{D}} = W_{\tilde{D}}(\lambda_1, \lambda_2, \tilde{D})$ and by inserting this definition in Eq.2.3, the condition of equilibrium becomes:

$$\left(\frac{\delta W_{\tilde{D}}}{\delta\lambda_1} - \frac{\sigma_1 - \sigma_3}{\lambda_1}\right) \delta\lambda_1 + \left(\frac{\delta W_{\tilde{D}}}{\delta\lambda_2} - \frac{\sigma_2 - \sigma_3}{\lambda_2}\right) \delta\lambda_2 + \left(\frac{\delta W_{\tilde{D}}}{\delta\tilde{D}} - \tilde{E}\right) \delta\tilde{D} = 0 \quad (2.4)$$

State equations

Eq.2.4 implies that the system reaches an equilibrium position in $(\lambda_1, \lambda_2, \tilde{D})$ for all the small variations $\delta\lambda_1, \delta\lambda_2$ or $\delta\tilde{D}$ if the three terms of the equations are cancelled. In other words, the system reaches an equilibrium state if the Eq.2.4 is ensured. Thus, this criterion provides the following state equations:

$$\sigma_1 - \sigma_3 = \lambda_1 \frac{\delta W_{\tilde{D}}}{\delta\lambda_1}(\lambda_1, \lambda_2, \tilde{D}) \quad (2.5)$$

$$\sigma_2 - \sigma_3 = \lambda_2 \frac{\delta W_{\tilde{D}}}{\delta\lambda_2}(\lambda_1, \lambda_2, \tilde{D}) \quad (2.6)$$

$$\tilde{E} = \frac{\delta W_{\tilde{D}}}{\delta\tilde{D}} \quad (2.7)$$

These equations are similar to those obtained in [67] and which describe the deformation of a thin dielectric elastomer through three state variables.

Ideal dielectric elastomer

In order to define the final form of the potential energy and its corresponding state variables, let us discuss the electrical nature of the elastomer. Indeed, another assumption in the domain of DEA concerns the model of the dielectric which is considered as ideal. It implies that this parameter could be defined through a constant permittivity. This hypothesis means that this variable does not depend on different parameters (stretch, activation frequency, temperature,

...). Thus, the elastic and the electric terms of the model could be separated like introduced by Suo.

The proposed potential energy $W_{\tilde{D}}$ which guaranty the condition of equilibrium (Eq.2.4 - Eq.2.7), is:

$$W_{\tilde{D}}(\lambda_1, \lambda_2, \tilde{D}) = W_s(\lambda_1, \lambda_2) + \frac{1}{2\epsilon} \tilde{D}^2 \frac{1}{(\lambda_1 \lambda_2)^2} \quad (2.8)$$

where ϵ corresponds to the permittivity of the film.

This equation is composed of two distinct terms with different nature, i.e. the elastic (W_s) also called *strain energy density function* which is given by the hyperelastic model (e.g. Yeoh) and the electrical part. However, in the domain of DEAs, the parameter used to represent the effect of the electrical component is classically the voltage. In order to keep this habit, the Helmholtz potential defined in Eq.2.8 is transformed to obtain the supply voltage (or its image : \tilde{E}) like the state variable.

From the last state equation, the definition of the electrical charge ($q = Cu$) and the one for the planar capacitance: $\epsilon_0 \epsilon_r \frac{L_1 L_2}{L_3} (\lambda_1 \lambda_2)^2$, the thermodynamic potential is given by:

$$W_{\tilde{E}}(\lambda_1, \lambda_2, \tilde{E}) = W_s(\lambda_1, \lambda_2) - \frac{\epsilon}{2} \tilde{E}^2 (\lambda_1 \lambda_2)^2 \quad (2.9)$$

The three parameters $(\lambda_1, \lambda_2, \tilde{E})$ form the useful set of state variables. With this last definition, the term ϵE^2 could be highlighted in the state equations (Eq.2.5 - Eq.2.7). In the domain of DEA, this term is known as the Maxwell pressure.

Eq.2.8 and Eq.2.9 with their respective variables represent two equivalent definitions of the energy density useful in order to study such technology.

2.1.2 Homogeneous and inhomogeneous state - Intrinsic stability

Following the thermodynamic domain, the study of the internal energy (or the internal energy density) allows defining both the equilibrium and the stability of each state of the system. The previous hypothesis about the system defined in Fig.2.1 was to consider that the *global* system is deformed in a unique way and uniformly. However, in the domain of thermodynamics, it has been demonstrated that subsystems, *local*, could be in different states under certain conditions. Thus, the global system is named: inhomogeneous. This observation is consistent with Callen [68] who affirms: *Even within one subsystem, the system would find it advantageous to transfer energy from one region to another, developing internal inhomogeneities.*

In the domain of the DEA, this phenomenon could appear (Suo [67]). When the film is globally deformed, two possibilities of deformations are available. The first one is the *homogeneous* deformation where the stresses and stretches are equivalent in the film. The second possibility

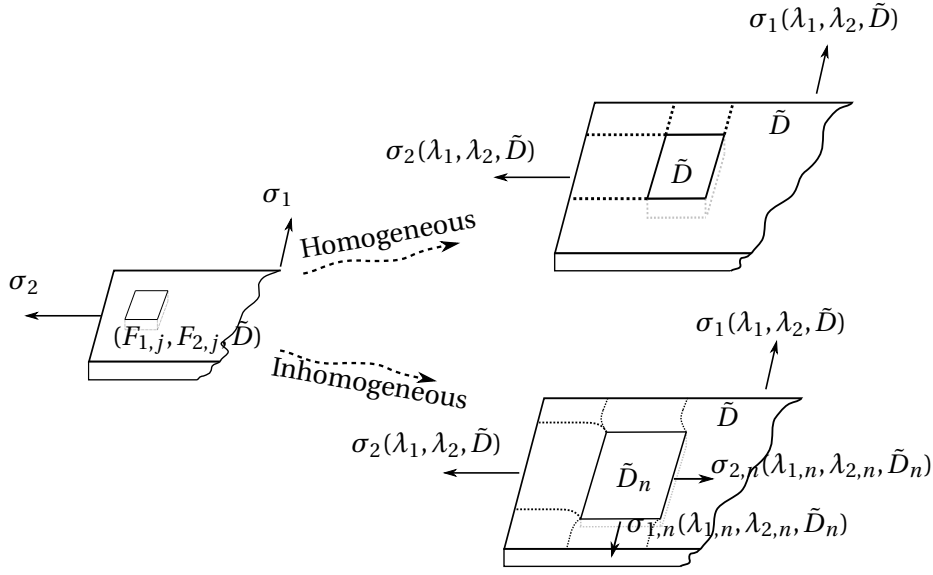


Figure 2.2 – Two possible states of deformations for a planar DEA

is to be deformed in an *inhomogeneous* state where several zones could appear. Each of them is then defined through their local variables $(\lambda_{1,n}, \lambda_{2,n}, \tilde{D}_n)$ which could not directly be obtained from external constraints. However, even in this configuration, the system could be stable and has the same global states $(\sigma_1, \sigma_2, \sigma_3, l_1, l_2, l_3)$.

To highlight the inhomogeneities, the term *intrinsic stability* is introduced in order to keep in mind the possibility of the separation between two states of all the subsystems $((F_{1,j}, F_{2,j}, q_i), (F_{1,k}, F_{2,k}), \dots)$, by guaranteeing the global stability.

The inhomogeneous deformation is complex, and the previous state equations are no more valid because the hypothesis of homogeneity was made. Finite element analyses can solve this kind of problem by defining all the zones with several elements and nodes. However, this solution is substantial in terms of computation time. Thus, based on the thermodynamic domain, an analytical solution is proposed to overcome this problem with the objective to adapt the previous state equations in order to obtain the global behaviour by considering the possibility of inhomogeneity, also called phase transition. The intrinsic stability consists in the possibility of each subsystem to reach a different state in order to guaranty the global stability, as explained in the next section.

2.1.3 Phase transition

Huang [56] and Zhu [69] have studied this topic by describing this effect on DEAs. They have demonstrated the criterion and the implication on the deformation when DEA is uniaxially stretched. Here, the analogy with the thermodynamic system is introduced to explain such a topic.

A general system whose internal energy is similar to the one in Fig.2.3a and where x_i represents its elongation (λ_1 for a membrane uniaxially stretched in the direction 1), is considered. Moreover, this system is composed of two subsystems. In order to reach the global position x_i , one inhomogeneous possibility is that the first subsystem states in the position $(x_i - \Delta x_i)$ and the second in the position $(x_i + \Delta x_i)$. The other homogeneous solution is that the two subsystems are equivalent deformed.

Thus, for the inhomogeneous possibility, the intrinsic energy of all the system, divided into two subsystems, is equal to $W_{q,int}(d^*)$ where d^* represents a particular point (Fig.2.3a). The energy at this particular position being smaller than the homogeneous internal energy $W_{q,int}(d)$, the system tends to prefer being subdivided into two parts for the same global position x_i in order to minimise its equivalent total energy. This development highlights the possible presence of inhomogeneity like in Fig.2.3b which represents the internal energy according to strain for different electric fields. Therefore, for the system defined through this $W_{q,int}$, the preferential path tracked in order to minimise its total energy, is changed.

In terms of mathematical expression, the condition which insures that the system will not be subdivided is given by:

$$\frac{1}{2}[W_{q,int}(x_i - \Delta x_i) + W_{q,int}(x_i + \Delta x_i)] \geq W_{q,int}(x_i) \quad (2.10)$$

In keeping with the thermodynamic theory developed by Callen [68], the condition highlights in Fig.2.3a is equivalent to ensure the convexity of the characteristic.

By considering the system defined by $W_{q,int}(x_i)$ and given in Fig.2.3a, through the previous definitions, the state for all the positions of the segment abc and efg are locally stables (convex). Concerning the states for the segment cde , they are unstables (concave). However, in order to minimise its internal energy, the system prefers to state on the straight line bf , which implies to ensure the intrinsic stability for all the positions because with such situation the criterion of convexity is respected.

DEA could be split into two states (inhomogeneity) in order to stabilise. Thus, while the positions on the segment cde are unstable according to Eq.2.11, the elastomer is subdivided into two states, b and f (with two strains and two stresses), in order to allow to the global system to reach any positions between these two ones. This phenomenon consists of the *phase transition* induces by the intrinsic stability of the system.

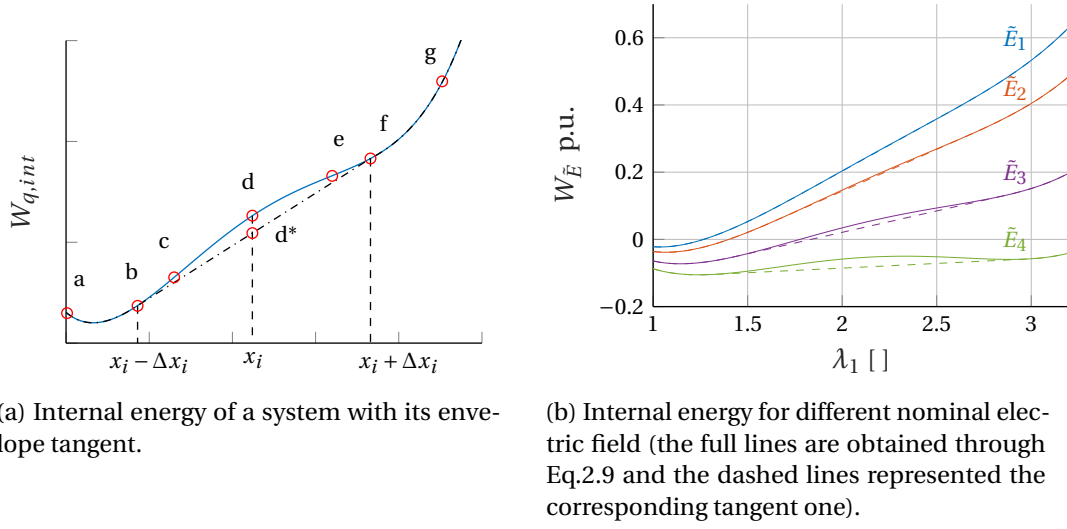


Figure 2.3 – Example of internal energy

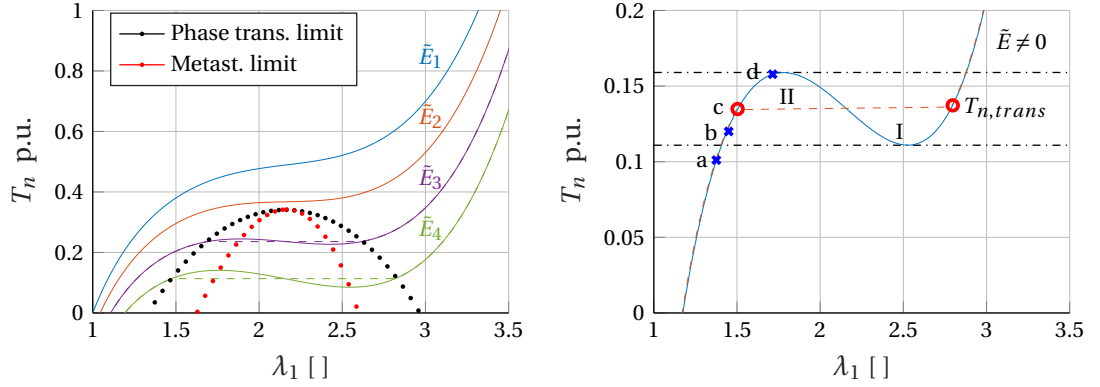
Eq. 2.10 could be generalised. When the Δx_i tends to zero, the differential form of Eq. 2.10 becomes:

$$\frac{dW_{q,int}^2}{d^2x_i} \geq 0 \quad \forall x_i \quad (2.11)$$

In conclusion, if a system does not satisfy the local criterion for any segments, the envelope defined by the tangent line which ensures to be always below the expected internal energy, determine the preferred path that the system follows in order to minimise its internal energy. In the domain of DEA, the internal energy $W_{q,int}$ depends on the nominal electric field and could be given by $W_{\tilde{E}}$. In Fig. 2.3b, the internal energy defined by the thermodynamic potential and its envelope tangent are given for four different nominal electric fields which highlights the discussed phenomenon.

2.1.4 Metastability

As previously explained, the criterion of stability could be summarised through the convexity of the internal energy characteristic of the system. This criterion is reached for the segments abc and efg (Fig. 2.3a). All the states on these segments are then locally stables. However, due to the minimisation of the internal energy the system prefers to follow the tangent line. Under certain conditions and because the segment bc and ef are locally stable, the system could reach these positions even if the probability is low. These locally stable states are defined as *metastable*.



(a) Nominal stress for different nominal electric field (Black dotted line represents the limit of phase transition and the red dotted line the limit of metastability.)

(b) Nominal stress $T_n(\lambda_1, \lambda_2, \tilde{E})$ for a nominal electric field. Dashed line: phase transition and full line: complete behaviour without considering phase transition.

Figure 2.4 – Nominal stresses

2.1.5 Nominal stress - uniaxial actuator

In order to study the behaviour of a DEA, the stress characteristic should be studied. From the definition of the internal energy of a system, the corresponding nominal stress (T_n) is obtained through the derivative of this internal energy according to the studied direction of deformation. The studied case in the next sections is focused on a uniaxial actuator (direction 1) while the other directions (2 and 3) are dependent on this studied one.

The nominal stress (Eq.2.12) allows representing the force without considering the geometrical parameters of the elastomer. Thus, several force-displacement characteristics could be obtained from the definition of the nominal stress by tuning the geometrical parameters of the actuator. An advantage of this representation is that the area enclosed by the x-axis (stretch) and y-axis (nominal stress) provides directly the energy density available in the system.

$$T_n = \frac{\delta W_{\tilde{E}}(\lambda_1, \lambda_2, \tilde{E})}{\delta \lambda_1} \quad (2.12)$$

Concerning the four examples of Fig.2.3b, the corresponding nominal stress for the internal energy ($W_{\tilde{E}}$) and the one defined through the tangent lines are given in Fig.2.4a. The true stress with the consideration of the phase transition is given through the dashed lines. The full lines represent the stress characteristic when the phenomenon is ignored.

Fig.2.4b provides the nominal stress for a given nominal electric field. Through the previous definitions about the stability, all the nominal stress-stretches to the position c respect the criterion of convexity. The phase transition occurs when the stress $T_{n,trans}$ is reached. Concerning the stresses in d (local maximum), these particular points are metastables.

For the phase transition, the typical characteristic concerns the flat region determined by the

nominal stress transition ($T_{n,trans}$). When a global position is imposed on this line, a part of the subsystems reaches the position on the left-hand side ($\lambda_1 = 1.5$), and the other one has the feature ($\lambda_1 = 2.75$) which ensures the global position on the flat region. The global position in this region determines the per cent of subsystems which is located on the two intrinsic stable positions ($\lambda_1 = 1.5$ or 2.75). According to the imposed nominal electric field, these positions of the subsystems are defined by the black dotted curve in Fig.2.4a. From the measurements obtained by Kollosche [70] of the voltage according to the stretch, the presence of the flat region is validated.

2.1.6 Discussion

Stable equilibrium - common definition

An image of the definition of stability is often given by tracking the minimum of the energy of the system.

In the case of DEA, the Gibbs free energy ($W_{\tilde{E}}(\lambda_1, \lambda_2, \tilde{E}_i) - T_n \cdot \lambda_1$) could be introduced through the Legendre's transformation in order to obtain such criterion of stability. The nominal stress T_n is obtained through Eq.2.12 which is dependent on the potential $W_{\tilde{E}}$. Fig.2.5 gives several Gibbs free energy definitions for different nominal electric field (\tilde{E}_i). The corresponding nominal stretches, for each electric field, are given in Fig.2.4b - nominal stress (a, b, c, d).

For example, when the analysed stress is a , the corresponding Gibbs free energy allows to find the intrinsic stability of the system, through the minimum of the bowl. In position b , two local minima exist, but the barrier between the lower and the upper position is such that the probability is low to pass from the first to the second position. On the contrary, for the state in d , the probability of passing from the first local minimum to the second one, which is lower in terms of energy, is high. This region is the *metastable* one which means that it is possible to reach these positions but under certain conditions.

Concerning the particularity of the stress c , the two local minima have the same Gibbs free energy. This situation allows highlighting the transition phase.

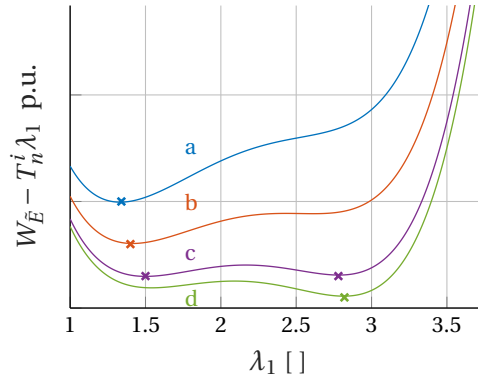


Figure 2.5 – Gibbs free energy for different constant stress

The previous example shows that through the right definition of the free energy, it is possible to find a graphical representation of the energy density where the local minima correspond to the stable positions.

Pull-in instability

In the literature, the pull-in instability (or electromechanical instability) is defined as the limiting voltage for which a small increase induces a snap-through in deformation with a much smaller thickness. In most cases, the electrical breakdown limit is exceeded which induces the break of the actuator.

Generally, this maximum voltage is considered as the local maximum [54] which belongs to the metastable region (Fig.2.4a).

However, it has been shown that the voltage for which the phase transition occurs is much smaller. Thus, the actuator risks breaking for an applied voltage smaller than the local maximum. Therefore, two limits should be differentiated. The one at the phase transition which corresponds to the most probable case and the local maximum, which is already defined in the literature.

2.2 Global characteristic of an uniaxial DEA

Now that the state equations of the DEA with its specifications like the phase transition have been treated, a solution to obtain a good prediction of the nominal stress characteristic of any uniaxial actuator is proposed. The phase transition as well as the consideration of the variation of the stress due to the special boundary conditions in the width direction are considered to obtain a better predictive model. In this study, one main hypothesis is to consider the width direction of the actuator constant and should be contrasted with the width of the elastomer which could vary. According to the condition of stress in the width direction, the unwanted out-of-plane deformation could appear in the form of wrinklings.

2.2.1 Deformation model of DEAs - "0D" analysis

In this section, a model is proposed in order to define the behaviour of any elastomer submitted to a voltage in order to create a linear actuator (deformation in one direction). The common models and geometrical configurations are adapted in order to improve this model without considering a specific pattern, like the pure-shear configuration.

The proposed model does not provide any information on the local aspect of the deformation (no spacial information). Only the presence of particular effects such as the phase transition are determinable. This phenomenon describes the presence of one uniform or two zones of the deformed film. However, the "0D" model does not provide information on the stress and stretch of each subsystems, only the global behaviour is determined.

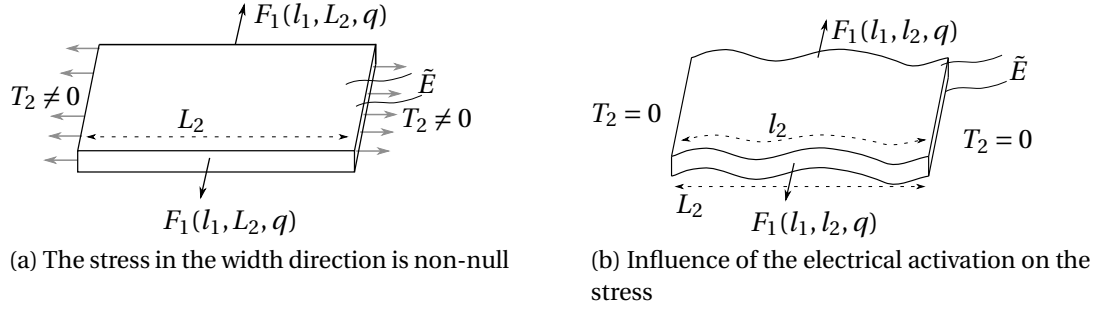


Figure 2.6 – Two possible states of the elastomer submitted to \tilde{E} and F_1

This model is the basis in order to obtain the performance (stretch, displacement and energy density) for any elastomer knowing the hyperelastic parameter (W_s), the permittivity and the electrical breakdown limit of the film.

Particular attention may be paid to obtain the parameters of the hyperelastic model without considering any geometry. Because the considered one in this thesis is close to a pure-shear configuration, the unknown hyperelastic parameters have been determined by stretching a membrane in a configuration with a length to width ratio equal to 1:10. These parameters are then used for the proposed "0D" model.

2.2.2 Variation of stress conditions

Generally, when an actuator is analysed and designed in order to perform a deformation in one direction, several hypotheses should be given concerning its length to width ratio.

The "0D" model assumes that the width of the actuator is constant (L_2). However, it is not always the case. The width could vary due to the wrinkling of the film (out-of-plane), according to the applied voltage. Indeed, when the constraints in the direction of deformation tend to decrease the width of the film, reaction stress ($T_2 \neq 0$) is induced due to the boundaries (Fig.2.6a). However, the stress could be cancelled ($T_2 = 0$) for other constraints induced through the mechanical and electrical deformation (Fig.2.6b). Thus, the wrinklings are a consequence of the elongation in the width direction while the width of the actuator is kept constant (for example through mechanical frames). Thus, the total stretch (l_2) of the film in the width direction is no more constant.

This effect should be considered in the model of the nominal stress characteristic in order to obtain more realistic energy density and stretch. It is possible to imagine a situation where the model passes from one configuration to another and comes back to the first one. Koh [71] has proposed in his study to take into account this change of assumptions ($T_2 \neq 0 \rightarrow T_2 = 0$ - relaxation). Here, a more efficient way of resolution is proposed by considering all the aspects (phase transition and relaxation of the membrane).

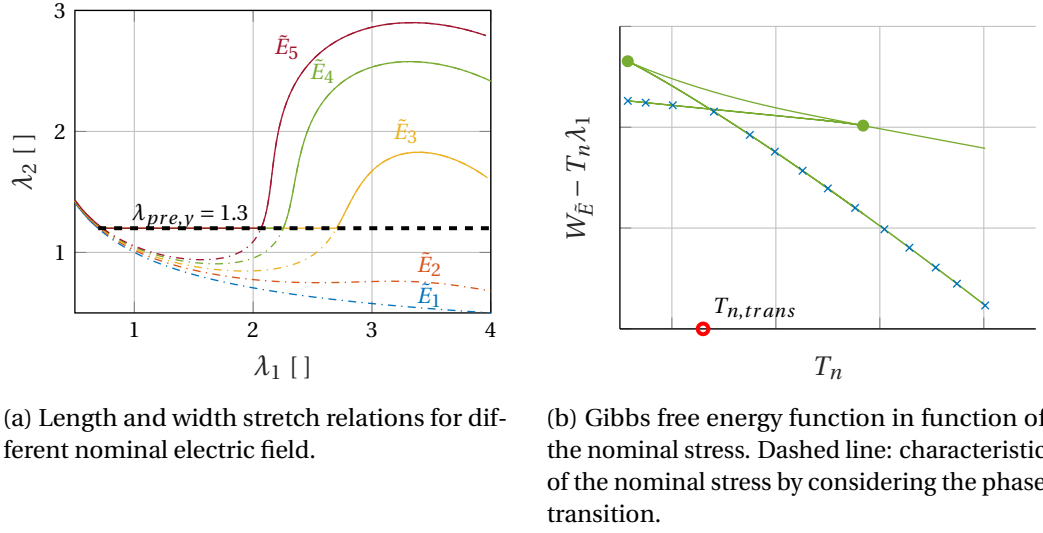


Figure 2.7 – Characteristics for the "0D" model

2.2.3 Relation between stretches

The first step in this analyse is to obtain all the pair (λ_1, λ_2) for a given nominal electric field (\tilde{E}_i) which cancels the stress in the width direction ($T_2 = 0$). The objective is to define when the actuator pass from the state $T_2 = 0 \rightarrow T_2 \neq 0$ and vice versa.

Let's consider a membrane pre-stretched in the width direction with $\lambda_2 = 1.3$ (Fig.2.7a). The case where the stress in the direction mentioned above is null allows determining the special characteristic for each nominal electric fields (corresponding colours). However, due to the incompressibility of the film, the stretch λ_2 lower than 1.3 are not reachable. Thus, the pairs (λ_1, λ_2) are defined by the full lines when λ_2 is higher than the pre-stretch ($T_2 = 0$) and by the value of the pre-stretch (dashed black line) when the membrane is supposed to be in compression (dash-dotted lines). This last case corresponds to the stress $T_2 \geq 0$.

From the derivative of the potential energy (Eq.2.12) and the pairs (λ_1, λ_2) , the characteristic of the nominal stress for each electric field could be obtained by considering the possibility to change the stress boundaries in the width direction (T_2).

2.2.4 Determination of the phase transition

The DEA technology has the particularity to reach inhomogeneous states in the same system in order to guaranty the intrinsic stability. Now that the relation between the stretches in all the directions (pairs of λ_1, λ_2) and the model of the nominal stresses (Eq.2.12) are known, the influence of the phase transition could be added.

One solution used to determine the nominal stress-stretch characteristic of the elastomer submitted to one electric field and the phase transition is explained here. It allows to numer-

ically compute these values easily and permits to demonstrate another similitude with the thermodynamic domain.

Generally, the Gibbs free energy density function characteristic (Eq.2.13) is given in function of the stretch λ_1 . A solution to track the phase transition and proposed by Koh [71] is to determine the different minima of the function.

$$g = W_{\tilde{E}}(\lambda_1, \lambda_2, \tilde{E}_i) - T_n \lambda_1 \quad (2.13)$$

Another solution is to provide the Gibbs free energy function in function of the nominal stresses (T_n) (Fig.2.7b). The previous characteristic creates a loop due to the specific N-shape characteristic of the nominal stress. The advantage of this representation is that when the characteristic intersects, it provides the stress for which the phase transition occurs (red dot: $T_{n,trans}$). By considering the phase transition, the nominal stress characteristic is then provided through the points defined by the blue crosses (Fig.2.7b).

2.3 Graphical criterion of stability: ideal elastomer

One major problem concerning the DEA consists of the electrical breakdown between the electrodes which limits the performance of the actuator. Due to the phase transition, even if only one part of the elastomer reaches the more significant stretch and if the electrical breakdown limit is exceeded during this transition, the film is damaged. Thus, the ability of the DEA to be in an inhomogeneous configuration in order to guaranty the intrinsic stability is not necessarily helpful if the electrical breakdown occurs. The majority of the standard material used to create DEA has this limit.

In the next section, the previously defined criterion of stability is used to determine an *ideal elastomer* defined by a linear true stress - stretch relationship. It is demonstrated that this ideal material allows reaching higher energy density and displacement without crossing the electrical breakdown. Through its energy density, a figure of merit is proposed involving both the electrical and mechanical parameters of the material.

Criterion	Comment
$\frac{\delta W_D^2}{\delta^2 \lambda_1} \geq 0 \Leftrightarrow \frac{\delta \sigma_1(\lambda_1, \lambda_2)}{\delta \lambda_1} - \frac{\sigma_1(\lambda_1, \lambda_2)}{\lambda_1} > 0$	/
$\frac{\delta W_D^2}{\delta^2 \tilde{D}} \geq 0 \Leftrightarrow \frac{1}{\epsilon} \frac{1}{(l_1 l_2)^2} > 0$	Always true
$\frac{\delta W_D^2}{\delta^2 \lambda_1} \cdot \frac{\delta W_D^2}{\delta^2 \tilde{D}} > \left(\frac{\delta W_D^2}{\delta \lambda_1 \delta \tilde{D}} \right)^2 \Leftrightarrow \frac{\delta \sigma_1(\lambda_1, \lambda_2)}{\delta \lambda_1} - \frac{\sigma_1(\lambda_1, \lambda_2)}{\lambda_1} > \epsilon_0 \epsilon_r \tilde{E}^2 \lambda_1 \lambda_2^2$	/

Table 2.1 – Stability criteria for uniaxial DEA

2.3.1 Criterion of convexity for DEA

In the previous section, Eq.2.11 was introduced in order to explain the general criterion of convexity for a state variable (x_i). In the case of the uniaxial DEA, three criteria should be verified in order to validate the stability. The first one is for the state variable λ_1 defined to consider the stretch in the considered direction of deformation. The two others are the one due to the variation of the electric field ($\frac{\delta W_p^2}{\delta^2 D}$) and the mutual contribution (Suo [67]). By developing these three definitions through the state equations (Eq.2.5-Eq.2.7), the obtained results are given in Table 2.1.

By observing the criteria in this table, the second one is always true, and the first one is the same that the third one when no voltage is applied to the electrodes ($\tilde{E} = 0$). Thus, the last criterion is the most restrictive one, and only this should be considered. This last criterion corresponds to ensure the convexity of the internal energy of the system and is called: *convex criterion*.

The objective is to verify that the criterion is valid for all the nominal electric field (\tilde{E}), provided to the membrane, before reaching the electrical breakdown (EB). Thus, the maximum performance with the actuator is achievable. The limiting value is the voltage for which the electrical breakdown occurred. Thus, if the intrinsic stability is insured up to this value, the stability is true for all the supply voltage. By introducing EB in the third criterion, the following equation is obtained:

$$\frac{\delta \sigma_1(\lambda_1, \lambda_2)}{\delta \lambda_1} - \frac{1}{\lambda_1}(\sigma_1(\lambda_1, \lambda_2) + \epsilon_0 \epsilon_r EB^2) > 0 \quad (2.14)$$

This criterion is ensured to the electrical breakdown if the derivative of the true stress characteristic of the elastomer evaluated in λ_1 given by $\frac{\delta \sigma_1(\lambda_1, \lambda_2, 0)}{\delta \lambda_1}$ is bigger than $(\sigma_1 + \epsilon_0 \epsilon_r EB^2)/\lambda_1$. This definition could be interpreted as the slope (S) of a new linear function and given by:

$$\sigma_1^* = S \cdot \lambda_1 - \epsilon_0 \epsilon_r EB^2 \quad (2.15)$$

In Fig.2.8, the true stress characteristic of common elastomer is given in blue with the derivative evaluated in two particular positions A and B (red and green lines). The intrinsic stability is guaranteed if the slopes of the line given by the pink dashed lines (Eq.2.15) are more significant than the one of the respective derivative. Thus, the position in A ensures intrinsic stability but not the position in B .

Through such representation, it is easy to determine if the elastomer will guaranty the intrinsic stability to the electrical breakdown only with the non-activated true stress characteristic of the material, its permittivity and its electrical breakdown.

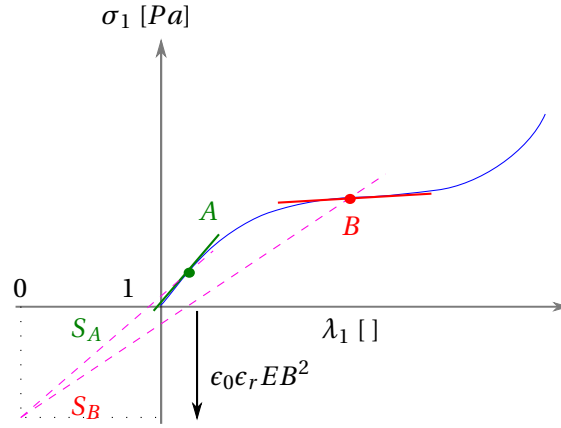


Figure 2.8 – Convex criterion applied to DEA: $\frac{\delta W_D^2}{\delta^2 \lambda_1} \cdot \frac{\delta W_D^2}{\delta^2 D} > \left(\frac{\delta W_D^2}{\delta \lambda_1 \delta D} \right)^2$. Full blue line: true stress characteristic of the elastomer (σ_1), dashed pink lines: criterion of convexity evaluated in different λ_1 (A and B) and green and red lines: derivative of true stress in A and B.

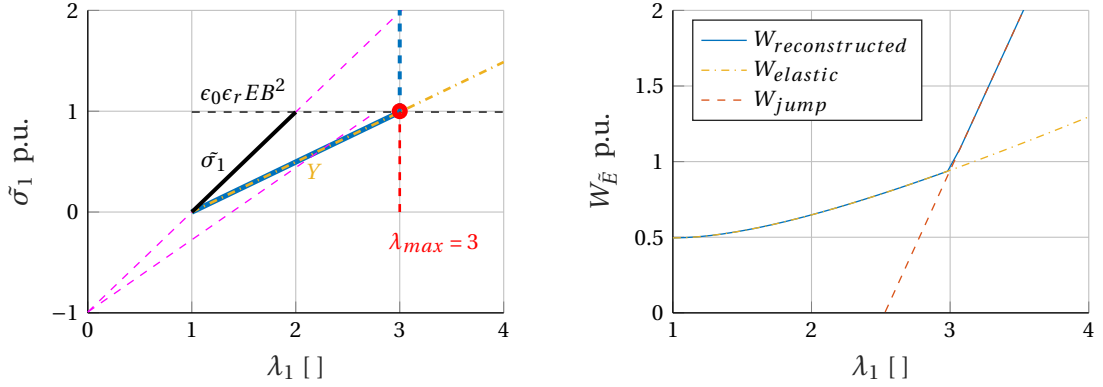
2.3.2 Study of the ideal elastomer

Now that the criterion of stability was discussed for a common elastomer with a characteristic described as in Fig.2.8 (blue line), another material with a *linear* characteristic is studied. This stress stretch relationship is assumed to have a slope given by $\epsilon_0 \epsilon_r E B^2$ like represented through the black line in Fig.2.9a ($\tilde{\sigma}_1$). The electrical breakdown limit could be represented in the true stress characteristic through the constant value: $\epsilon_0 \epsilon_r E B^2$. Thus, the linear $\tilde{\sigma}_1$ characteristic allows to respect the criterion provided by Eq.2.14 for all the voltages to the electrical breakdown.

By keeping the same consideration about the linear elastomer (constant Young's modulus Y), let us study another stress characteristic which does not ensure the convex criterion (orange dash-dotted line in Fig.2.9a). According to the criterion of the "pink line" (slope of the pink line bigger than the orange one), this material is unstable for all the stretches. It means that it reaches the phase transition from the beginning of the characteristic and thus directly exceeds the electrical breakdown. However, if this situation is avoided just before this electrical limit, the actuator could survive. To perform such improvement, a vertical *jump* is added to the characteristic when the linear true stress is crossing the electrical breakdown limit (blue line in Fig.2.9a). For the energy density characteristic, this is equivalent to add a jump at the maximum position λ_{max} (red dashed line in Fig.2.9b). In terms of physical property, it is equivalent to infinitely stiff the elastomer at this fixed position.

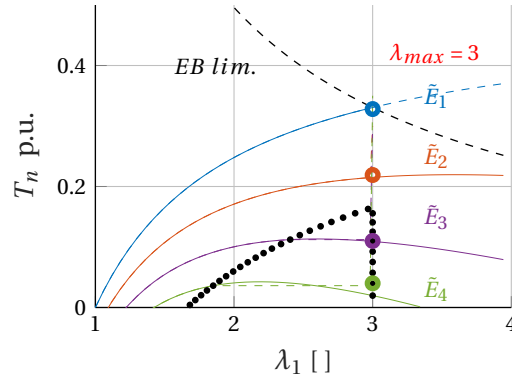
The reconstructed energy density (Fig.2.9b) allows to obtain the nominal stress characteristic of the proposed ideal elastomer for different nominal electric field (Fig.2.9c). For low electric fields (\tilde{E}_1, \tilde{E}_2), no phase transition occurs, and the maximum strain could be reached without exceeding the electrical breakdown limit. Concerning higher electric fields (\tilde{E}_3, \tilde{E}_4), the phase transition appears without reaching the electrical limit. Indeed, the subsystems which are in the bigger stretch (λ_{max}) in the phase transition, do not cross the electrical breakdown. Thus,

2.3. Graphical criterion of stability: ideal elastomer



(a) Stress characteristic of ideal elastomer. Dashed pink lines: criterion of convexity, full dark line: the criterion up to $\epsilon_0 \epsilon_r E B^2$ is ensured, dash-dotted orange line: elastomer which does not respect the criterion and full blue line : ideal elastomer

(b) Corresponding energy density function of the ideal elastomer (blue line in Fig.2.9a)



(c) Nominal stress for the ideal elastomer with its limits (dotted black line: limit of phase transition)

Figure 2.9 – Ideal elastomer

even if the phase transition occurs, the elastomer survives due to the presence of this jump.

Moreover, because the energy density is proportional to the area below the nominal stress characteristic of the elastomer, more significant energy density and higher stretch are reachable with the proposed ideal elastomer (blue line in Fig.2.9a) than the one which ensures the intrinsic stability (black line in Fig.2.9a).

2.3.3 Performance of the ideal elastomer

The maximum strain which is reachable is given by the intersection between the constant electrical breakdown limit ($\epsilon_0 \epsilon_r E B^2$) and the characteristic of the linear elastomer defined

through its Young's modulus (Y). This stretch is defined by:

$$\lambda_{max} = \frac{\epsilon_0 \epsilon_r E B^2 + Y}{Y} \quad (2.16)$$

where Y is the slope of the true stress characteristic. In order to *guaranty the convexity* of the material, the elastomer with a slope Y equal to $\epsilon_0 \epsilon_r E B^2$ was defined. Therefore, with such characteristic, the maximum variation of stretch is $\lambda_{max} = 2$. This maximum strain is independent of the permittivity and the electrical breakdown limit of the material.

For the other intrinsic stable elastomer (blue line in Fig.2.9a), done possible through considering the presence of a *jump* characteristic, the maximum strain becomes the one which induces the mechanical rupture. Indeed, if the characteristic of the elastomer such as the blue one in Fig.2.9a is created and that any Young's modulus is possible, the objective is to obtain Y such that λ_{max} becomes the maximum mechanical stretch.

Concerning the energy density, it is defined by the area enclosed in the nominal stress-stretch relationship. From this specification, the energy density for a linear material becomes:

$$W_{ideal} = \int_1^{\lambda_{max}} T_n(\lambda_1) d\lambda_1 = Y(\lambda_{max} - \ln(\lambda_{max}) - 1) = \epsilon_0 \epsilon_r E B^2 - \frac{\ln(\lambda_{max})}{\lambda_{max} - 1} \quad (2.17)$$

Through the definition of the maximum strain (Eq.2.16) and the Taylor series expansion, the energy density becomes:

$$W_{ideal} = \frac{1}{2} \frac{(\epsilon_0 \epsilon_r)^2 E B^4}{Y} \quad (2.18)$$

In comparison with the elastomer define through the linear stress characteristic and which ensures the stability everywhere (black in Fig.2.9a), the energy density is not only dependent on the electrical properties but also on the mechanical characteristic which provides another degree of freedom in order to improve the performance of the elastomer.

In addition to provide the energy density, Eq.2.18 represents a figure of merit which links the electrical properties of the film (permittivity and electrical breakdown limit), as well as the mechanical one (Young's modulus). However, the proposed FOM in this section is not sufficient to guaranty a suitable elastomer. The presence of the *elbow* (or *jump*) right before the electrical breakdown is a second condition. Without this mechanical behaviour, the phase transition brings a part of the elastomer in a state above the electrical breakdown limit.

2.3.4 Discussion on the figure of merit

The objective of the figure of merit is to compare different elastomer through their intrinsic parameters in order to determine the best one. This FOM could be used to compare the

different elastomer, not necessary with a linear stress characteristic, i.e. hyperelastic material. With such material, an equivalent Young's modulus is then needed.

Eq.2.18 shows that a good elastomer which is stable with the presence of phase transition and with an *elbow* at the adequate position, should be as soft as possible and have a permittivity and an electrical breakdown limit as large as possible.

If the elastomer is already fabricated with known electrical and mechanical parameters, the objective is to determine a solution in order to improve the performance through external systems by decreasing the stiffness (e.g. section 2.6).

However, if the objective is to create a new material with the best performance, the first solution is to play with all these parameters. Another solution could be to rewrite Eq.2.18 as : $\frac{\epsilon_0 \epsilon_r EB^2}{2} \cdot \kappa$ where $\kappa = \epsilon_0 \epsilon_r EB^2 / Y$. From this equation, either the ratio κ or $\epsilon_0 \epsilon_r EB^2$ could be improved. Indeed, Young's modulus could be increased if $\epsilon_0 \epsilon_r$ and EB increase as well. The new way to write the figure of merit tends to join the one often found in the literature in terms of Maxwell pressure ($\epsilon_0 \epsilon_r EB^2$) [6] with κ which tends to 2.

2.4 Energy density of DEAs

In the previous sections, the models of the DEA have been recalled by considering the inhomogeneous deformation. The material prefers to be subdivided into two parts to minimise its internal energy and ensures the intrinsic stability of the actuator. From these equations, the phase transition has been integrated. This particularity limits the energy density of this technology. Indeed, if one part of the deformed DEA crosses the electrical breakdown, all the actuator is damaged. Then, from the study of the stability of the DEA of all the state variables, a figure of merit has been proposed which allows defining the essential parameters of the material to obtain large energy density.

In this section, several energy densities defined by considering appropriate limitations are introduced in order to understand the real performance of such technology. Indeed, the values observed in the literature, do not image exactly the performance when the DE is used such as an actuator.

The considered actuator consists in the uniaxial one studied in the section 2.1 and 2.2. The characteristic of the elastomer is the one given through the hyperelastic model.

2.4.1 Limits of the DEAs

The conventional mechanical and electrical limits of the DEA technology is well defined in the literature. Besides these limits, the phase transition could be added as seen previously. The combinations of all of them allow determining the different reachable zones and thus evaluating the energy density. These limits are given in Fig.2.10 where the stretch and the nominal stress are represented. The area enclosed by any closed loop in this representation provides the energy density considering four cases.

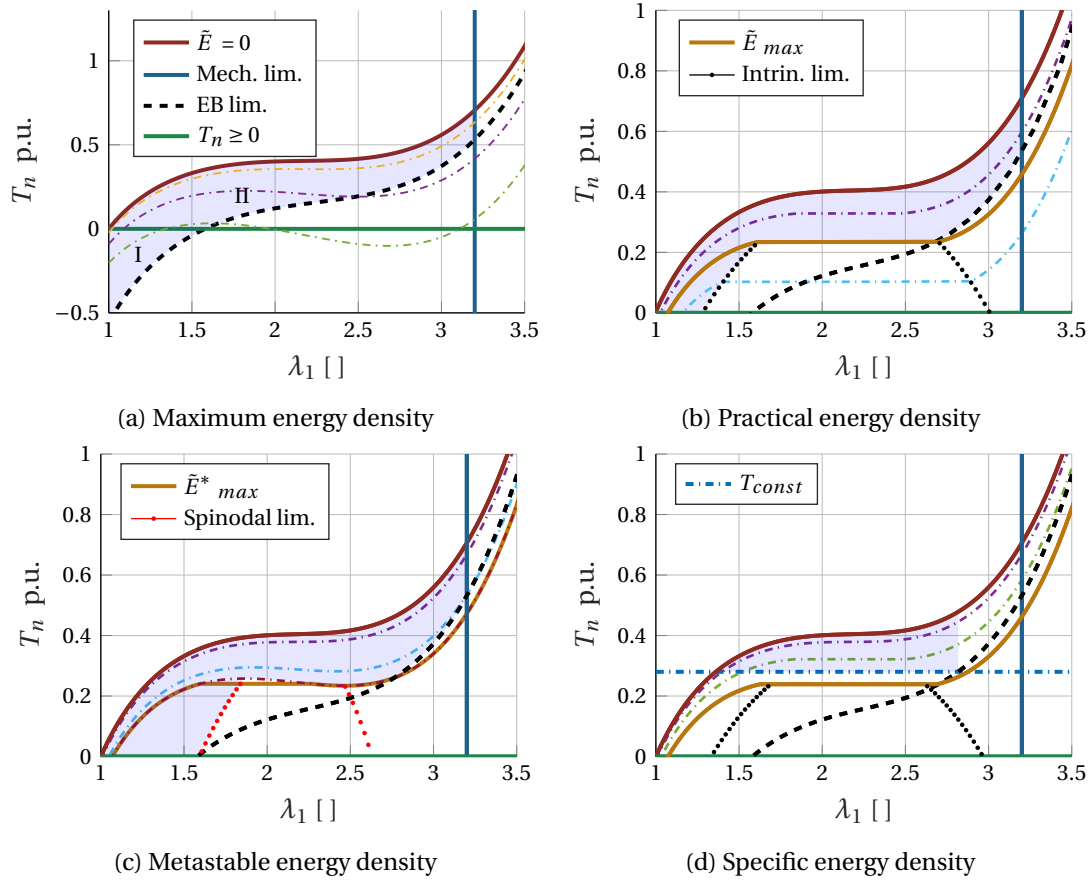


Figure 2.10 – Definitions of different energy densities. The dash-dotted lines correspond to the stress-strain characteristic for different nominal electric fields.

The upper limit is always given by the characteristic of the membrane when no voltage is applied between the electrodes (dark red lines). The maximum strain which is reachable before that the elastomer mechanically breaks is given by the dark blue lines. In terms of electrical limits, the limiting stretch and stress for which the electrical breakdown occurs are given by the black dashed lines. According to the considered energy density, other limitations are introduced and explained in the following section.

2.4.2 Definitions of the energy density

According to the considered limits several energy densities could be defined. The loop for which the energy density is maximum is presented in Fig.2.10a (Part I + II), i.e. *maximum energy density*. Generally, all this cycle is not realistic because the elastomer could not be in compression. Thus, the limit $T_n \geq 0$ (green lines) is introduced in order to remove the possibility to have a compression state. With this limit, the *theoretical energy density* is introduced (Part II) and corresponds to the realistic maximum energy density potentially available. However, this definition does not represent a realistic energy density of any actuators.

In the first section, it has been shown that the characteristic of the DEAs is dependent on the phase transition, the membrane being split into two states for a given global position. For each nominal electric field, this limit is provided by the black dots in Fig.2.10b). A problem occurs when for a specific applied voltage, a state is further than the electrical breakdown limit. This limit is highlighted in brown (\tilde{E}_{max}) in Fig.2.10b). The area enclosed by this zone is the *practical energy density*.

Even if the probability is low, the metastable region could be reached. The spinodal limit defines the local maxima and minima for all the applied voltage (red dotted line). In this case, another maximum voltage is defined (\tilde{E}_{max}^*). The *metastable energy density* is provided in Fig.2.10c and corresponds to the maximum energy density that the actuator could reach if all the cycle is performed through particular external conditions (e.g. mechanical or electronic control).

2.4.3 Influence of external loads

Optimising the energy conversion between heat and mechanical work is a well-known topic in the thermodynamic domain and can be summarised with the *Carnot Cycle*. This cycle guarantees an optimum conversion process. For the DEG (dielectric elastomer generator) based energy harvesting systems, the square cycle in the characteristic u vs q is often represented. However, the problem is entirely different for dielectric elastomer actuators. The mechanical load and the application itself influence a lot the energy density and impose other boundaries.

Generally, the goal of any work in the domain of DEA is to increase the stretch. In the literature, several examples of moving masses are presented. In such a situation, the potential energy provided to the load is restored once the voltage is turned off.

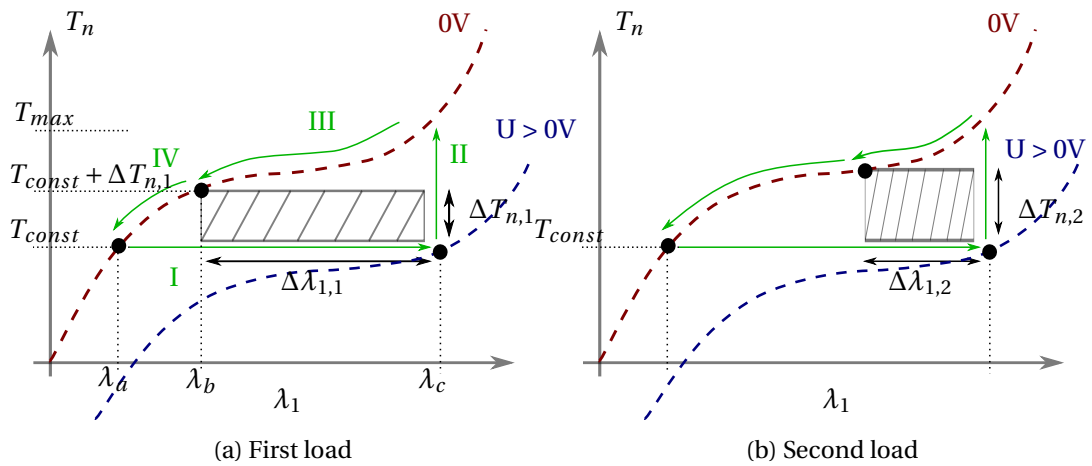


Figure 2.11 – Definition of the cycle for the energy density. Green arrows for the specific one and black rectangles for different loads and a given pre-load.

In order to create an actuator which provides some work to a load, the appropriate parameter becomes the energy density. Here, it has been decided to focus on a uniaxial actuator, fixed to a rigid frame at the top, to provide work to an external load against gravity (e.g. to lift a mass). Thus, the adequate cycle should be determined (appendix A). By considering the green cycle in Fig.2.11a, the *specific energy density* could be defined. A load submitted to the gravity and represented through its nominal stress equal to T_{const} is hanged to the membrane. The two components are initially stable in λ_a . Then, the voltage is slowly increased to reach the equilibrium position λ_c (step *I*). During the second step *II*, another load ($\Delta T_{n,1}$), located at this position (λ_c), is hanged to the system and ideally, at the same moment, the voltage is switched off. The elastomer and the two loads are stabilising in λ_b (state *III*). If the second load $\Delta T_{n,1}$ is let in this position (i.e. removed from the membrane), the stable position becomes λ_a (state *IV*), and the cycle is accomplished.

During this specific cycle, the load $\Delta T_{n,1}$ wins a potential energy equivalent to the dashed rectangle. Indeed, the load rose from its initial low position (λ_c) to the highest one (λ_b). In this presented case, the remaining energy is equivalent to a kinetic one provided to the masses during the deactivation. The activation of the membrane could be done through a jump of voltage. However, the damped energy is useless whereas the one during the deactivation could be used in a specific situation (e.g. pumping system). Thus, the jump of voltage is only considered for the deactivation in order to provide the green cycle.

Concerning the first constant load T_{const} , it could be assimilated to a constant pre-load which allows the system to be located in the targeted region of the characteristic of the elastomer.

For a given constant initial nominal stress T_{const} , another load ($\Delta T_{n,2}$) could be moved such as in Fig.2.11b. This second load is less risen during activation. However, the potential energy is not necessarily lower because the load is bigger. An infinite number of rectangles could be determined in the green cycle defining the specific energy density.

In the studied examples, the case of two constant loads has been treated by considering the same initial surface in contact with the load. Thus, the nominal stress for the constant load depends only on the weight of the mass. However, if the geometry is keeping adjustable, a specificity appears in order to tune the real force according to the nominal stress. Because the theory is about the nominal stress and the stretch, the rectangle provides information about the energy density. Once the load is defined, the force provided by the actuator is tuned according to the load to lift by connecting several DEA in series (more displacement) or parallel (more force). During the design of the actuator, the adequate rectangle should be decided in order to obtain the maximum potential or kinetic energy density.

2.5 Influence of the Mullins effect

Knowing the elastomer, the objective is usually to find a system which can bias the elastomer in order to improve the global performance, i.e. increase the specific energy density. One often neglected parameter which is highlighted in the proposed figure of merit is the Young's

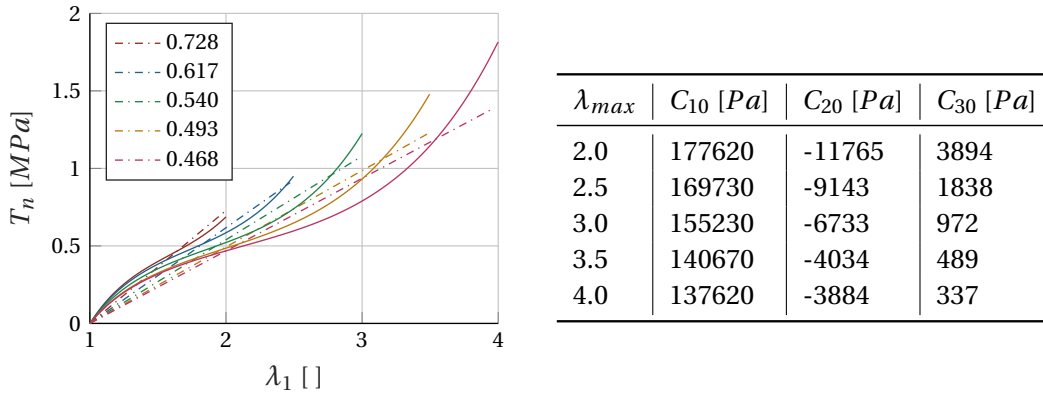


Figure 2.12 – Influence of the Mullins effect on Elastosil® . On the left, the nominal stress for each maximum strain with its corresponding equivalent Young's modulus. On the right, the value of the parameters of the Yeoh model.

modulus of the elastomer which is a particularity of this material [72]. The stress characteristic of the film softens when different maximum strains are reached during the "history" of the film.

In order to observe the influence of such effect on the performance, five films have been previously stretched ten times (to remove initial effects as previously explained) respectively with a stretch of 2.0, 2.5, 3.0, 3.5 and 4.0. Then, from these measurements, the corresponding parameters of the Yeoh model are computed. The characteristic, as well as the parameters of the model, are provided in Fig.2.12. The equivalent Young's modulus for each characteristic is also provided which corresponds to the mean value of the stresses over the stretches. These values allow studying the performance of the actuator through the "0D" model. The practical energy density and then the specific one are discussed according to the process mentioned above.

2.5.1 Effect on the practical energy density

The different characteristics for different final reached stretches (Fig.2.12) are compared to the same "targeted" maximum stretch (2^{th} and 3^{rd} columns of the table in the Fig.2.13). The practical energy density decreases when the initial stretch performed to the membrane is increased. The observation about the energy density is not coincident with the figure of merit previously defined (Eq.2.18) where the value is inversely proportional to Young's modulus. Indeed, between the different curves, more the film has been previously stretched, smaller is the equivalent Young's modulus (Fig.2.12). However, it is consistent with the importance of the *elbow* (when the stress characteristic passes from the "plateau" to the third convex region) which should be as close as possible of the targeted maximum strain (here $\lambda_1 = 2.0$ or 3.0). The area enclosed by the characteristic which has been initially stretched up to $\lambda = 2.0$ (area between full and dashed red line in Fig.2.13) is more important because the targeted stretch is after the *elbow* contrary to the initially stretched membrane $\lambda = 3.0$.

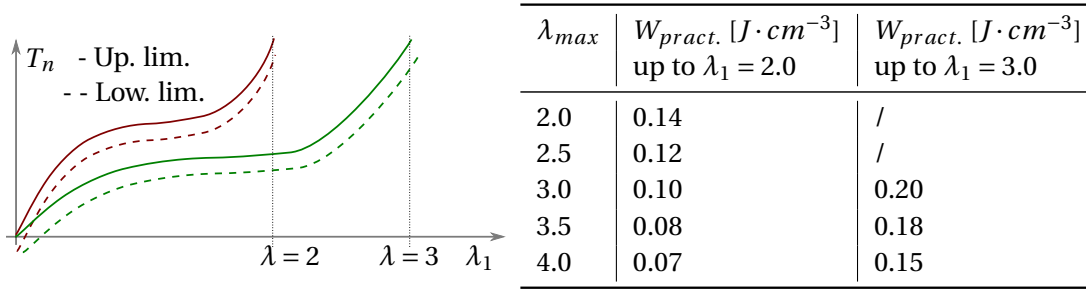


Figure 2.13 – Practical energy density for different targeted stretches

Concerning $\lambda_1 = 3.0$, it seems that the practical energy density decreases more slowly. It could be explained by the fact that the *elbow* of $\lambda_{max} = 3.5$ and $\lambda_{max} = 4.0$ are closer to the targeted stretch (Fig.2.12). Not only the stiffness of the material seems essential but the presence of the *elbow* and its location should also be considered.

2.5.2 Effect on the specific energy density

In the previous section, it has been demonstrated that the Mullins effect influences the practical energy density (50% between $\lambda_{max} = 2.0$ and 4.0).

In this section, this phenomenon is compared for the specific energy density and different constant loads and pre-stretches (Fig.2.14). It could be noticed that the " $\lambda_{pre,y}$ pre-stretch" and the "*initial pre-stretch*" to a targeted maximum stretch λ_{max} are not equivalent. The first one concerns the pre-stretch submitted to the width direction and maintained in this position. The other one is an initial stretch performed to the membrane in the deformation direction before to release the film.

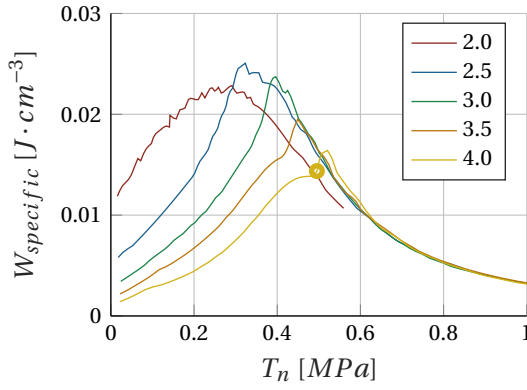
Without pre-stretch ($\lambda_{pre,y} = 1$)

Without pre-stretch (Fig.2.14a), the maximum specific energy density is obtained for the membrane initially pre-stretched up to $\lambda_{max} = 2.5$ and the worst for the membrane initially stretched with the maximum value ($\lambda_{max} = 4.0$). Before reaching the maximum for each characteristic, the specific energy density is always better when smaller initial stretches (λ_{max}) have been performed to the film. After the local optimum, the tendency is reversed. If the membrane is initially stretched to a significant value, the specific energy density passes from $0.016 J \cdot cm^{-3}$ to $0.024 J \cdot cm^{-3}$.

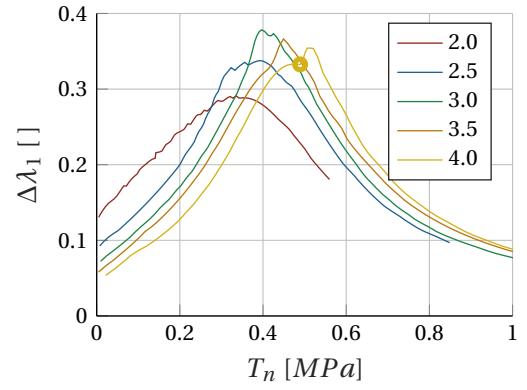
As previously discussed, the constant load helps to reach the smoother region of the characteristic. However, in this case, it seems that it does not consist of the only condition to reach an optimum. Indeed, the membrane which has been initially stretched 2.5 times has the maximum specific energy density.

As previously explained in Fig.2.16a, the optimum is reached when the limit due to the electrical breakdown passes from the phase transition which induces the breakdown to a normal stretch (intersection of dark and light blue lower limit) in the flatter region.

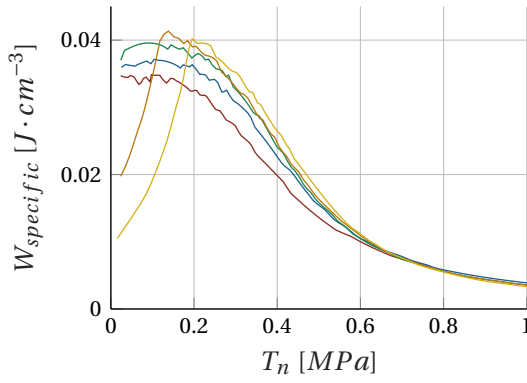
2.5. Influence of the Mullins effect



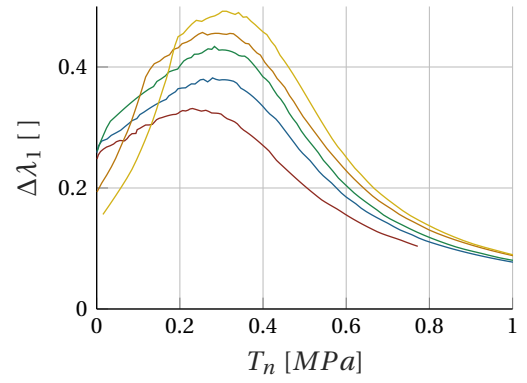
(a) Specific energy density - $\lambda_{pre,y} = 1$



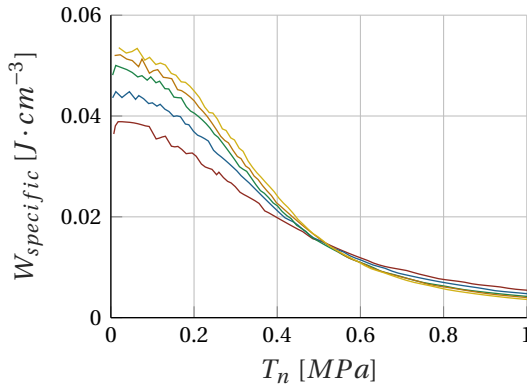
(b) Displacement - $\lambda_{pre,y} = 1$



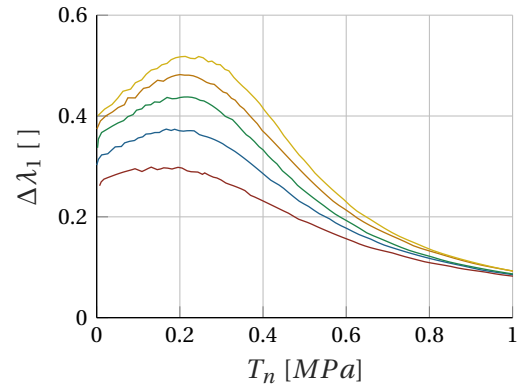
(c) Specific energy density - $\lambda_{pre,y} = 1.5$



(d) Displacement - $\lambda_{pre,y} = 1.5$



(e) Specific energy density - $\lambda_{pre,y} = 2.0$



(f) Displacement - $\lambda_{pre,y} = 2.0$

Figure 2.14 – Performance of Elastosil® film with the influence of the Mullins effect and different pre-stretches in the width direction. The wavy shape of the curves comes from the numerical resolution of the system ("0D" model).

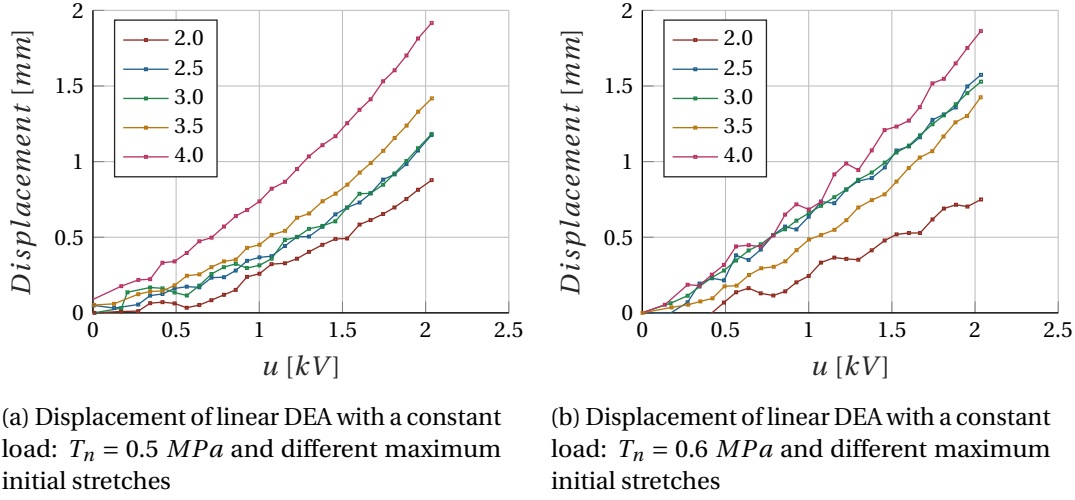


Figure 2.15 – Variation of the displacement according to the Mullins effect

However, a second previously mentioned condition to reach an optimum is the presence of an *elbow* (stiffer region after the "plateau") as close as possible of this specific location. Over the different presented stress characteristics, the 2.5-case has the ideal behaviour in the sense the flatter region is followed by a stiffer characteristic right at the intersection of the "dark" and "light" lower blue limit (Fig.2.16a). Thus, this characteristic induces the optimal specific energy density.

From the obtained results, another observation concerns the 3.5 and 4.0 cases. A sharp transition of specific energy density is present (dot in Fig.2.14a). This "jump" consists in the case where a phase transition is present, but the electrical breakdown is not exceeded. Thus, the phase transition helps to obtain a more significant energy density for the given stress characteristic but does not necessarily provide the best solution.

Concerning the variation of stretch, the conclusion is quite similar. However, the maximum stretch is obtained with $\lambda_{max} = 3.0$, and the difference between each maximum is not as significant as for the specific energy density. The specificity of the stress characteristic induces such results. However, it is difficult to explain this phenomenon carefully.

In order to validate the observations about the variation of stretch, linear actuators with pure-shear configuration and composed of an Elastosil® membrane with a thickness of $50 \mu\text{m}$ have been tested with two different constant loads (0.5 MPa and 0.6 MPa). The electrodes are done with carbon grease. The voltage has been increased from 0 to 2.5 kV . The results are provided in Fig.2.15. The chosen loads being after the theoretical optimum of each characteristic, the Mullins effect allows increasing the displacement as predicted by the model.

With pre-stretch ($\lambda_{pre,y} = 1.5, \lambda_{pre,y} = 2.0$)

When the pre-stretch is applied to the different studied curves, the values of the specific energy density and the variation of stretch are increased. Moreover, by increasing the pre-stretch, the

optima seem to be achieved when no constant nominal load is applied. This effect is more present for the specific energy density than for the displacement.

By applying the pre-stretch, the Mullins effect starts playing a role to improve the performance of the elastomer precisely such as the for the constant loads located after the optimal performance (Fig.2.14). Whatever is the pre-stretch, this observation is done.

Trough the pre-stretch, the stress-stretch characteristic is softened. Moreover, the pre-stretch allows to reach the "plateau" zone of the characteristic, and the Mullins effect also helps to decrease the slope of this particular zone. Therefore, through the mix of these two specificities, the performance are improved. Moreover, the specific energy density becomes maximum for $T_n = 0$ when the pre-stretch is large enough ($\lambda_{pre,y} = 2.0$), and over the different stress characteristic, the one initially stretched with a maximum value (4.0) provides the best performance. It could be explained by the fact that when the pre-stretch is sufficiently high, the limiting parameters induces through the phase transition is suppressed (only light blue limit). Thus, the presence of the *elbow* is no more important. The softer material becomes the one which provides better performance as observed in the studied cases. The pre-stretch tends to stabilise the elastomer. However, if the pre-stretch is too important, the stress characteristic and the advantage of the pre-stretch is lost because of the stiffening of the membrane (not shown in the figures).

2.6 Biasing elements

Another approach in order to improve the performance is studied in this section. The constant biasing loads are the most famous tools, and their influence is analysed.

A common elastomer engineered for the DEA and commercially available is the Elastosil® from Wacker. This film is studied through the "0D" model (section 2.2). Then, the specific energy density is evaluated and compared to the values found in the literature. The objective is to obtain a more realistic value of energy density for a linear actuator according to the discussion as mentioned earlier about the practical energy density.

2.6.1 Performances of common silicone

The Elastosil® film has been characterised with a pull-tester in order to obtain the parameters of the hyperelastic model through a fitting process. The studied sample consists of a membrane with a width, a length and a thickness of 100 mm, 10 mm and 50 μm respectively and fixed to a rigid frame. The membrane has been stretched ten times before starting the measure in order to remove the problem of the Mullins effect (section 2.5) and the shift of the force due to the first deformations. The considered dielectric constant and the electrical breakdown limit are 2.8 and 100V $\cdot \mu m^{-1}$ respectively. The speed of deformation for the pull-test is fixed to 1 mm $\cdot s^{-1}$ and the membrane has been stretched up to $\lambda = 3.5$. Considering the Yeoh model, the parameters which describe the elastomer are obtained (Table 2.12 fourth row).

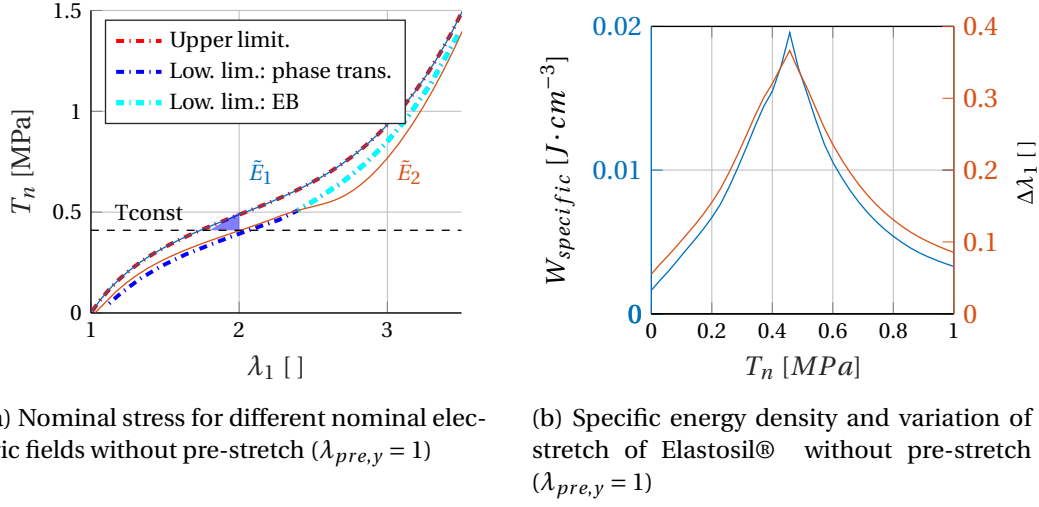


Figure 2.16 – Performance of Elastosil®

The practical energy density found for this elastomer is $0.22 \text{ J} \cdot \text{cm}^{-3}$ which is in the same order of magnitude than the one in the literature for ordinary silicone ($0.3 - 0.4 \text{ J} \cdot \text{cm}^{-3}$ [73]). Moreover, the energy density found in the literature is generally provided through $\epsilon_0 \epsilon_r E B^2$ which gives $0.25 \text{ J} \cdot \text{cm}^{-3}$, for the studied elastomer. Thus, the practical energy density provides a good prediction of the maximum value. However, such a cycle is difficult to follow. Considering a uniaxial actuator and as previously discussed, this definition is certainly not suitable but provides a good idea about the maximum energy density potentially usable with the elastomer in perfect conditions.

2.6.2 Influence of constant biasing elements

The studied biasing element concerns the constant load which is assimilated to a constant nominal stress. The "0D" model is adapted in order to consider such a biasing system and to evaluate the specific energy density presented in Fig.2.10d. Fig.2.16b provides the results of the specific energy density of the Elastosil® and the variation of the stretch of the film for different loads ($T_n = T_{const}$).

The nominal stress characteristic is given in Fig.2.16a for different nominal electric fields with the two boundaries. The specific energy density for the example of T_{const} is provided by the blue area. The lower limit could be subdivided into two parts, i.e. dark and light blue lines. The dark one is provided by the stress-strain value for which the phase transition occurs and exceeds the electrical breakdown. The light blue part concerns the limiting stretches which have no phase transition.

Concerning the studied elastomer, the optimum specific energy density is around $0.02 \text{ J} \cdot \text{cm}^{-3}$ for a stretch of around 37% and a T_n of 0.46 MPa . It is evident that this value of energy density is ten times lower than the values provided in the literature and the one given through the maximum energy density ($0.25 \text{ J} \cdot \text{cm}^{-3}$). However, this cycle is more realistic in terms of

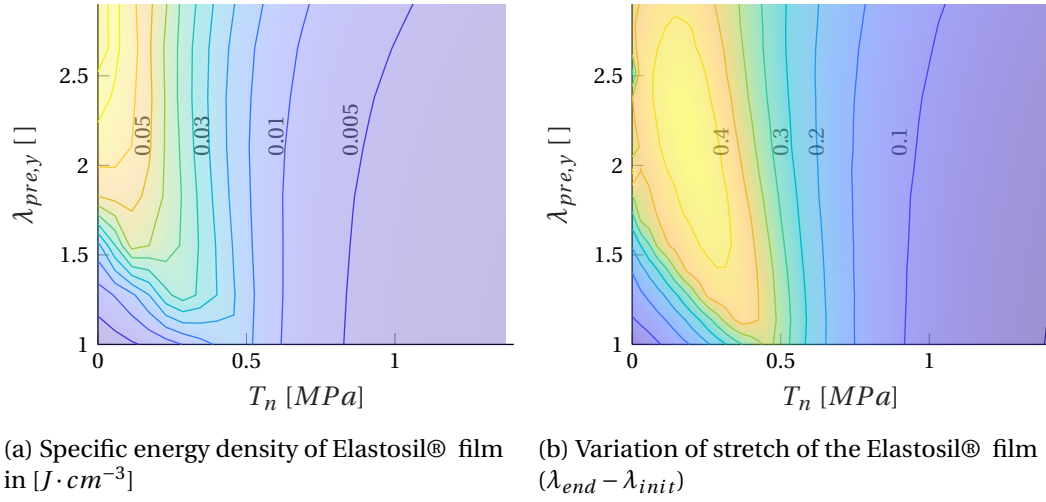


Figure 2.17 – Performance of Elastosil® film with the influence of pre-stretch and pre-load

actuation than the practical energy density.

As previously mentioned, an optimum for the specific energy density as well as the stretch is present (Fig.2.16b). The load of the optimum represents the constant load for which the intersection with the dark and the light blue lower limit occurs.

The nominal stress characteristic of the elastomer is divided in three part with the first one which increases rapidly with a concave shape, then a flatter region ("plateau") occurs, and finally, an increase of the stiffness with a convex curve is present. When getting close to the flatter region, the equivalent Young's modulus (stiffness) is lower which tends to improve the specific energy density. The advantage of the well-chosen constant load is the fact that the actuator could work near this flat region. According to the proposed figure of merit, this parameter helps to increase the specific energy density which is confirmed in this example.

2.6.3 Influence of the pre-stretch in the width direction

Another essential parameter consists of the pre-stretch in the in-plane direction opposite to the considered one. It consists of initially stretching the membrane in the direction as mentioned above before maintaining it in this pre-stretch form. The model is also able to consider such an influence. Thus, the specific energy density and the variation of stretch are obtained according to the load and the pre-stretch (Fig.2.17).

Concerning the specific energy density, it is clear that the pre-stretch improves the performance: up to $0.05 J \cdot cm^{-3}$. The influence of this parameters tends to "stretch" or "bunk" the characteristic which induces a softening of the elastomer in the preferential direction and then the energy density is increased as described by the FOM. By pre-stretching the membrane, the stress characteristic is smoothed and tends to remove the first concave region of the stress characteristic and thus cancelled the phase transition which is limiting due to the electrical

breakdown. The "plateau" is reached for smaller constant loads. For a certain pre-stretch ($\lambda_{pre,y} = 2.25$), no more load is necessary to reach the optimum because the softer region starts from the beginning of the characteristic.

For the variation of the stretch, the effect is similar. However, an optimum appears which is not coincident with the optimum of specific energy density. In terms of improvement, the effect on the stretch is not as significant as for the specific energy density. Indeed, the variation of stretch is improved by a factor 1.3 versus 2 for the energy density.

In order to obtain better specific energy density, either the load could be adapted, or the pre-stretch is also useful. Both allow working near the flatter region of the characteristic. However, it is difficult to explain the presence of optima for different conditions due to a large number of variables.

2.7 Conclusion

An original comparison of the DEA to the thermodynamic domain has been performed to understand and to provide the state equations of such technology. Through the nominal stress characteristic, the variation of condition on the width stress and the implication of the phase transition, the model of the dielectric elastomer actuator is better understood and better developed than common assumptions on the configuration of the elastomer (e.g. pure-shear). Moreover, another definition of the pull-in instability is introduced which is more limiting. The graphical representation of the criterion of intrinsic stability has allowed defining an ideal elastomer. This material helps to define a figure of merit which implies electrical and mechanical characteristics of the material. The importance of the stiffer region (*elbow*) of the stress characteristic is also introduced.

Several definitions of the energy density are provided in order to understand the meaning of all of them and to define the more useful one in terms of actuator. The influence of an external load has also been considered and has allowed defining the specific energy density as being the most appropriate definition for this kind of actuator.

Through the previously defined "0D" model, the Elastosil® film is analysed. The practical energy density of $0.22 \text{ J} \cdot \text{cm}^{-3}$ is obtained. This value is close to the one found in the literature. However, the value computed considering the specific energy density, being more appropriate from our point of view is ten times lower. Even if the pre-stretch and load could improve the value by a factor 2, this energy density stays low compared to the practical energy density, which seems to be the reference in the literature.

Concerning the observations obtained through the variation of the stiffness of the elastomer with the Mullins effect and the influence of constant loads and pre-stretches, a global conclusion about the ideal film could be given.

The lowest, the stiffness is, the highest the performance (variation of stretch and specific energy density) are. However, if the phase transition occurs, it should be guaranteed that it will

not limit the performance through the fact that a part of subsystems of the material reaches a deformation which could induce an electrical breakdown. Thus, with the presence of phase transition, the *elbow* (third region of the stress characteristic) should be present and as stiff as possible right after the "plateau" of the characteristic.

For an existing material, if its stress characteristic is fixed (no chemical improvement possible), the constant load helps to reach the region of the characteristic with the lower stiffness, and improved performance are achievable. Through the pre-stretch which softens and brings closer the "plateau", the phase transitions are suppressed and the performance are increased. Moreover, the Mullins effect allows increasing the performance by reducing the stiffness of the elastomer.

Finally, in the literature, the primary objective is to increase the stretch of the DEA. Some researchers are using particular material with high permittivity (VHB™ from 3M), the encapsulation of the material in oil increases the electrical breakdown limit [74], the dielectric constant is increased by creating composite, e.g. IPN (interpenetrating polymer networks) [75] or the design of special spring [76] is considered. The idea being that if the stretch is increased, the specific energy density is also increased. The studied results have demonstrated that if the stretch is increased, the specific energy density is also increased for particular values of the biasing parameters. However, the optimum of this energy density is not coincident with the optimum of the variation of the stretch.

Another solution mentioned in the chapter 1 concerns the negative biasing element which is analysed in the next chapter.

The hypothesis of the constant electrical breakdown limit has been made in order to define the energy density. One whole thesis was dedicated to analyse the variation of the electrical breakdown [77]. It has been shown that this electrical field increases with the stretch. Thus, better energy density could be expected. However, a model of the variation of the electrical breakdown limit according to the stretch should be performed.

3 Cylindrical negative biasing system

In terms of performance regarding DEA, the research has principally focused on the possibility to increase the displacement of this kind of actuator. The most often cited one concerns Pelrine [6] who has demonstrated the possibility to reach more than 300% of deformation. However, when so considerable stretches are obtained, it is principally with the 3MTMVHBTM-tape used such as an elastomer. Regarding the number of actuation cycles, this material is not adequate due to its high viscosity. These high performances have been generally reached once for the demonstration.

A solution proposed in order to increase the displacement of the DEAs for more or less viscous material is a negative biasing element (load system). It consists of spring with a particular characteristic. The objective is to adapt the working characteristic of the DEA and the one of the biasing element in order to reach the best performance of the coupled system. Wingert [78] has related the first linear actuator which has such specific spring. In order to obtain a negative stiffness spring, the authors have used bistable components for which a specific zone of the *force vs displacement* characteristic is negative. Firstable, the spring is pre-compressed and is placed into contact with the membrane. Then, it is released, and an equilibrium position between the two elements is reached (initial pre-load). Berselli [76] and then Hodgins [79] have also studied such bistable elements. The first one has used the spring in order to create a linear actuator which can provide a constant stroke. The second author has studied this bistable element and he has demonstrated the possibility to increase the displacement of the actuator. This solution is benefit for all kind of elastomer. The main disadvantage of the bistable solution is that the zone between the two mechanical stable positions is not reachable (unstable). Hodgins has proposed to use a mechanical stop in order to be able to use the spring over a certain range of positions on the negative characteristic.

All these authors have focussed on the possibility to increase the displacement without considering the energy density. This first aspect is studied in the first section of this chapter in order to understand the two topics carefully. Contrary to the previous chapter, the pre-stretch in the opposite direction of the targeted deformation is not studied.

Then, the design of a cylindrical spring with such a negative characteristic is proposed, tar-

getting the application of a tubular pump. The main characteristic of this particular spring is the radial deformation without variation of its length. The radial force according to the deformation of the radius has the specific negative characteristic. To obtain such behaviour, arch-beams have been used which improves the achievable stable positions in the negative zone contrary to the solutions proposed through bistable elements. In order to study the influence of the geometrical parameters on the force-displacement relationship, a design of experiment is proposed through FE analysis. The relatively high number of parameters induces a significant computation time for this numerical analysis. Thus, before the analysis of the parameters, a simplification is proposed in order to reduce them. Finally, a prototype is designed and its characteristics, obtained through measurements, are compared to FE results.

3.1 Negative biasing element

In the previous chapter, the specific energy density has been defined and studied with a standard loading solution, i.e. constant force. Moreover, the pre-stretch in the opposite direction of the deformation has also been discussed. In this chapter, the negative biasing element is introduced, and the pre-stretch is not considered. In the nominal stress (T_n) and stretch (λ_1) representation, the ideal negative stiffness spring, characterised through the equation of a line, is represented in Fig.3.1. Two different negative characteristics (s_1 and s_2) are presented with the specific energy density for one of them (enclosed area). It is easily understandable that with such a load, better performance in terms of displacement could be obtained compared to constant load or positive stiffness spring. It could be explained by the fact that the slope of the characteristic of the membrane and the one of the load have the same sign (monotonically increase).

Influence of the slope

This specific biasing element is characterised through a slope and its intercept. Thus, their influences will be analysed. For the same slope, the intercept could be varied in order to shift downward or upward the linear characteristic. The corresponding intercept is defined as the *initial* T_n . This stress is equivalent to a pre-load of the elastomer (non-activated).

A large variety of possible characteristics exists for this biasing element. In this section, three interesting results of the various characteristics have been studied (Fig.3.2a to Fig.3.2c). The first one consists in a case where the energy density is higher than the one observed with positive or constant biasing elements. The second one is a case where the stretch has been increased even if the energy density has not been improved in the same proportion. The last case is a special one where better performance has been reached. However, some problems are highlighted for specific T_n .

The first two cases show that the maximum energy density is around $0.03 - 0.04 \text{ J} \cdot \text{cm}^{-3}$.

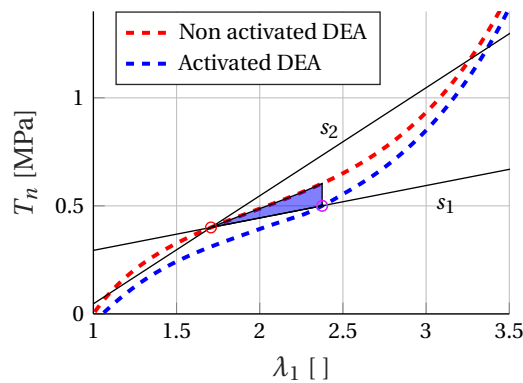


Figure 3.1 – Characteristic of the "0D" model of Elastosil® film with two different negative stiffness biasing elements

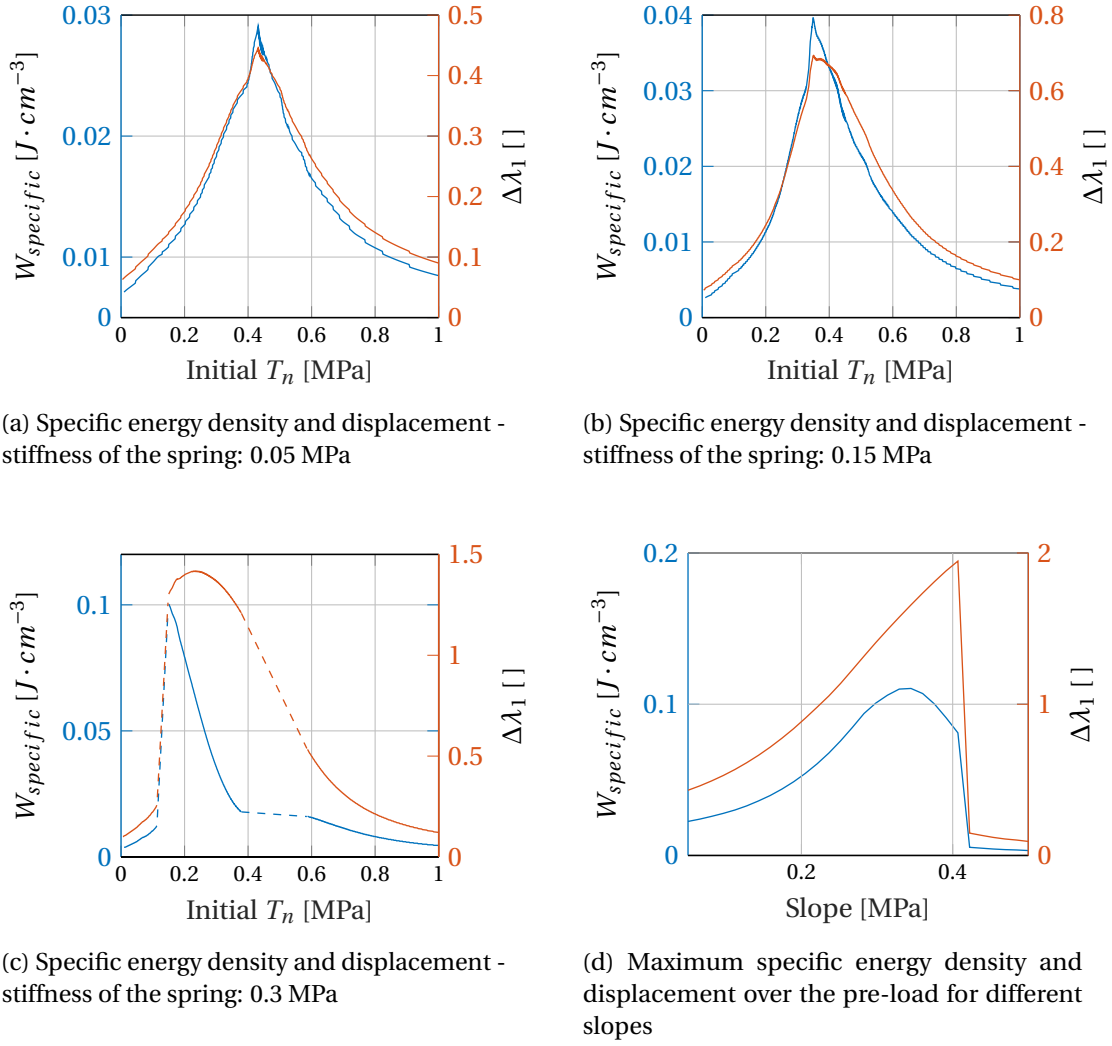


Figure 3.2 – Performance of Elastosil® film with the influence of negative biasing elements

These values are higher than the one obtained in the previous chapter without pre-stretch. Concerning the case in Fig.3.2b, the per cent of the increase of the energy density is not as high as expected compare to the stretch improvement. It is difficult to find an explication to this phenomenon due to the high number of parameters. The particular stress characteristic, with or without voltage, of the elastomer could be seen as a possible reason. By studying the stress characteristic (Fig.3.1) and the smaller slope (s_1) which induces the working of the actuator in the flatter region of the characteristic, an explanation could be provided. It could be imagined that for another negative line which passes through the same lower position ($\lambda_1 = 1.7$) but with a bigger slope, the stretch is increased quite fast. However, the area enclosed by the loop (specific energy density) does not necessarily increase as fast.

For the slopes 0.05 MPa and 0.15 MPa, the maximum stretch corresponds to the maximum energy density. In this sense, the idea to increase the stretch in order to reach the maximum energy density is validated.

For the results in Fig.3.2c, this conclusion is no more verified. It exists a configuration for which the optimal displacement does not correspond to the optimal energy density. The explanation is similar to the one of the case with the slope of 0.15 MPa and the fact that the per cent of energy density does not grow as fast as the stretch. Moreover, energy densities around $0.1 \text{ J} \cdot \text{cm}^{-3}$ seems reachable.

The solutions given by the dashed lines represent "non-reachable" ones. This zone has been considered non-reachable because of the uncertainty of the stable position. The characteristics of the negative load cross several times the polymer stress characteristic, which implies several stable positions (e.g. s_2 in Fig.3.1). Thus, it is challenging to predict in which one the system will exist. Moreover, the system could pass quite easily from one state to another one because of tiny perturbations.

According to the previously studied case, it should be noticed that the wish to work near the optimal energy density (initial T_n around 0.1 MPa) is sensitive to small perturbations. Indeed, if the actuator is designed to work right at this maximum energy density, a small perturbation could balance the performance to a much lower one (e.g. from $0.1 \text{ J} \cdot \text{cm}^{-3}$ to $0.01 \text{ J} \cdot \text{cm}^{-3}$). While, if the two first cases are considered, a small perturbation will change the performance but just around the optimal solution.

In comparison with the constant load, better performances are reachable with the negative biasing element. In chapter 2, an important conclusion was about the smooth region of the characteristic of the elastomer. By tuning the initial pre-load, better performances are reached if the pre-stretch allows working in this specific region. Through a negative biasing element, this region of the characteristic is amplified due to the similar sign of the slopes of the elastomer and the biasing element. It confirms that better results are reached with this kind of element.

Optimal performances

In order to study the optimal solutions, it has been chosen to track the optimal value of the energy density over the different initial T_n , for a given slope. This process has been performed for different slopes. The results are provided in Fig.3.2d. A maximum energy density of around $0.12 \text{ J} \cdot \text{cm}^{-3}$ could be reached. This solution does not correspond to the maximum stretch. The reason is the same than previously provided for the case 0.15 MPa . Concerning the stretch of the elastomer, 200% is reachable with the adequate slope. Once again, it seems that the stretch could be increased faster than the energy density with this biasing element.

This solution of the biasing element has been used for a long time in order to increase the stretch of DEAs. Here, the fact that the energy density is improved through such load is demonstrated for the first time. Moreover, with this kind of characteristic, it is shown that reaching an optimal stretch does not necessarily correspond to track the maximum energy density of the DEA. Finally, for the studied Elastosil® film, the negative biasing element allows reaching more than twice the energy density obtained with constant load with a pre-stretch

which makes interesting such element.

3.2 Design of the spring

3.2.1 Geometrical specifications

The objective in this section is to propose the design of a particular spring with a negative characteristic which allows improving the performance of a cylindrical DEA by increasing the energy density and the stretch of the actuator.

The elastomer is rolled around the initially pre-compressed spring. Releasing the spring pre-loads the DEA reaching the initial T_n previously studied and thus the first stable position.

Arch-shape beam

One problem met by authors [78], [76] who have used negative biasing elements, is the bistability of the spring. These springs are built with pre-compressed beams which confer two mechanically stable positions when deformed by its center. The anchorings of the beam are equivalent to pivots which allow such displacements. The in-between positions are unstable or metastable. The last definition represents an unstable equilibrium point (local maximum) in the mechanical energy characteristic. According to this characteristic, when the center of the beam, which is displaced, passes through the metastable equilibrium point, the beam jumps to its second stable position (by considering the center of the beam pushed and not hold). If the limiting metastable position is not overpassed and the center of the beam is released, this component stabilises in its first stable state.

Hodgins [79] has proposed to add a mechanical stop in order to prevent the mechanism from jumping from one stable position to the other one when the metastable position is passed. Through such improvement, the negative characteristic of the bistable beam is usable. Later, he has added a linear spring for which the stiffness is tuned in order to make the system (*bistable beam + spring*) stable when controlled in position by removing the two mechanically stable positions.

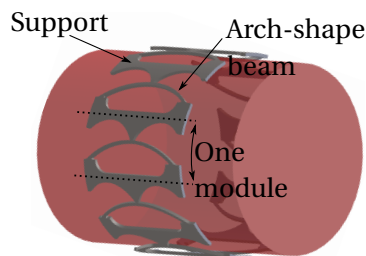


Figure 3.3 – Design of the radial cylindrical spring

Design of the spring

The proposed solution is inspired by medical stents where the design consists of a cylindrical spring with two stable mechanical positions. Once the stent is placed in the aorta, the expanded position is reached, and it stays in this shape in order to keep open the artery which was previously obstructed.

Instead of using a pre-compressed beam such as the one presented by Hodgins [79], the solution is to use an arch-shape beam (Fig.3.3). This initial shape confers a unique mechanical stable position of the mechanism when deformed by its center. However, particular attention should be drawn to the ratio *height of the beam / thickness of the beam*. Indeed, in the domain of MEMS, Qui [80] has observed that the negative characteristic could be removed according to the choice of these parameters.

The proposed design is given in Fig.3.3. Every module are composed of an arch-shape beam and one unalterable support. The role of the support is to be in contact with the elastomer and to deform it radially. The design has a configuration such that the radial displacement of each module leads to a deformation of the beam in a pseudo tangential direction.

Definition of geometrical parameters

All the spring contains a high number of parameters defined in Table 3.1 and in Fig.3.4a. The thickness of the cylinder ($t_{cyl.}$) also defines the width of both the beam and the module. The number of modules ($N_{segm.}$) should be defined according to the geometry of the beam to guaranty the spring to create a full cylinder (360°).

In order to validate the radial force characteristic, a FE analysis is performed. In Fig.3.4, one undeformed module is represented. By moving each supports of the spring radially, the beam reaches a shape such as in Fig.3.4b. Fig.3.4c gives the normalized radial force in function of the normalized radial deformation. This characteristic demonstrates the presence of the negative characteristic along a certain range of deformation, as expected.

Parameter	Definition
h_{NSS}	Height of the beam
t_{beam}	Thickness of the beam
L_{NSS}	Length between feet (see Fig.3.4)
$t_{cyl.}$	Thickness of the cylinder
D_{int}	Internal diameter of the cylinder ($2 \cdot r_{int}$)
$N_{segm.}$	Number of modules
α_{beam}	Angle of the beam
α_m	Angle of the module ($\frac{2\pi}{N_{segm.}}$)
$\alpha_{supp.,low}, \alpha_{supp.,up}$	Angle of the lower and upper support ($\frac{1}{2}(\alpha_m - \alpha_{beam})$)

Table 3.1 – Definition of the geometrical parameters

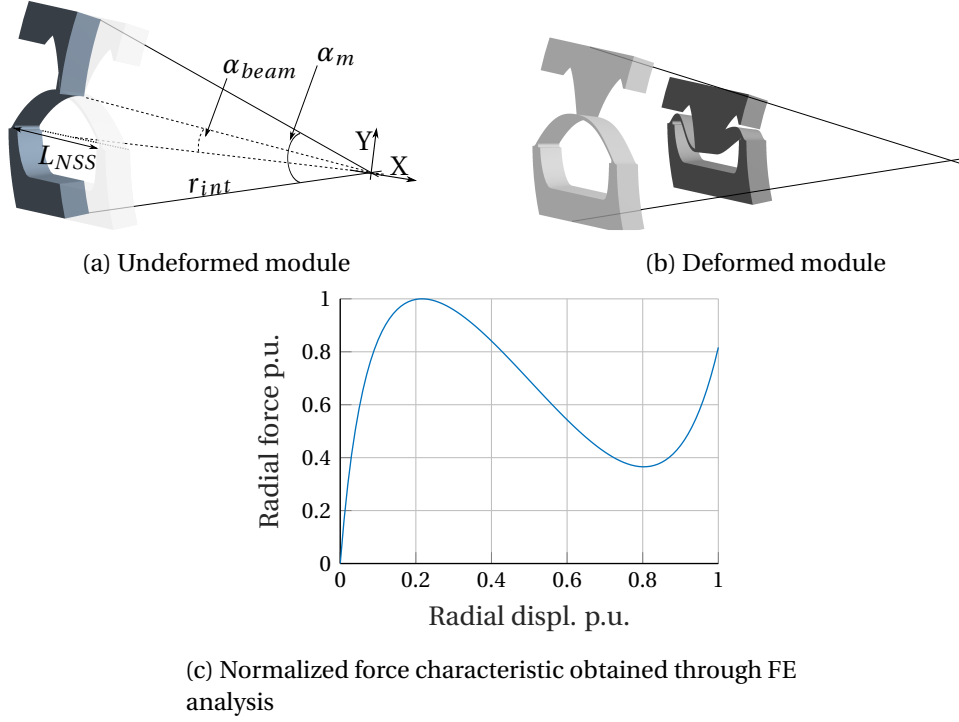


Figure 3.4 – Single module of the proposed spring and radial characteristic

Mechanical mode of deformation

In the domain of the bistable beams, one major problem raised in literature [81], [82] concerns the symmetric (M-shape) and the anti-symmetric (S-shape) shapes of deformation which consists in the two first elastic buckling mode of instability. Indeed, when a beam is displaced by its center, the deformation generally implies two shapes. The first one is the symmetric (first buckling mode). However, a small perturbation or default (e.g. due to the fabrication process) of the beam implies to be deformed with an anti-symmetric shape (second buckling mode) where the center of the beam rotates during the deformation. The force characteristic is then different and much more difficult to predict. In order to avoid such problem, authors have used two beams in parallel which prevents from the rotation and which imposes the symmetric mode to appear during the deformation. For this reason, the same trick is used for the proposed cylindrical spring. By placing the two beams as close as possible, the behaviour of the force characteristic is not changed, only the amplitude varies of a factor near two. For this reason, the studied design in the following sections consists of the one with a single beam and with the hypothesis of a symmetrical deformation.

3.2.2 Radial displacement and force relationship

As presented in the previous section, the study of the characteristic of the proposed spring is difficult due to the high number of geometrical parameters.

The analytical model of such spring is complex. Some studies of planar arch-beam, such as Beharic [83], have been done in order to propose a model of the force characteristic. However, even considering a planar configuration with few geometrical parameters, only numerical results with complex strategy of resolution (zero-tracking) is proposed. This solution is heavy in terms of computation time and the problem is difficult to define with the adequate assumptions.

Moreover, the FE analysis allows to provide the necessary information but the time of simulation is long and not easily repeatable for different geometries. Indeed, even for the same beam but different number of modules, the simulation should be run several times.

In order to decrease the computational time through FE analysis, a solution to reduce the number of parameters is proposed. The FE analysis could be then done more rapidly.

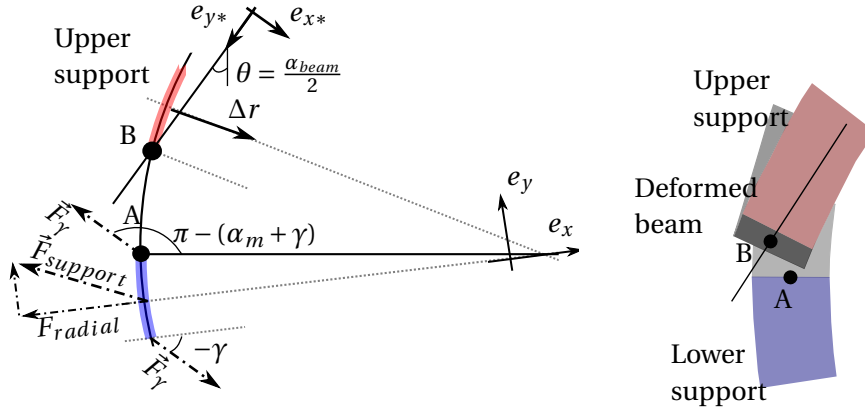
Radial deformation

The first considered parameter is the radial displacement of the module. The easiest solution, in order to decrease the time of numerical computation, is to simulate only one module (Fig.3.4). This solution decreases the number of elements in the FE analysis.

Let's consider this module with its upper (red) and lower (blue) supports (Fig.3.5a). These supports are displaced radially along a straight line over a distance defined by Δr and equivalent to the one presented in Fig.3.4b. An interesting observation concerns the displacement of the two points A and B . Indeed, by considering the displacement of these two points, it could be demonstrated that the upper point (B) moves, according to the lower point (A), along a straight line defined by:

$$y_B = \cot\left(\frac{\alpha_{beam}}{2}\right) \cdot x_\Theta + r_{int} \cdot (\sin(1) - \sin(\alpha_{beam})) \quad (3.1)$$

where x_Θ is the displacement along the line in the referential (e_{x*}, e_{y*}) . This means that the upper support moves, according to the lower support, along a straight line defined by $\theta = \alpha_{beam}/2$ (Fig.3.5a). This result is true if the arc length of the lower and upper supports $(\alpha_{supp.,low}, \alpha_{supp.,up})$ are equal which consists of the only assumption of the proposed development.



(a) Equivalent displacement along the straight line defined by θ . The upper support is used to highlight the radial displacement and the lower one for the forces.

(b) Side view of the radially deformed beam with its upper and lower supports

Figure 3.5 – Equivalent deformation of a module and its parameters

The radial displacement of each supports is linked to the equivalent displacement on the straight line (e_{x*}) (or vice versa) through:

$$\Delta r = \frac{1}{2 \sin\left(\frac{\alpha_m}{2}\right)} x_\theta \quad (3.2)$$

This equation, combined to the definition of α_m , shows that according to the angle of the module, a small displacement along the straight line induces a bigger one in the radial direction if the number of modules is higher than six. Generally, the stress of the deformation of a beam is a limiting factor. With such a solution, the radial deformation could be higher before reaching the yield strength of the beam.

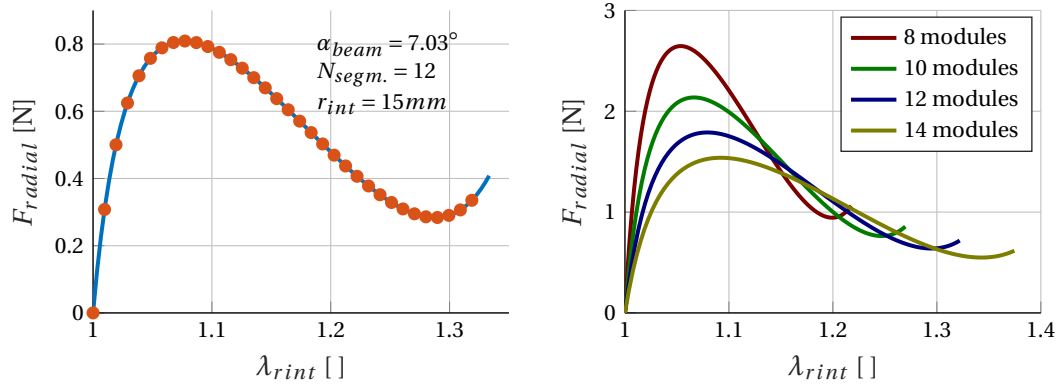
Amplitude of the force

Now that the relationship between the radial displacement and the one along an equivalent straight line dependent only on the angle of the beam is done, the force is analysed.

When the two supports are displaced radially, each of them provides a reaction force $\vec{F}_{support}$ composed of two components, the radial (F_{radial}) and the tangential one ($F_{tang.}$). Concerning the beam, the upper part (B) sees a force \vec{F}_γ (in the provided schematic, the presented one is for the beam placed before this module) with an angle γ according to the radial displacement. The lower part (A) sees the same amplitude of the force with a different direction which could be linked to γ through the geometry.

The force of the support is linked to the one of the beam through:

$$\vec{F}_{support} = F_\gamma \cdot ((\cos(\gamma) - \cos(\alpha_m + \gamma))e_x + (\sin(-\gamma) + \sin(\alpha_m + \gamma))e_y) \quad (3.3)$$



(a) Validation of the radial force relationship. Beam geometry: $t_{beam} = 150 \mu m$, $h_{NSS} = 1.85 mm$ and $L_{NSS} = 20 mm$, $t_{cyl.} = 1.5 mm$

(b) Force vs radial strain for different angle of support and the same arch-beam

Figure 3.6 – Force characteristic of the special spring

Then, a study of the sum of the forces on the supports (lower and upper) in the referential (e_{x*}, e_{y*}) and by highlighting the radial component along e_{x*} from Eq.3.3, the following relationship is obtained:

$$F_{radial} = 2 \sin\left(\frac{\alpha_m}{2}\right) \cdot F_\theta e_{x*} \quad (3.4)$$

Therefore, it is possible to link the force obtained along the e_{x*} -axis, by displacing the point B along this axis, with the equivalent radial force of the system.

The development of the previous relationship between the radial displacement and the force with the deformation of a single beam could be found in [84] .

Validation and discussion

The relationship which links the radial displacement and the radial force to the one along a straight line defined by the θ -angle (Eq.3.5a and Eq.3.4) demonstrates the possibility to simulate one module without considering the support. Then, it is possible to predict the two equivalent considered radial characteristics by defining the number of modules in post-processing. Indeed, only the geometry of the beam is necessary to obtain F_θ and x_θ .

In Fig.3.6a, the previous results are proven through FE simulations. The beam given through the parameters in Fig.3.6a was deformed along a straight line define by $\theta = \alpha_{beam}/2$. The FE analysis provides the relationship between the displacement x_θ and the reaction force F_θ .

In Fig.3.6a, the full line corresponds to the results obtained for all the spring where the supports have been moved radially, and the dots are the one obtains through the previously presented process. The error is less than 0.5%.

Chapter 3. Cylindrical negative biasing system

From the force F_θ obtained via FE analysis, by the help of Eq.3.2 and Eq.3.4, the radial force characteristic is easily determinable with post-processing for a large number of modules. For example, if this force is analysed for the previously simulated beam, the results of the force characteristic in the radial direction for different number of modules are given in Fig.3.6b. By increasing the number of modules, the width of the negative slope is increased. However, it affects also the amplitude of the radial force which decreases.

Through an optimisation process and according to the characteristic of the elastomer, with the same geometry of the beam, the number of modules could be adapted in order to either create more displacement or more force. It should be noticed that it exists a maximum number of supports in order not to overpass 360° of the circumference. Moreover, according to the targeted rigidity of the support, they should be well designed. Indeed, the support should be more rigid than the beam in order to deform it and not the part in contact with the elastomer.

3.3 Influence of geometrical parameters

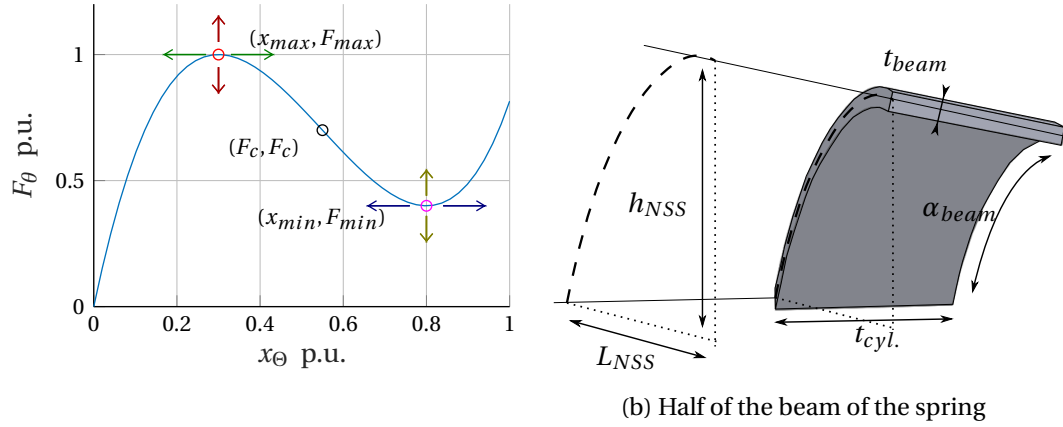
As previously mentioned, the study of the planar bistable beams is a large and complex domain in mechanic, and an analytical model is difficult to obtain. Contrary to the one proposed by Beharic [83] based on the numerical resolution of the complex system of equations, another solution to obtain a model based on the influence of the parameters, such as the geometrical ones, is the design of experiment (DOE). To perform the DOE, a certain number of experiments should be run in a predetermined domain of validity.

In the studied case, the objective is first to analyse the influence of the geometrical parameters (inputs) on the force-displacement characteristic (Fig.3.7a). It is too heavy to analyse all the points of the curvature. Thus, four output points are highlighted: (x_{max}, F_{max}) and (x_{min}, F_{min}) .

Thanks to the previously defined relationship between the radial spring and a single beam, only this single beam is analysed through the proposed DOE. Five geometrical parameters (inputs) are highlighted which correspond to the ones useful after the proposed simplification (Eq.3.2 - Eq.3.4). In Fig.3.7b, the half of a single beam is presented with the studied parameters. The height of the equivalent beam is given through $r_{int} \cdot \alpha_{beam}$, and it is used instead of the

Factor	Parameter	Unit	Min	Max
Height of the beam (h_{NSS})	X_1	[mm]	1	2
Thickness of the beam (t_{beam})	X_2	[mm]	0.1	0.2
Length between feet (half) (L_{NSS})	X_3	[mm]	10	20
Thickness of the cylinder ($t_{cyl.}$)	X_4	[mm]	1	2
Diameter of the cylinder (D_{int})	X_5	[mm]	20	35

Table 3.2 – Matrix of experiments



(a) Force characteristic of the radial negative stiffness spring with specific points

(b) Half of the beam of the spring

Figure 3.7 – Definition of the inputs and outputs parameters for the DOE

internal radius and the angle of the beam in order to further reduce the number of geometrical parameters.

The model used to make this DOE is the Doehlert one. The objective is to analyse different combinations of the input parameters (X_i) in order to study the influence between them. For a five-element model, 31 experiments should be performed (appendix B). In this case, FE analysis is used to provide the experiments. The boundaries for the geometrical parameters are provided in Table 3.2 which have been defined according to the feasibility of the manufacturing process.

Different models exist to link one output response to the input parameters. In this study, three models are analysed. The linear model is firstly defined. Then, a linear model with interaction is used. Finally, the quadratic model which links the two previous one with the quadratic influence of each input parameters is investigated and are defined in appendix B (Eq.B.1-Eq.B.3). In order to validate the model, 200 other beams have been simulated. These beams have been designed randomly in the boundaries. Then, the errors between the results obtained through the models and the results of the FE are computed in order to validate or not the models.

3.3.1 Displacement characteristic

The two positions of the local optima (x_{max} , x_{min}) are firstly studied (Fig.3.7a). The results of the DOE for these parameters and the three models are given in appendix B. In Fig.3.8 only the results for the linear model are provided.

For these two parameters and the three models, only one geometrical input influences the position (x_{max} , x_{min}), i.e. the initial height of the beam ($r_{int} \cdot \alpha_{beam}$). It means that the interaction effects between the geometrical parameters (a_{ij}) and the quadratic effects (a_{ii})

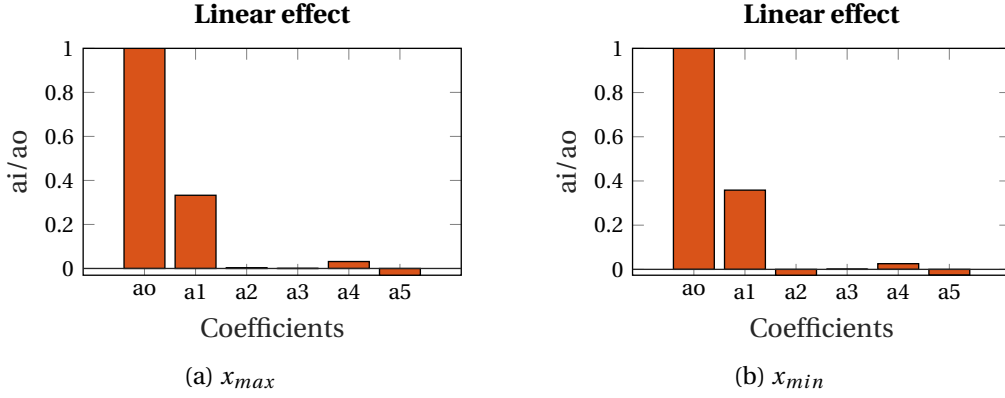


Figure 3.8 – Results for linear model for x_{max} and x_{min} .

does not influence the position x_{max} and x_{min} . Thus, the two positions could be estimated through a linear model:

$$X_{\theta, x_{max}} = 0.33 \cdot 10^{-3} \cdot h_{NSS} + 1.47 \cdot 10^{-5} \quad (3.5)$$

and

$$X_{\theta, x_{min}} = 0.00135 \cdot h_{NSS} - 1.46 \cdot 10^{-4} \quad (3.6)$$

The proposed models (Eq.3.5 and Eq.3.6) are applied to estimate the position of the optima for 200 beams used as validation. The errors of the proposed models for the 200 tests are lower than 7% for x_{max} and lower than 5% for x_{min} . It means that the two previous equations could be used to predict x_{max} and x_{min} if the equivalent height of the beam is confined within the boundaries (Table 3.2).

3.3.2 Force characteristic

In the case of the amplitude of the force at the local maximum and minimum, the conclusion is not as evident as for the positions. In Fig.3.9, only the coefficients for the quadratic model are provided. Indeed, they allow having an overview of the influence of the parameters and the interactions.

The main parameters which influence these forces are the thickness of the beam (a_2, a_{22}), the length between the feet (a_3, a_{33}) and the thickness of the cylinder (a_4). Moreover, the interaction between the length of the extremities of the beam (length of the feet) and respectively the thickness of the beam (a_{23}) or the thickness of the cylinder (a_{34}) are also important. A negative parameter (a_i) means that it should be subtracted in the model.

However, none of the models is useful in this situation. Over the 200 tested beams, the linear and the linear with interaction models predict forces with an error nearly 50% for 85% of the tested beams. Concerning the quadratic model, the model provides an error of less than 25%

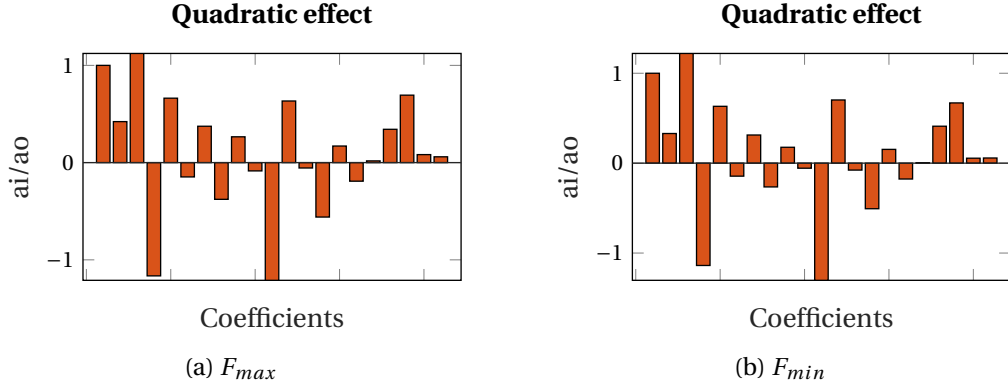


Figure 3.9 – Results for the quadratic model for F_{max} and F_{min} . The labels of the coefficients are not provided, the first one being a_0 and so one.

for 95% of the tested beams. Thus, no model is proposed for the amplitude of the forces, only the influences of the parameters are considered here.

One possible reason for the difficulty to predict the amplitude of the forces consists of the choice of the geometrical parameters to perform the design of experiment. Indeed, other definitions, like the ratio between two parameters, could be studied.

Without providing any models, Qiu [80] has observed for bistable beams that the ratio h_{NSS}/t_{beam} influences a lot the amplitude and the characteristic of the force. He has demonstrated that above a particular value, the beam becomes monostable. Here, it has also been observed that this ratio influences the amplitude of the force. Concerning the proposed geometry and for specific values of the ratio, the monostability is guaranteed, but the negative region of the characteristic could be lost. However, the geometrical parameters used for the design experiment have been chosen to avoid such issue.

3.4 Characterisation of the spring

In this section, a prototype is presented. The fabrication process is explained which allows understanding the boundaries fixed in the design of experiment. Finally, through a test bench, the force characteristic of the prototype is compared to the results obtained via FE analysis.

3.4.1 Fabrication of the prototype

Prototype

The chosen material for the prototype consists of titanium grade 5, contrary to the standard used material, the stainless steel. The titanium is characterised through a Young's modulus of 114 GPa and a yield strength of 795 MPa [85]. This material has two main advantages; the first one is the high yield strength limit. Moreover, this metal is biocompatible and already

used in the medical domain.

In order to build this spring, several ways have been studied. Due to the emergence of the 3D printing tools and the possibility to print metals, such technic was promising. However, the sintering metal powder has much lower yield strength than uniform material. Thus, a conventional method has been used. Indeed, the CNC machining was chosen with a 5-axis machining. Due to the limiting size of the drill wick, all the dimensions are not possible. The smallest available diameter of the tool is 0.5 mm .

The spring has been cut in a solid cylinder with the CNC over a depth bigger than the defined thickness $t_{cyl.}$, i.e. 1.55 mm . The CNC is not able to machine a depth of more than 2 mm . Moreover, the maximum length of the tube is around 60 mm which limits once again the final geometry.

When the shape of the beams and the supports are cut, the spring was free with an electrical discharge machining by removing the center of the cylinder. The final prototype is presented in Fig.3.10.

The geometrical parameters of the prototype are the same than presented in Fig.3.6a, as a recall: $t_{beam} = 150\text{ }\mu\text{m}$, $h_{NSS} = 1.85\text{ mm}$, $L_{NSS} = 20\text{ mm}$ and $t_{cyl.} = 1.5\text{ mm}$. Because for the prototype the double beams have been manufactured, the distance between both should be defined. In this case, 0.55 mm was chosen. It consists in the dimension of the drill wick with a small gap ($50\text{ }\mu\text{m}$). For the tolerances, none have been fixed. It was the first geometry with such configuration manufactured by the company. Thus, only testing prototypes were built in order to understand the feasibility of such geometry.

3.4.2 Measure of the spring

Test bench

A test bench (Fig.3.11a) has been used in order to measure the force characteristic of the spring which is placed at the center of the measuring tool. This test bench is constituted of the same

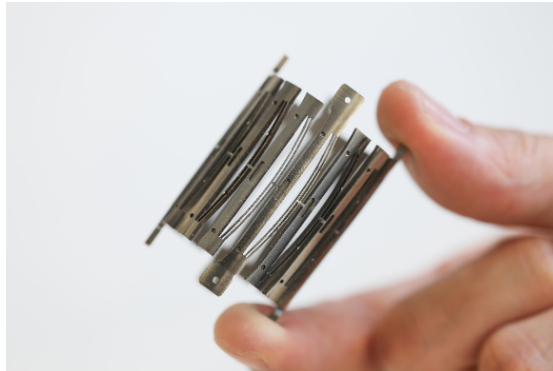
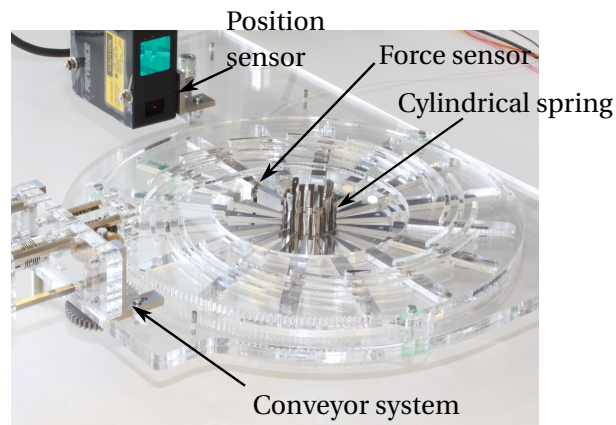
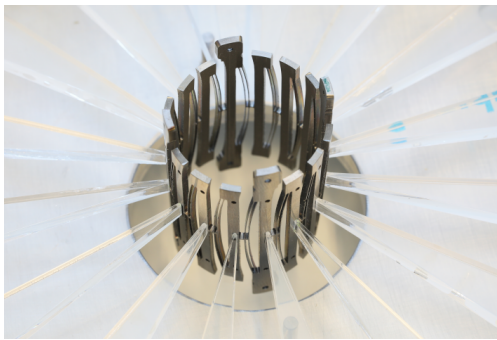


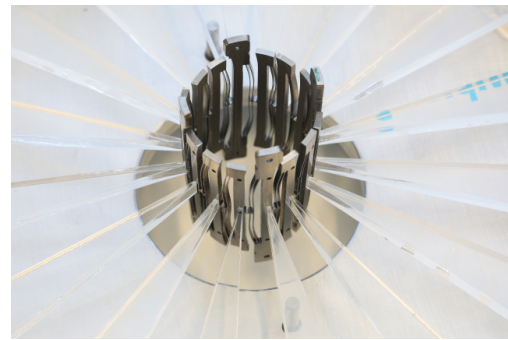
Figure 3.10 – Prototype of the negative stiffness cylindrical spring



(a) Global view of the system including the spring



(b) Non-deformed spring



(c) Deformed spring

Figure 3.11 – Test bench for measuring the force-displacement characteristic of the proposed cylindrical spring

number of "fingers" than the number of supports (sixteen in this case). These fingers push all the supports radially. In one of these part, a force sensor has been placed in order to obtain this radial information. A displacement sensor (laser) is used to measure the radial position of the spring. A conveyor system has been used in order to do the measurement automatically. A non-deformed state is presented in Fig.3.11b and a deformed one is shown in Fig.3.11c for which the specific M-shape of the deformed arch-beam is highlighted.

Force characteristic

Through the test bench, the measure of the force characteristic of the prototype is done and is compared to the one of the FE analysis (Fig.3.12a). In this figure, two measures are provided where the difference comes from the manipulation. The spring has been placed, removed and turned several times. The results are not repeatable. More than two measurements have been performed. However, two radial forces from measurements are provided in Fig.3.12a, the only difference between these two results is the assembly and the manipulation of the spring. The position of the local maximum and minimum (dashed vertical black lines) is provided through the proposed model (Eq.3.5 and Eq.3.6).

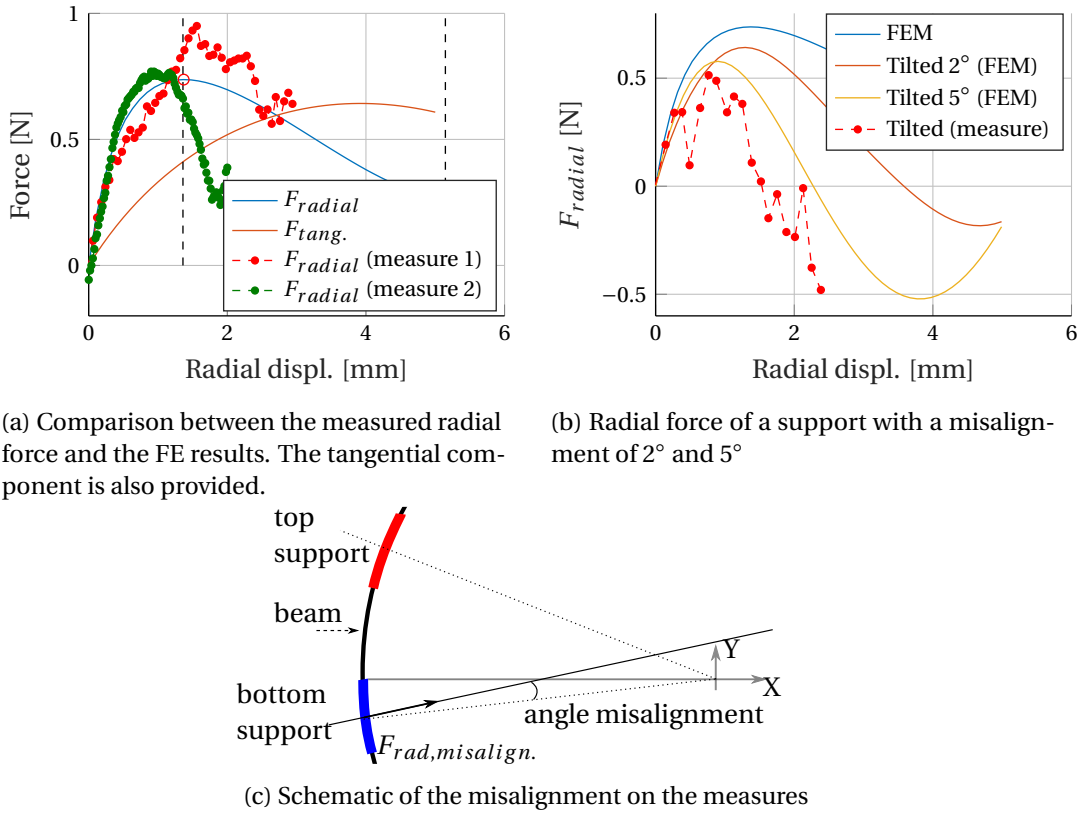


Figure 3.12 – Measurements on the prototype

First, for this specific design, the previous model of the local optima provides an error of around 2% compared to the FE results.

Concerning the first measurement (measure 1 in Fig.3.12a), the location of the local maximum seems close to the model (difference of 3%). The amplitude is not so far as well with 13% of difference. The slope becomes negative which confirms the presence of this characteristic in the prototype and the value is nearly the FE result (5% of difference).

For the second measurement (green), the result is close in terms of position but much less for the amplitude than the simulation (respectively 2% and 22%). The negative slope of the prototype with this measure is too big compared to the one of FEM with a factor four.

It was challenging to measure the radial component of the force. The tangential one (Fig.3.12a) being significant (same order of magnitude than the radial component), the fact to push the supports does not allow to prevent from the rotation. Thus, the test bench has been improved in order to prevent from this rotation. However, it was still tricky and out of the expected range.

Moreover, a small angle of misalignment between the displacement of the finger and the one of the support induces a different radial force characteristic ($F_{rad,misalign.}$ in Fig.3.12c). In the example in Fig.3.12b, the results for a simulated beam with a direction of deformation tilted

with an angle of 2° and 5° are given. These angles correspond respectively to a direction of displacement shifted of $500\ \mu m$ and $1.3\ mm$ (upward or downward) from the center (Fig.3.12c). The results of a measurement which seems to be deformed with an angle shows the apparition of negative force as predicted by the simulation. According to the results obtained with FE analysis, the tilted angle for the measure seems to be near 5° .

Finally, the measured thicknesses of the different beams of the prototype are between $120\ \mu m$ and $180\ \mu m$. A thickness of $150\ \mu m$ has been chosen for the simulation.

Thus, all these observations could explain the difficulty to obtain repeatable measurements and the associated errors.

3.5 Conclusion

Due to the improvement of the energy density and stretch studied with the negative biasing elements and because of the particular considered geometry of actuator, a special cylindrical spring has been designed with such characteristic. This spring with the special force characteristic has been protected through a patent.

The full model is complex and not provided. However, a solution to reduce the computational time through FE analysis of the spring is proposed. It is difficult to estimate the time won through the proposed simplification because the simulation of a beam allows providing information for an infinite number of modules (different number of modules for the same beam). The influence of the geometrical parameters has been performed for the force (two optima) through a design of experiment. Concerning the positions of two important states (local maximum and minimum), a simple model is given with a prediction error of these parameters of less than 7%. Through the understanding of these four parameters, it is easier to optimise any radial actuator which combines this spring with a cylindrical DEA.

Even if the measurements of the force characteristic of the spring are not ideal, the FE analysis provides a good estimation. In the following chapter, the radial spring is merged with a tubular DEA in order to create an actuator. Through the variation of the voltage, the deformation will be studied.

4 Tubular DEA

The developed cylindrical spring with the negative force characteristic presented in the previous chapter was designed in order to increase the performance of a cylindrical DEA. In this chapter, a system composed of a tubular DEA coupled to the aforementioned spring is proposed in order to create an actuator. The objective is to determine the displacement characteristic according to the applied voltage. Two thicknesses of membrane have been used in order to create the actuator.

An analytical model of the actuator and a FE analysis with different boundary conditions are proposed and analysed. The measurements of the prototype allow explaining the models. The study of the deformation of the actuator highlights a phenomenon similar to the one observed with the planar DEA (chapter 2) where the film could be split into two parts (inhomogeneity) in order to reach intrinsic stability. Due to this phenomenon, the deformation of the actuator is not necessary symmetric because all the arch-shape beams are not deformed in the same way. This particularity is also analysed.

4.1 Simplified Model of a cylindrical DEA

Before studying the prototype of the membrane mixed to the special spring, a model of the membrane radially deformed is proposed. The particularity of this model of the elastomer takes into account the interaction between the negative stiffness spring and the DEA. Indeed, the design of the proposed spring, which is inserted inside the tube, implies that the elastomer is not uniformly radially stretched. The configuration is such that the arc shape elastomer is deformed as a planar film which is elongated between two consecutive supports, located on the longitudinal edge of the membrane (Fig.4.1).

Fig.4.1 highlights how half of a circular arc ($s_{0,1/2}$) is deformed ($s_{1/2}$) when its left and right supports are displaced radially. An assumption is made according to the particularity of the circular arc. The length over the width ratio is supposed large enough (greater than 10) to use the pure-shear configuration and allows considering no stretch in the length direction, i.e. L_0 constant.

The radial force applied to the extremities is given by $F_{m,i}$. When the longitudinal edges of the film are radially moved with Δr , the equivalent reaction force in the radial direction ($F_{rad.}$) is given by:

$$F_{rad.} = F_{m,i}(\lambda_s) \cdot 2 \sin\left(\frac{\alpha_m}{2}\right) \quad (4.1)$$

where the equivalent force of planar configuration is dependent on the planar elongation (λ_s) of the elastomer. The force $F_{m,i}$ is provided by the Cauchy stress tensor (appendix C) and is equivalent to the well-known form established for planar DEA:

$$F_{m,i}(\lambda_s) = \frac{L_0 t_0}{\lambda_s} (2\lambda_s^2 - 2\lambda_s^{-2})(C_{10} + 2C_{20}(\lambda_s^2 + \lambda_s^{-2} - 2) + 3C_{30}(\lambda_s^2 + \lambda_s^{-2} - 2)^2) \quad (4.2)$$

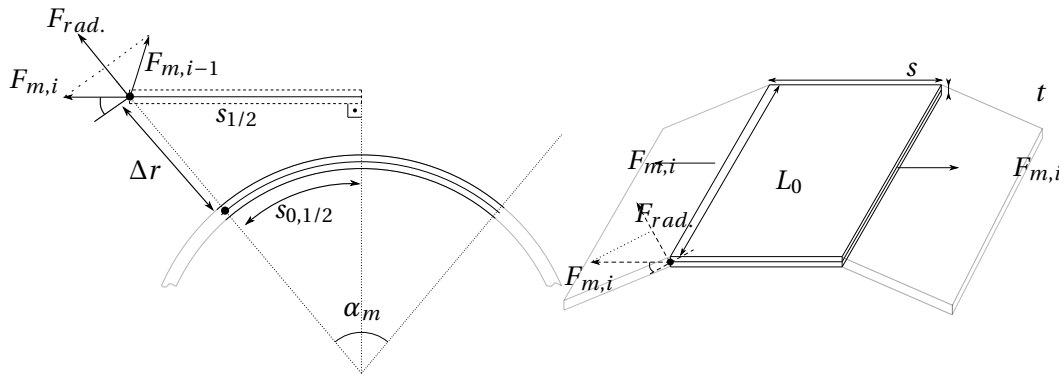


Figure 4.1 – Circular arc and its equivalent deformation in the pure-shear configuration

Concerning the link between the displacement, it could be demonstrated that the linear stretch (λ_s) of the planar membrane (right figure in Fig.4.1) is linked to the radial displacement (λ_r):

$$\lambda_s = \frac{2\sin(\alpha_m/2)}{\alpha_m} \lambda_r \quad (4.3)$$

In appendix C, it has been demonstrated that the radial stretch could be approximated by the planar elongation of the membrane if the number of modules is larger than six which ensures a margin of error lower than 4.5%.

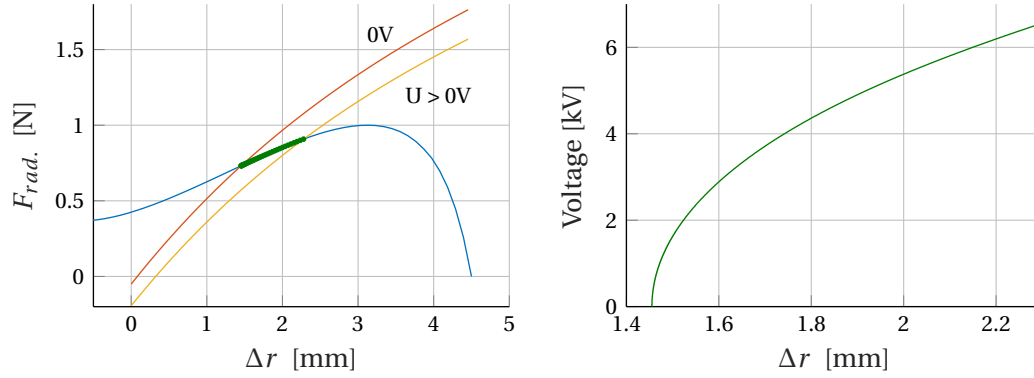
4.2 Actuator with specific cylindrical spring

4.2.1 Prototype

In this section, a prototype of a dielectric elastomer actuator coupled to the previously discussed negative biasing cylindrical spring is proposed. The characteristic presented in Fig.4.2a is considered. It consists of the radial force relationship according to the variation of the internal radius of the cylinder. The considered radial force ($F_{rad.}$) represents the reaction force of the supports in the radial direction. If all the supports move purely radially, this force is the same for all these supports (blue line in Fig.4.2a). Concerning the elastomer, the radial force represents the one given through Eq.4.1 and depends on the activation voltage (red and orange lines in Fig.4.2a and the ones in-between). The intersections of these curves (green dotted lines) allow determining the working positions of the actuator for different supplied voltages. The theoretical radial displacement of the actuator according to the supply voltage is presented in Fig.4.2b. In order to validate the working principle of such an actuator, the *displacement characteristic* is discussed.

The negative stiffness spring used for the actuator is the one presented in chapter 3.4. The design of this spring allows being initially radially pre-compressed of 4.5 mm. The internal diameter of the tubular DEA is imposed (25 mm) by the spring. The length of the tube is chosen to be the same such as the spring, i.e. 50 mm.

Concerning the elastomer, the Elastosil® 2030 film from Wacker is used. According to the different possibilities provided by the manufacturer, a thickness of 100 μm and 200 μm have been investigated. The parameters of the hyperelastic model have been determined by stretching an elastomer with the same geometry than the one of the circular arc (pure-shear configuration) considering the Yeoh model (C_{i0}). In chapter 2, the Mullins effect has been discussed, and it has been shown the importance of the final stretch reached by the membrane in order to determine the parameter of the model. In this case, the elastomer has been stretched 1.5 times with a pure-shear configuration and the following parameters have been obtained: $C_{10} = 0.62 \text{ MPa}$, $C_{20} = -54.4 \text{ mPa}$ and $C_{30} = -3.8 \text{ kPa}$.



(a) Radial force and displacement characteristic

(b) Displacement relationship of the actuator

Figure 4.2 – Working principle of the actuator based on the DEA and the negative stiffness pre-compressed spring

4.2.2 Deformation characteristic

The test bench used to obtain the deformation characteristic of the actuator according to the supply voltage is presented in Fig.4.3a. The DEA consists of a membrane rolled around the compressed spring (Fig.4.3a). Four out of sixteen titanium supports are extended (*A*, *B*, *C* and *D*). One of them (*A*) is used to fix the actuator, the others are free. In order to reduce the friction between the membrane and the elastomer, narrow supports of PTFE have been glued on each titanium supports.

The membrane is composed of two parts (*I* and *II*). The first one is active and the second is not. The reason is to let a small part of elastomer without electrode in order to decrease the possibility to have a breakdown between the external electrode (+) and the spring connected to the internal electrode through the air. The length of the activated part (*I*) corresponds to the length of the smaller supports (2,3 and 4). The planar membrane constituted of one electrode on each side with a thickness of around $5 \mu m$, is rolled around the compressed spring. The extremities of the film are glued with a silicone (close to the support *C* in Fig.4.3a). The internal electrode (-) is directly in contact with the metallic spring which is directly used for the electrical connector. The external electrode (+) is connected as shown in the figure.

A ramp of *voltage* is applied to the DEA in one second, then the voltage is maintained during another second and finally decreased with the same time. For the two studied membrane ($100 \mu m$ and $200 \mu m$), the maximum voltage was around $7.5 kV$. Above this value, an electrical breakdown in the air appears between the external electrode and the spring connected to the internal one. This breakdown does not damage the film like the well-known electrical breakdown through the elastomer. Thus, the actuator could be tested again with smaller voltages.

The displacement is measured with a laser sensor on single support (resolution $1 \mu m$). It is complicated to measure the displacement of all the cylinder at the same moment. A system with cameras could reach such an objective. However, the resolution is too low for standard

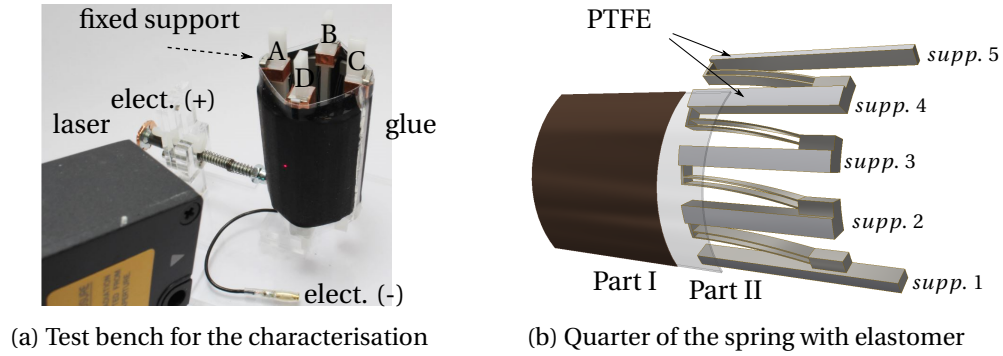


Figure 4.3 – Test bench and schematic for the FE simulation

ones. The measurements of the variation of displacement have been performed by placing the laser in front of one of the three measurements points (*B*, *C* or *D* in Fig.4.3a) in the same axis with its opposite support (e.g. *A* with *C* and *B* with *D*). In order to obtain the variation of displacement according to the voltage in different positions, the process is repeated.

To simulate the prototype in a proper manner where only four supports are bigger than the others (*A*, *B*, *C* and *D* in Fig.4.3a), the solution presented in Fig.4.3b (half of the total length) is simulated through FE analysis. The simulated design is also constituted of a quarter of the spring where the support *supp.1* and *supp.5* are longer.

4.2.3 Results - 200 μm thick membrane

Measurements

The first results concern an elastomer with a thickness of 200 μm . Four prototypes with the same spring but four different membranes have been tested. The measurements have been performed in the position *B* (Fig.4.3a) and the results are given in Fig.4.4a through the green dotted lines. The process seems repeatable due to the similar behaviour of the measurements. However, between the worst cases, a difference of 25% is observed.

In reality, the values given through the green lines correspond to the half of the measured value with the laser. Indeed, it has been observed that the opposite support *D* hardly moved (a few micrometers) due to the unsymmetrical deformation. Thus, the measured values are assumed as half of the radial displacement. Equivalent results are obtained by measuring the displacement in position *C* and by dividing it by a factor two.

Through this observation, it seems that each supports of the spring are not deformed identically.

The previously presented analytical model which does not consider any friction between the elastomer and the spring is given through the light blue line. It predicts a more significant variation of displacement for the same supply voltage compared to the FE results, but it is

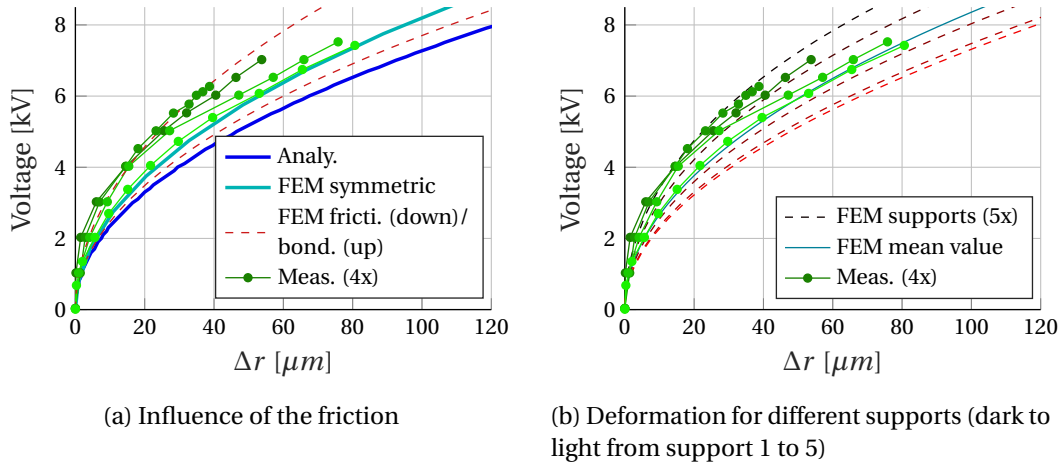


Figure 4.4 – Results for 200 μm thick elastomer

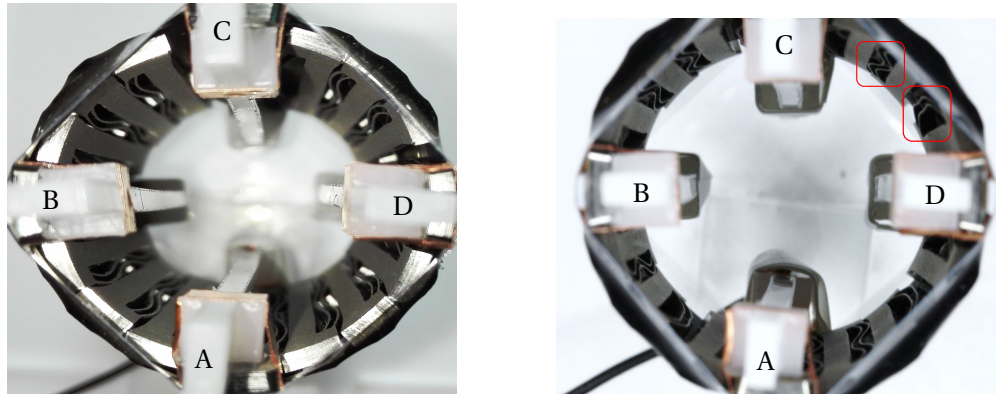
quite close to the frictionless case. The analytical model does not consider the two parts of the elastomer, and all the membrane is considered as active. Thus, more displacement could be reached because of more considered active surface.

Concerning the results obtained via FE analysis, the displacement of each supports have been forced to move purely radially.

It is difficult to estimate the friction between the contact of the membrane and the support (PTFE) of the spring. For this reason, two cases have been simulated with the design presented in Fig.4.3b. The first one is without friction between the elastomer and the supports and the second one when the two elements are considered as glued. These two cases allow delimiting the results (red dashed lines). The upper one corresponds to the case where the elastomer is bonded, and the lower one is for the frictionless case. The characteristic of the glued membrane provides lower displacement because of stiffer behaviour. Moreover, it should be noticed that the stiffness of the membrane is bigger due to the presence of the electrodes (between 5 μm and 10 μm thick). This parameter could also influence the difference between the measurements and the FE results.

Another case for the FE result is provided (FEM symmetric in Fig.4.4a). This case represents a design where the elastomer is composed of the two parts (*I* and *II*), each supports of the modules has the same length than the *supp.1* and *supp.5*, and no friction is considered between the film and the spring. The main advantage is that only one module could be simulated. The result obtained via this case is close to the measurements and is between the more realistic glued and frictionless cases.

From the measurements point of view, the friction difference with or without electrode is easily felt, it seems that the part *I* of the elastomer which is covered with electrode slides more efficiently than the part *II* electrode free. However, it is observed that the obtained measurements belong to the zone delimited through the previously defined cases. Thus, it validates that the effect of the contact is essential in order to obtain realistic FE results.



(a) Initial position of the arch-beams (completely compressed spring)

(b) Different pre-deformed shape of arch beams

Figure 4.5 – Influence of the special deformation of the arch-beam on the results

Concerning the ideal case (symmetric), it predicts well the behaviour of all the actuator. For this case, the main advantage is the computation time, because only one module is simulated.

4.2.4 Stability of the system

Complexity of the displacement

Even if the measured displacements are well defined through the frictionless and bonded cases, some differences between the measurements are observable which could be explained through different origins.

In the section 3.4.2, the analysis of the forces of a beam displaced along a straight line defined by the geometry of the beam which could be characterised through its (F_θ, x_θ) relationship, shows that a tangential component of the reaction force exists. Thus, another situation has been studied through FE analysis. The system presented in Fig.4.3b has been simulated but contrary to the previous cases, the displacement of the *supp.2*, *supp.3* and *supp.4* are not imposed purely radial. The tangential direction is let free. Thus, all the in-between supports are free to move in order to allow the subsystems to reach different states. Moreover, a frictionless contact has been considered between the spring and the silicone (*Part I* and *Part II*).

The radial displacements of all the supports are provided in dashed lines in Fig.4.4b. The displacement for each of them are not similar, an inhomogeneity is observed in the simulation. The blue line corresponds to the mean radial displacement of the elastomer. As for the frictionless and bonded simulation, the measurements are well delimited by these different possibilities of deformation of each beam.

The influence of the tangential force and the friction could explain the fact that not all the beams of the spring are in the same state when the stability between the elastomer and the spring is reached and when no voltage is applied. Moreover, the spring has beams with a random thickness between $130\ \mu m$ and $180\ \mu m$ which could influence the asymmetry. In

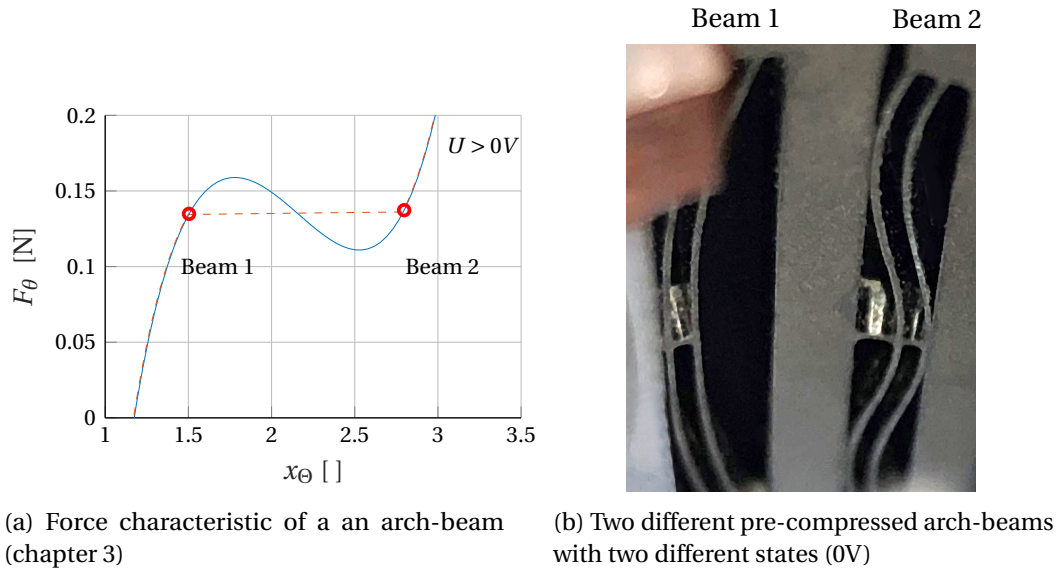


Figure 4.6 – Intrinsic stability of the proposed spring

Fig.4.5a, the actuator is shown when the spring is completely compressed ($\Delta r = 0$). It could be noticed that all the beams are in the same *closed* state (M-shape). When the system is released, the two elements reach an equilibrium position ($\Delta r \neq 0$) such as in Fig.4.5b. In this situation, not all the beams have the same state. Indeed, several of them are already more released than the others (red squares). All these observations could explain that the deformation of the actuator is not symmetric. According to the state of all the beams without voltage, the measurements of the displacement could vary.

Intrinsic stability

The global behaviour of the actuator is challenging to obtain. However, by analysing the characteristic of the spring, an explication could be proposed.

The force-displacement relationship of the spring with the negative stiffness region recalls the behaviour of the elastomer such as the one presented in chapter 2. The elastomer was described as an infinite number of subsystems. The intrinsic stability was introduced to explain the possibility of the system to reach all the *global* position by splitting itself into two states in order to guaranty the stability (inhomogeneity).

The force characteristic of one beam is presented in Fig.4.6a. This representation highlights the force characteristic of one beam displaced along its equivalent θ direction (chapter 3) but represents an image of the radial component. Because the nature of the beam does not allow to be split into two states, the behaviour of one module is not similar in this case. No subsystems of the beams exist to allow such inhomogeneity through splitting states. However, when several beams are assembled in a global system like the cylindrical spring, all these beams could be considered as subsystems. Thus, the global behaviour of the spring allows

such inhomogeneity. It could explain why not all the beams of the spring reach the same state during the deformation. In Fig.4.6b, two adjacent beams are presented with two different shapes. The *Beam 1* is less compressed than the *Beam 2*. In the force characteristic (Fig.4.6a), these two states could be represented through the red dots which are present when the transition force occurs.

Therefore, by linking together several systems which are not able of inhomogeneity, a new system is created and allows such behaviour. When the force transition occurs, the beams could reach at least two states. However, it is impossible to predict individually how the beams will be deformed. The two different states could be seen by a pre-open one (*Beam 1*) or a closed one (M-shape - *Beam 2*).

4.2.5 Results - 100 μm thick membrane

Measurements

For the 100 μm thick film, four prototypes have been tested precisely in the same conditions that the 200 μm one. With such a film, the deformation seemed almost symmetric. Thus, the measured deformations have not been divided by two.

In comparison with the former thickness and by considering the same nominal electric field ($35 V \cdot \mu m^{-1}$), the displacement obtained with the smallest thickness is better (more than 10%). In Fig.4.7a, the characteristic of the activated and non-activated of the two thicknesses and the one of the negative spring are represented. The force characteristic of the elastomer with a thickness of 100 μm shows more important displacement. This characteristic could be reached because it is more adequate than the 200 μm . Indeed, the stiffness is lower. The slope of the characteristic of the elastomer and the one of the spring are closer.

Moreover, the displacement could be more significant because higher nominal electric field could be reached before the electrical breakdown in the air for the thinner film. As a reminder, the maximum voltage is around 7.5 kV.

Concerning the results obtained through the FE analysis with the different analysed cases, the conclusions are similar to the previous film (Fig.4.7b).

Intrinsic stability during activation

The previous theory about the possibility for each beam (subsystems) to be split into at least two categories, or two states, is also analysed here. The pre-open and the M-shape configurations of the beams are observed as well (Beam 1 and Beam 2 in Fig.4.6b). It seems that the system composed of the elastomer and the spring reaches initially a more symmetric configuration which could explain the fact that the measurements are more repeatable (bigger difference 16%). Moreover, the characteristics for the different supports of the FE analysis (Fig.4.7c) are less dispersive (Discrepancy of 30% in the worst case) with such thickness.

The main advantage of this film is the possibility to target higher nominal electric field before

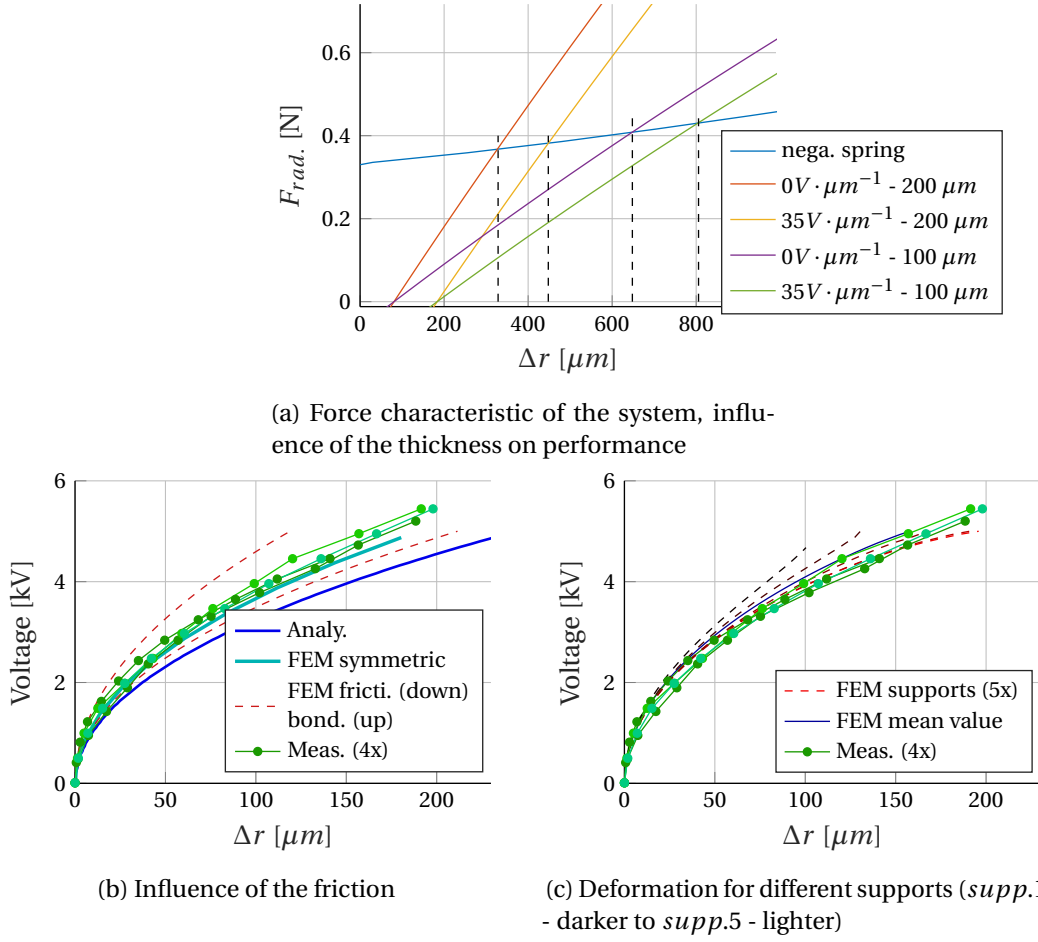
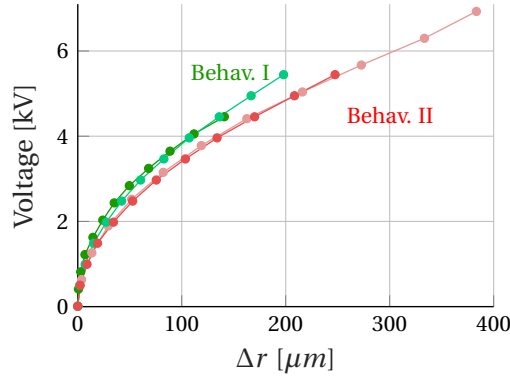


Figure 4.7 – Results for 100 μm thick elastomer

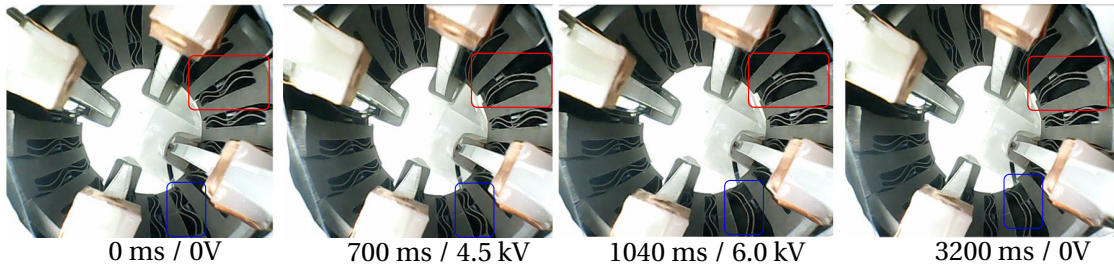
reaching the breakdown in the air. In Fig.4.8a the results for actuators supplied up to $55\text{V} \cdot \mu\text{m}^{-1}$ and up to $70\text{V} \cdot \mu\text{m}^{-1}$ are compared. Two out of the four previously discussed prototypes (DEA) have been used for these measurements. It could be observed that the characteristics have two behaviours (*Behav. I* vs *Behav. II*).

During the activation of the actuator up to the maximum nominal electric field, a specificity was observed. Once a certain threshold is reached (around 6 kV), several beams "jump" from the M-shape to the pre-open one, when the supply voltage returns to zero, the new rest states are different from the initial positions. It means that the initial configuration of the spring has changed. One reason is the friction which prevents from reaching once again the first initial shape.

In Fig.4.8b, the different configurations of the beams during the activation are provided. The first image corresponds to the starting position of the spring. During the activation, a first jump occurs at 6.0 kV (second image). The beam enclosed by the red squares jumps to the pre-open position. At 6.5 kV, the beam in blue jumps as well (third image). When the voltage is switch off, the beams which have jumped, do not return to their M-shape. The next activation starts with the new configuration of the beam and follows the characteristic of the *Behav. II*.



(a) Measurements for different maxima nominal electric field



(b) States of beams before and after the "jump"

Figure 4.8 – Special behaviour of the actuator

However, if the spring is totally closed once again such as in Fig.4.5a and reactivated, the characteristic of the first behaviour is observed.

4.2.6 Discussion

Special behaviour of planar beams

The global behaviour of all the spring is challenging to study and to predict. To highlight such difficulties, a planar configuration has been studied (Fig.4.9a) which is constituted of two pairs of planar beams in series. The thickness of the beams are 150 μm . In this study, the amplitudes are not important, the behaviour during the deformation is important.

The test for the first measurement consists of blocking the deformation of one of these pairs of beams and in measuring the force-displacement relationship (green curve Fig.4.9b). The measure shows the presence of the negative characteristic of the beams as expected.

The second performed test consists of controlling the displacement of the beams in series and measuring once again the reaction force (red curve). In this case, the global behaviour is special. It seems that for the first part of displacement, only one beam is deformed and at a certain threshold, the second one starts to move while the first one is mechanically blocked.

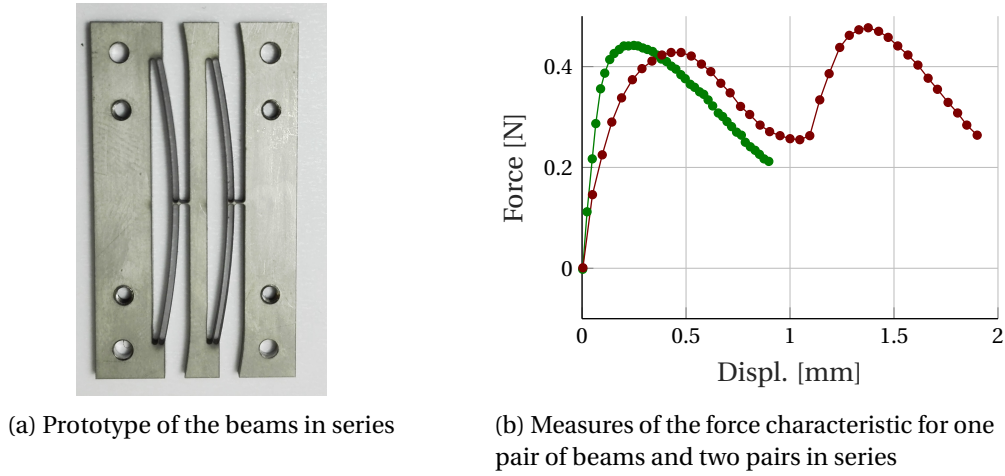


Figure 4.9 – Study of the global force characteristic

Such observation allows validating the difficulty to predict the behaviour of coupled beams even in a planar configuration. For the cylindrical spring, sixteen beams are coupled in a cylindrical shape which makes it difficult to foresee the global behaviour.

Negative characteristic

From the previous results with the prototype, it has been highlighted that the global behaviour of the spring and the DEA is complex. In literature, a good example is provided by Hodgins [79] where the characteristic of the biasing elements and the one of the elastomer was split and analysed separately. However, in the proposed actuator, this analysis is not possible. The fact to link the membrane to the spring does not allow to study the two elements one after the other. Thus, it is essential to validate that the global behaviour with the proposed spring provides better displacements than other biasing elements even if the deformation of all the beams are not controllable. The study is performed with FE analysis on the $200\ \mu\text{m}$ thick membrane.

Two other biasing elements, i.e. the constant load and the positive stiffness spring, are generally used to study the performance of the DEA. According to the literature [79], the constant load provides better performance than the positive stiffness spring. Thus, the idea is to demonstrate that an increase of the mean variation of the radius is obtained with the proposed spring compared to the constant load (F_{const}).

The characteristic of the elastomer and the ones of the two biasing elements are presented in Fig.4.10a. Concerning the negative one, the targeted behaviour of the compressed spring is given by $F_{neg,1}$. When the spring is inserted in the tube (Fig.4.3b) and released, the radial displacement r_1 is reached. In the FE analysis, this position corresponds to the mean value of the displacement of the surface (*Part I*) of the membrane, because the results change according to the considered supports (*supp.1* - *supp.5*), as discussed in the previous section.

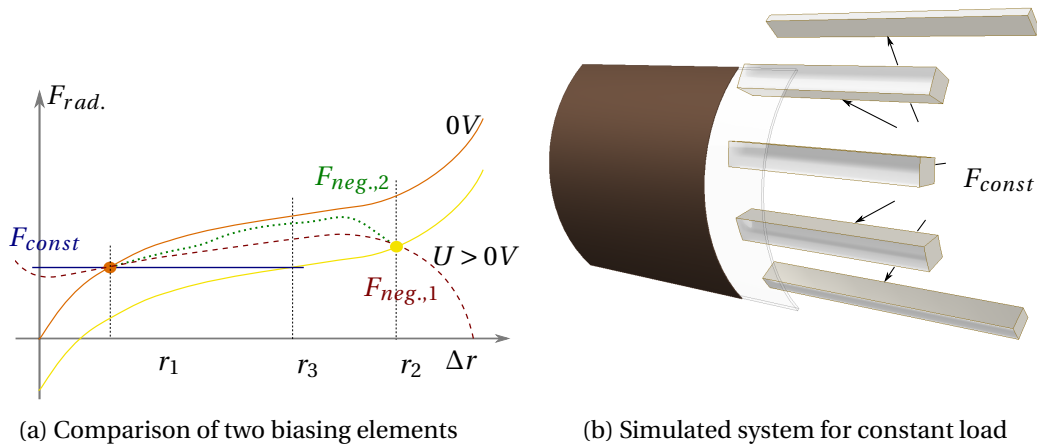


Figure 4.10 – Comparison between constant and negative biasing element

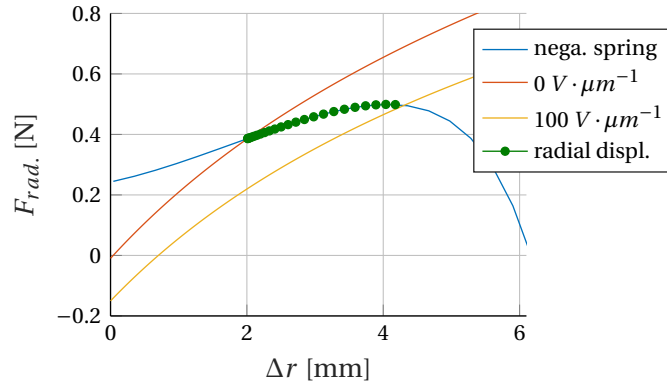


Figure 4.11 – Displacement analysis with the improved design of the actuator

When the DEA is activated ($\tilde{E} = 50 \text{ V} \cdot \mu\text{m}^{-1}$), a mean radius r_2 is reached. In order to analyse the effect of the constant force, the same design than the one presented in Fig.4.10b is used. The supports are inserted in the elastomer, and a constant force is applied to the supports (*supp.1 - supp.5*) in the radial direction. The amplitude of this force is determined so that the stable position of the elastomer is equal to r_1 when no voltage is applied. Then, the actuator is supplied, and the displacements could be compared according to the voltage.

For an activation voltage of 5 kV and 10 kV, the variation of the radius is respectively, 33% and 15% times bigger with the proposed spring. It means, that whatever is the path followed to go from r_1 to r_2 , globally, the cylindrical spring allows to reach larger displacements and thus provides a global negative characteristic. Indeed, even if instead of the targeted path $F_{neg,1}$, the $F_{neg,2}$ one is followed (because of the previously discussed instabilities), the displacement is more significant than with the constant biasing element.

The primary objective of the negative biasing element is to increase the performance of the actuator. However, through the prototype, no significant deformation was reached. When

the design was performed, wrong parameters of the Yeoh model were used. A softer film was considered and more significant displacements expected.

In order to prove the possibility to obtain bigger displacement with such spring, a new design is proposed. Because the relationship between the force characteristic of the beams (F_θ) and the radial component (F_{radial}) is dependent on the number of modules, the same geometry of the beams is considered for the new design. By adjusting the thickness of the membrane and the number of modules, the objective is to find a solution to obtain better performance. The final geometry is constituted of 22 modules (16 modules for the prototype in chapter 3) with a $50\ \mu m$ thick elastomer. The expected result is provided in Fig.4.11. With such spring, a variation of $2.2\ mm$ of radial displacement is reached which consists in a radial stretch of 13.5 %. In comparison with the results obtained with the $100\ \mu m$ thick membrane and the previous spring, the displacement is ten times bigger with this new spring, for the same activation.

4.3 Conclusion

In this chapter, the proposed prototype has been tested and discussed. Two thicknesses of membranes have been investigated. For each thickness of the membrane, four DEA have been analysed with the same spring. The obtained displacements characteristics were repeatable for the $100\ \mu m$ thick membrane but less for the $200\ \mu m$ one. Concerning the results, maximum radial displacement of around $300\ \mu m$ was reached for the thinner film due to its closer force characteristic with the spring than the $200\ \mu m$ thick film.

The first tested membrane, with a thickness of $200\ \mu m$, has allowed highlighting the importance of the friction between the membrane and the spring. Because of the different covered and uncovered part of the elastomer with electrodes, the choice to delimit the results with a FE analysis where the contact was considered as wholly frictionless or bonded was done. The measurements seem to belong to this boundary. Another way studied to delimit the results concerns the non-symmetric way of deformation of the different beams. Due to the different friction condition and the presence of a tangential component, the actuator is not deformed symmetrically. Once again, the FE solutions of the displacements of different supports where the tangential force is unblocked, provide a good delimitation for the measurements. Moreover, as explained in the previous chapter, the prototype of the spring has beams with a thickness ranging from $130\ \mu m$ to $180\ \mu m$ which could also explain the unsymmetrical behaviour.

These observations have also been done with the second membrane with a thickness of $100\ \mu m$. Better results were obtained from the displacement point of view, with this initial film thickness.

Concerning the two studied thicknesses, the intrinsic stability of the system (membrane and spring) was highlighted. Even if a single beam does not allow intrinsic stability (inhomogeneity) by splitting itself into two states as it is possible with the silicone (chapter 2), this phenomenon

was observed for all the spring. By assembling several of these arch-shape beams, all the system is transformed into a system able to reach at least two different states. Thus during the deformation, the beams could reach one completely closed M-shape or a pre-open one.

The proposed cylindrical actuator was more complicated than expected. Some researches [79] have studied the elastomer and the biasing element separately. However, due to the specific configuration and the high number of parameters, like for example the way chosen to maintain the cylinder to perform the measurements, make challenging to study the influence of each parameter separately and their interactions. The system including DEA and the spring should be considered as one set. Thus, it is not so easy to determine the contribution of the proposed spring. However, it has been demonstrated through FEM analysis, that the actuator with the proposed spring has provided more displacements than considering other biasing elements. Thus, the fact that the cylindrical spring works in its negative force characteristic is validated.

Concerning the possibility to increase the displacement, a real optimisation process of the spring and by considering single or multilayer membranes with different thicknesses should be performed. The former design has demonstrated the feasibility and its advantage, however, the intrinsic performance could be improved.

5 Cylindrical DEA as cardiac assistance

In terms of disruptive innovation, it makes sense to consider DEA as an alternative technology for cardiac assistance. In this chapter, this application is studied in order to determine the feasibility to use DEA as assist device.

In the first part, the state of the art of current assist devices is presented and the proposed solution is compared to them. Then, the strategy of assistance is introduced which explains how the cylindrical DEA could interfere in the human circulatory system and potentially release the heart. In order to simulate such a cycle, lumped parameter models are often used. It consists of proposing an equivalent electronic circuit of the circulatory system in order to study the different parameters in the body (pressure, the variation of volume, flow rate, ...). One of these equivalent circuit is proposed which models the cardiac cycle and for which the zone including the DEA such as assistance is highlighted. The objective is to study the influence of the actuator on the physiological parameters. The cylindrical DEA is modelled through the pressure-volume characteristic with and without electric field.

An activation of the DEA is proposed based on the working principle of the intra-aortic balloon pump [86] (IABP) which is an existing device used by surgeons and able to relieve the natural pump, i.e. the heart. Tuning the different parameters of the proposed system (parameter of the lumped model, shape and synchronisation of the activation, geometry of the cylinder), will provide a fair number of possible responses. To interpret these responses, several specifications are introduced in order to answer the question: "is the heart relieved?". Finally, due to the variation of the pressure induced by the left ventricle to the DEA and the appropriate supply, the negative biasing behaviour could be studied. However, the negative stiffness spring previously presented is not considered in this model, only the heart itself plays this role.

5.1 Ventricular assist device

Artificial hearts or implantable ventricular assist devices (iVAD) have been developed for a long time even if the heart is undoubtedly the most complex organ we can find in the human body. Research aspects for such system are intricate and require expertise in many fields. Its overall working, including the blood properties, the pump system, the control and the biocompatibility, is difficult to understand and thus implement in a single artificial system. Research on this domain has started since more than a half-century, and today the artificial heart still enthral the scientific community. Recently, a French group has tested an artificial heart on a human [87]. This device has a new biocompatible skin that facilitates integration. In Switzerland, a group in Zurich [88] tends to create a complete heart system with a magnetic material. Few research projects have investigated only part of the heart through some assist devices [89]. It means a device that helps the heart to work correctly without changing the entire organ. This kind of device is less invasive in terms of surgical operation and more compliant with the body.

Existing artificial devices aiming to replace or help the heart working correctly could be separated into three main types. The first kind of system is a fully artificial heart which consists of a complete mechanical heart wrapped with a biocompatible skin or not. The challenge is the adaptability of the patient's body and the problem linked to the blood. This method is not yet often used, and only some cases of implementation are listed even if the research is actual (Carmat [87]). The second kind of artificial device consists of cardiac stimulators (pacemaker). This technology provides electrical signals to the heart useful to control the working of the heart correctly. The last category is the ventricular assist devices. It includes all the artificial pumps that allow transferring the blood from one cavity of the heart to the body. Contrary to the previous assistances, some regions of the heart are still working and generally one of the ventricles is assisted.

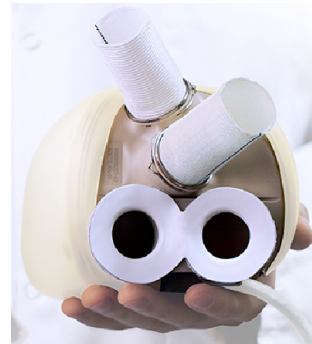
The main proposed systems are in contact with the blood that unfortunately leads to hemolysis. Generally, the patient needs to take medical treatment against this problem. The blood being very sensitive, a system of valves (non-biological one) is not adequate for such actuators.

Full artificial heart

In some cases, the heart could not work by itself and needs to be replaced entirely. This kind of technology generally consists of four main cavities (like in the natural heart) to transfer the blood through the body. The left and right ventricles and atrium should be present in such a pump system. They allow to manage the blood precisely such as a real heart would do. The system of pump is generally driven by two main technologies: pneumatic and electro-mechanical.



(a) Abiomed [90]



(b) Carmat [87]

Figure 5.1 – Artificial hearts

The operating principle of the *Abiomed* system is based on a mechanical rotary motor that transfers the blood everywhere, within parallel, a valves system to control the flow. The new approach for this product is the implanted controller, the system of lithium battery and the TET (transcutaneous energy transmission) system that avoids wires through the skin. The Carmat product is the latest product on the market. The main novelty is the biocompatible skin. Such a skin is constituted of animal tissues and is chemically transformed in order to avoid problems of blood contact and immunotolerance. The transfer's system for the blood is based on a pump constituted of a propeller which imposes the cardiac frequency. This solution is the most concluding system on the market. All these technologies are not yet widely commercialised due to the difficulty of body approval.

Pacemaker

In many cases, the problem comes from the malfunction of the electrical signals sent to the heart in order to restore the heart's rhythm. The pumping system is no longer ensured with a sufficient heartbeat frequency (bradycardia). A solution consists in providing electrical impulsions at specific points in order to correctly activate the heart. This technology requires a soft surgical operation for the patient. A battery is placed inside the pacemaker. The life cycle is in the range of 5 to 10 years. Afterwards, a surgical operation to change the device is compulsory.

Ventricular assist device

Other solutions exist in order to help the deficient heart without completely replacing the organ. These systems work such as a pump. The heart still works, but its mechanical power is not sufficient to transfer the blood. This solution is chosen during or after surgery (until the heart recovers), while the patient is waiting for a heart transplant and sometimes as a long-term solution to permanently help the heart. The ventricular assist device could be used into both ventricles, the left one (LVAD) and the right one (RVAD). The mainly used is the LVAD

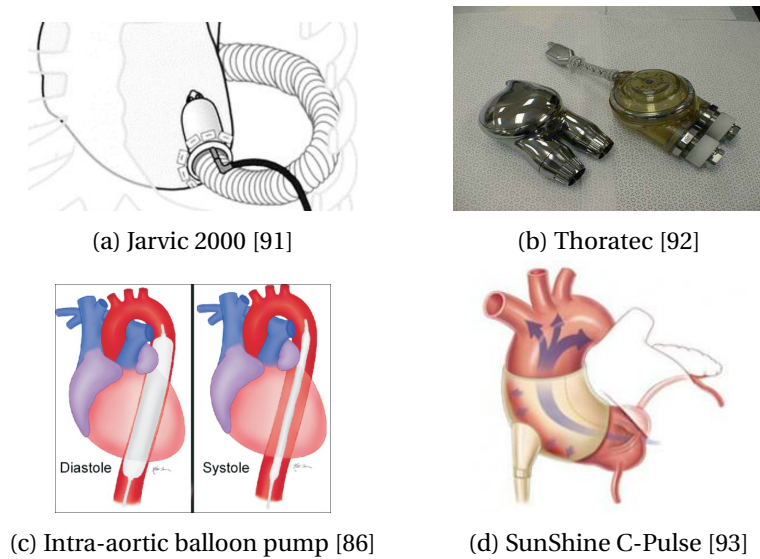


Figure 5.2 – Assist devices

to help the heart to transfer oxygen-rich blood from the heart to the body through the aorta. Both VADs could be found. First, the transcutaneous ventricular assist device where the power source and the pump are located outside the body and secondly, the implantable ventricular assist device where the pump is generally inside the body. The first solution is mainly used for invalid people or those waiting for surgery.

In these two examples of VAD, the blood is pumped by a mechanical rotor. The size is significant and not negligible for implementation into the body. The electronics control and the battery are located outside the body and are linked by wires. The main problem of the external part is the high risk of infections. Additionally, each cumbersome system outside the body is physically heavy for the patient. The *Thoratec* is an example of an external VAD.

The *Jarvik* and *Debakey* systems have the advantage to be small and directly implantable into the patient's body. These two solutions have small mechanical propeller able to transfer the blood. The batteries are located outside the body and wires go through the skin. It induces the same problems such as the two previous systems. Other problems for all these solutions are the direct contact between the blood and the mechanical part which creates hemolysis by damaging the globules.

Another solution used by the surgeon is the intra-aortic balloon pump (Fig.5.2c). A balloon is placed in the descending aorta through an artery of the leg. Then, this balloon is inflated and deflated according to the heart's functioning in order to propel the blood in the rest of the vessels. When the aortic valve is closing, the balloon inflates and help the blood to be propelled in the body. Before, the opening of the valve, the balloon is deflated. One main advantage of such a system is the decrease of the maximum pressure in the left ventricle and

Criterion	Abiocor	Carmat	Thoratec	Jarvik	C-Pulse	IABP	DEAs
Weight	+	+	++	--	-	-	++
Biocompatibility	-	++	++	-	++	-	+
Infection risk	+	--	--	+	-	--	+
Non-invasive	--	--	-	+	+	-	++

Table 5.1 – Summarize of the different artificial heart systems and criteria of comparison. + and - stands respectively for interesting or not

the aorta when the balloon is deflated. The main disadvantage of the IABP is the direct contact with the blood and the permanent presence of the tube which passes through the artery of the leg in order to control the pressure in the balloon. Moreover, there is a risk of obstruction, rupture of the aorta or the balloon. This solution is used in an emergency and is not kept for a long time.

The last solution is the one proposed by the group SunShine,i.e. the C-Pulse [93]. The device is placed around the ascending aorta, and it consists of a kind of balloon which could be inflated through air pressure (Fig.5.2d). When the aorta is squeezed, the blood is ejected in the circulatory system. The assistance should be supplied with air. Therefore an external source of air is placed outside and a wire which passes through the skin brings the air in the body.

Comparison of existing solutions

As previously discussed, many solutions exist when it consists of relieving or replacing the heart. Even if all of them are used for specific diseases, a comparison is proposed in Table 5.1. Because the diseases treated with the pacemaker are not the ones which are studied, this device is not compared in this section. Besides all these current solutions, the technology of DEA could be added to the list. Actually, no commercially available devices are operational, but through the knowledge of this technology, an indicative comparison is performed.

5.2 Cardiac cycle

Before entering in the particularities of the lumped models, an overview of the working principle of the heart is recalled. The strategy chosen to activate and place the DEA is also provided.

5.2.1 Working principle of the circulatory system

The main objective of the heart is to provide the oxygen-rich blood to the rest of the body (Fig.5.3a). The organs, through their cells, use this oxygen and essential nutrients and eject

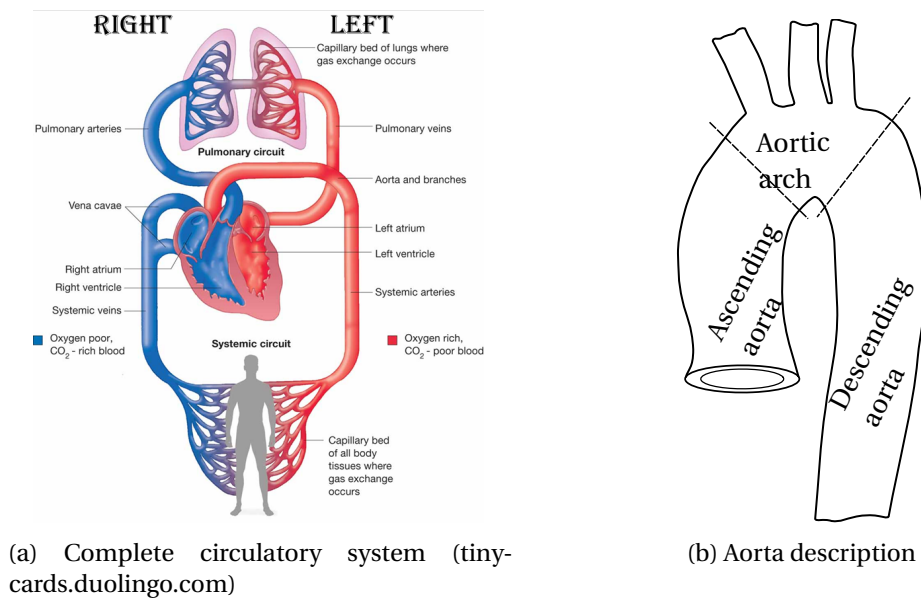


Figure 5.3 – Circulatory system

the carbon dioxide. The blood leaves the left ventricle to reach the small capillaries at the extremities. Then, the blood deficient in oxygen comes back up to the right atrium. By crossing the tripuscid valve (between the right atrium and right ventricle) and then the pulmonary valve (between right ventricle and lungs), the oxygen-rich blood arrives in the left atrium after passing in the lungs. This fluid passes through the mitral valve (between the left atrium and left ventricle) and finally through the aortic valve (between the left ventricle and ascending aorta) to continue through the aorta to go back to the capillaries. The left part of the heart, especially the left ventricle provides sufficient energy to reach all the regions of the body.

By observing the different zones of the body which tends to act such as a pump, three main muscles help the blood to be propelled. The first one concerns the heart itself where its main objective is to guaranty the body to have a constant mean flow rate. The second one is the skeletal muscle pump in the legs which helps the blood deficient in oxygen to come back in the right part of the heart. By walking, the muscles of the legs are contracted and compressed the arteries to help the venous return. Finally, the third one does not precisely act such as a pump but stored potential energy and re-inject it at the appropriate moment. It consists of the compliance part of the body like the aorta. Indeed, when the blood is ejected by the left ventricle, and it passes through the aortic valve, the tissues of the aorta are sufficiently elastic to be deformed and stored potential energy. When the aortic valve is closing, the aorta contracts itself in order to continue to provide blood to the body. All the elastic parts are defined according to their compliance or elastance (inverse of the compliance) which is defined by the variation of pressure over the variation of the volume in the studied zone. A tissue with a high elastance means that its stiffness is high and inversely.

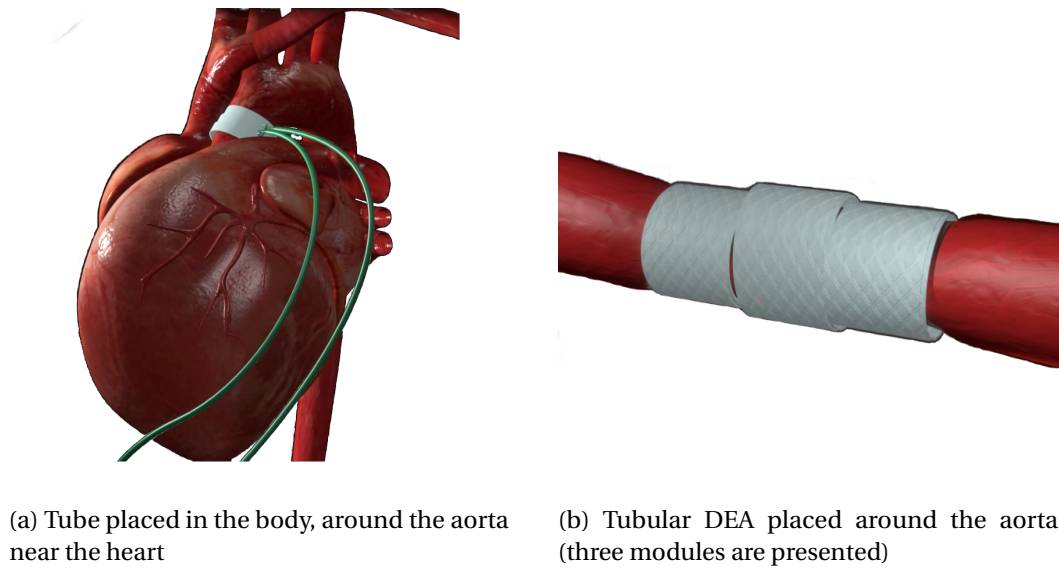


Figure 5.4 – Working principle of the proposed solution for the cardiac assistance

5.2.2 Strategy of assistance

Several authors have mentioned the possibility to use the technology of DEA such as cardiac assistance [94]. However, only the idea is provided without trying to validate such a proposal. It seems that it is an adequate solution in order to create artificial assistance for the heart. The main advantage concerns the size and the possibility to place it easily. According to the strategy defined to place this actuator, a safety risk could exist if the system is in contact with blood. However, no artificial valve is present, thus hemolysis could be avoided. Moreover, the natural behaviour of the DEA is close to the one of arteries and other organs in the body. However, the challenge remains to produce high power with this kind of actuator.

The proposed solution is related to the working principle of the aorta. However, contrary to the natural one which is passive, the objective of the assistance is to provide some energy. Indeed, the idea is not to replace a part of the heart but to relieve it. Precisely like the aorta, the DEA consists of a soft membrane able to be deformed and to store elastic energy.

The aorta is composed of three main parts (Fig.5.3b). Right after the aortic valve, there is the ascending aorta with a length of around 80 *mm* for adult, the aortic arch with three arteries (brachiocephalic, left common carotid and left subclavian) and finally the descending aorta with a length of around 300 *mm*. The intra-aortic balloon pump is placed in this part of the aorta (Fig.5.2c). Right after the aortic valve, at the beginning of the ascending aorta, few vessels supply the heart with oxygen-rich blood. These vessels are not presented in the schema.

The proposed system consists of a tubular DEA placed at the end of the left ventricle (Fig.5.4a). Due to the length of the ascending aorta (80 *mm*), it has been decided to let half of the natural aorta without actuator in order to not weaken too much this vessel. The second part of the natural aorta is replaced with the tubular actuator. This solution is close to the one proposed

by Ioannou [95] where the authors have studied the effect of the increase of the compliance of the aorta by placing rigid tube at this location (no actuation).

By activating and deactivating the DEA according to the heartbeat, the module could provide energy to the blood. In the proposed study, only one module is placed around the aorta. However, a peristaltic system could be imagined with at least three modules (Fig.5.4b).

5.2.3 Energy from the left ventricle

When a patient suffers from a cardiac disease, a reaction could be that the heart and especially the left ventricle provides more energy. In order to evaluate the amount of energy provided by the left ventricle, the pressure (blue curve in Fig.5.5a) and the volume (green curve in Fig.5.5a) should be determined. Through the integration of the volume over the pressure for one cycle, the provided energy by this organ is determined (Fig.5.5b). This energy corresponds to the area enclosed by the loop. It should be recalled that the left ventricle is filled through the left atrium during *diastole* and is emptied during *systole*.

In order to define the two previous terms, let's consider the so-called *PV-loop* (Fig.5.5b) describing the pressure-volume characteristic in the left ventricle. By starting the loop at the end of diastole (e.g. 90 mL for 10 mmHg), the pressure increases through iso-volume state due to the fast contraction of the left ventricle. Then, the aortic valve opens, and the pressure in the left ventricle and aorta varies, and the blood passes into the ascending aorta. This period corresponds to the *systole*. Then, the pressure in the left ventricle decreases without variation of volume before the left ventricle being filled again through the mitral valve, known as the *diastole*.

The obtained *PV-loop* which is provided through the intersection of the characteristic of the external loads of the heart (all the impedance) and the intrinsic characteristic of the left ventricle [96], corresponds to the energy provided by the left ventricle. The characteristic of the left ventricle is given through the elastance at each moment (t_1, t_2, t_3, \dots) and is considered such as specific to the patient and cyclic. This parameter images the variation of the stiffness of the walls of the left ventricle during one cycle. However, the loop does not provide any information on the heartbeat and thus the power.

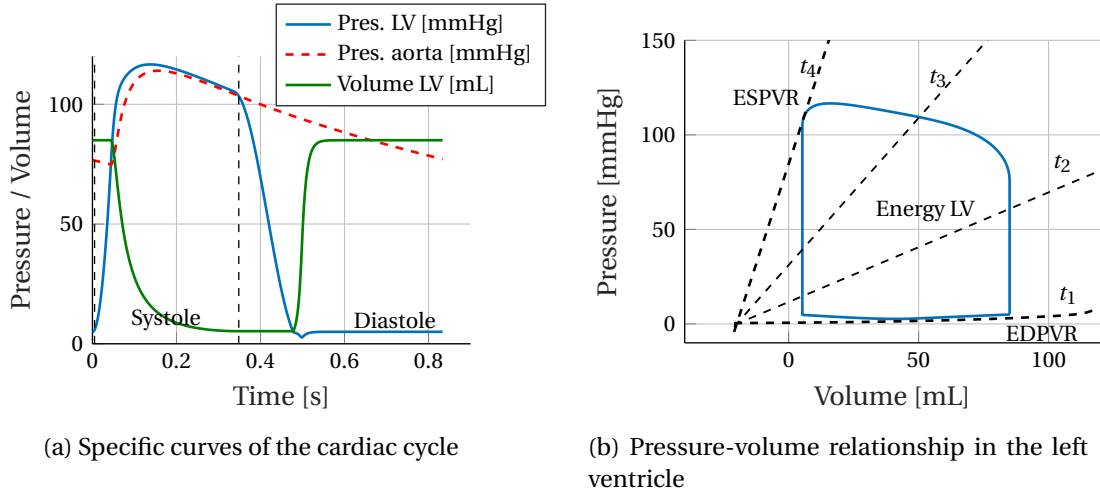


Figure 5.5 – Characteristics of the cardiac cycle

5.3 Integration of the DEA in the circulatory system

In order to determine the influence of the activation of the tubular DEA, the circulatory system is modelled through an analogy between physiological regions and electrical components. Indeed, the blood circulation could be represented through an equivalent electronic circuit in order to simulate easily the behaviour of the variation of impedance due to potential disease. In literature, different models are described, from the "0D" model [97], [98] to the 3D one (FEM). According to the wished accuracy and the studied zones of the body, the model is more or less complex with up to several tens of elements for all the body.

The "0D" model is used in this study due to its facility to represent the cardiovascular system and the possibility to include the DEA. This model is principally characterized by the conservation of mass used to describe the blood flow (equivalent to Kirchhoff's law in the electrical domain), the steady-state momentum equilibrium is provided by the Poiseuille's law (Ohm's law) and finally the Navier-Stokes relations are used in order to describe the unsteady state momentum balance. The main disadvantage of such a model is the incapability to describe the spatial distribution.

In order to represent the different regions of the circulatory system, different *RLC* blocks are assigned to the physiological zones [99]. The number of elements depends on the targeted precision of the model in the different regions of the body.

5.3.1 Lumped element model

Concerning the analogy between the physiological domain and the electronic one, the equivalent components are summarised in Fig.5.6. The resistance (*R*), the capacitance (*C*) and the inductance (*L*) allow to simulate respectively the viscosity, the compliance (or elastance) and the inertia of the fluid. More details about the analogy between the physiological component

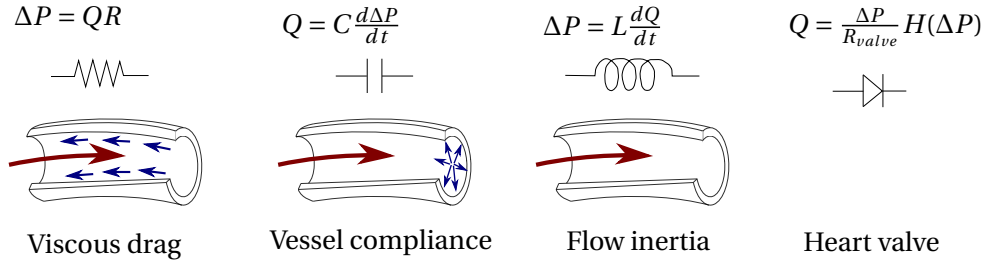


Figure 5.6 – Equivalent elements between the physiological and the electrical domains

and the electrical could be found in [98]. The theories developed in the domain of electronic allow solving such systems.

Through the computation of the voltages, the currents and the charges, the pressures, the flow rates and the volumes are respectively determined in the different regions of the body. Another analogy could be done by considering a bond graph [100]. However, in this chapter, only the electrical analogy is considered.

The Windkessel model [97] consists of the most simple and the most famous model which allows determining the influence of the total peripheral resistance (TPR) and the equivalent arterial compliance. The TPR [101] consists in the resistance that the blood encounters to reach different zones of the body and is mainly given by the capillaries (smallest vessels at the extremities of the circulatory system). The input of such model consists in imposing the flow rate in the circuit. This system allows determining an equivalent TPR according to the measured pressures and flow rates which provides useful information to surgeons. However, the influence of the left ventricle and the aorta is not highlighted in such model.

The objective of the heart is to regulate the flow rate in order to provide oxygen-rich blood to the body. If this flow is imposed in the Windkessel model, the influence of the variation of the impedance (e.g. activation of the DEA) does not allow to analyse its consequence on the flow. Another way used to solve this problem is to take into account the compliance of the left ventricle (C_{LV} in Fig.5.7). It should not be forgotten that this parameter is considered as specific to each patient and is cyclic.

5.3.2 Adaptation of the lumped model

In order to consider the influence of the DEA, the schema given in Fig.5.7 is introduced which represents the proposed lumped parameter model. Due to the chosen region where the actuator is placed, the lumped model is split into three parts (Fig.5.7). The first one (green rectangle) represents the heart mainly dependent on the elastance of the left ventricle as explained previously. Constant pressure in the left atrium (P_{atr}) is also added through a constant supply voltage. In reality, this pressure is not constant but fluctuate a little bit. This parameter simulates the moment when the left ventricle is filled through the left atrium.

The second one consists of the aorta with the ascending, the arch and the descending region

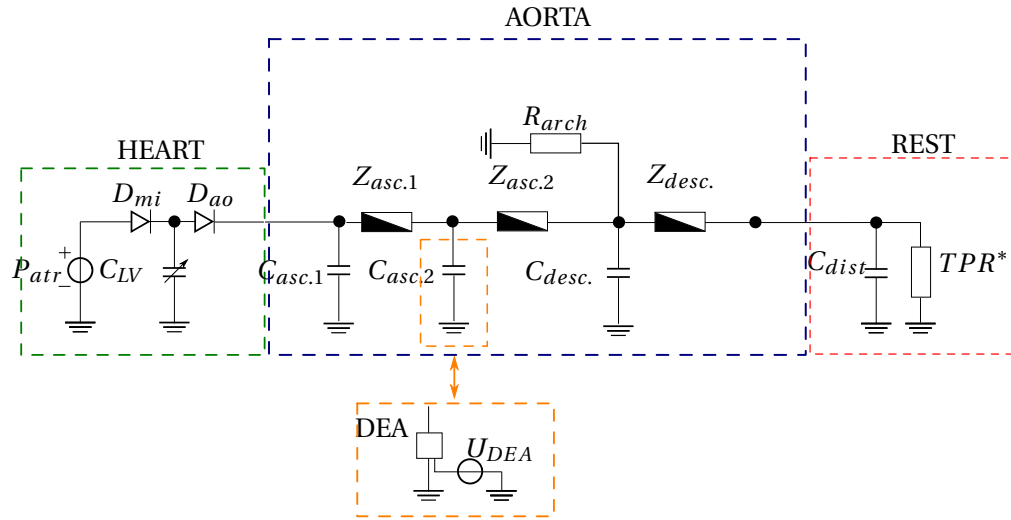


Figure 5.7 – Modified lumped model with DEA and its power supply voltage replacing part of the aorta compliance (orange square).

(blue rectangle). It has been chosen to replace all the zones by equivalent compliance (capacitor), inertance (inductance) and resistance (in the schema, the equivalent impedance is given).

The idea of the proposed solution is to place the tubular DEA instead of a part of the ascending aorta (Fig.5.3b). Thus, this zone should be highlighted in the model. Because this model is discrete, it is possible to perform such action by splitting the regions. The ascending aorta is divided into two similar parts of around 40 mm length. The closest one, near the aortic valve, is kept natural ($C_{asc.1}$ and $Z_{asc.1}$) and the second part ($C_{asc.2}$ and $Z_{asc.2}$) will allow to include the DEA. For the descending aorta, all this part is kept as a single zone ($C_{desc.}$ and $Z_{desc.}$). Due to the presence of the three vessels of the aortic arch, a resistance (R_{arch}) is placed at this location. Generally, this resistance is included in the total peripheral one of the Windkessel model.

The third zone, which consists in the rest of the body, includes the equivalent distal compliance (C_{dist}) of the rest of the body (arteries and capillaries) and the resistance TPR^* . Because this resistance does not take into account R_{arch} , this value is not equivalent to the well known TPR found in the Windkessel model.

Once the value of each element is determined, the circuit can provide information such as in Fig.5.5. In order to consider the effect of the tubular DEA in this system, the solution consists of replacing the compliance $C_{asc.2}$ with the *pressure-volume* relationship of the actuator (orange square in Fig.5.7). Thus, if the variation of volume which enters in the DEA is known, the equivalent pressure is determined.

Generally, in the literature [102], [103], [104], the cardiac assist device is placed in parallel of the aortic valve, which means that the assistance starts in the left ventricle and is connected to the aorta. Thus, a part of the blood does not cross the aortic valve. However, in the proposed

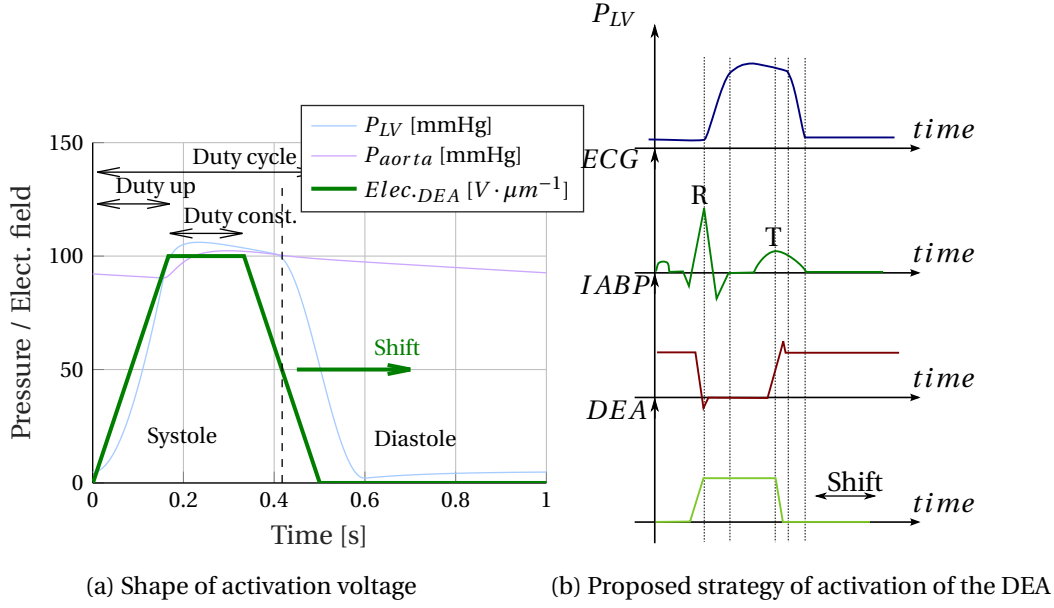


Figure 5.8 – Strategy of activation of the DEA

solution, the assistance is placed in series. Moreover, the DEA is driven by its external source, U_{DEA} , in order to transfer the energy to the fluid.

Through the *PV-loop* and other parameters, the model allows analysing the effects of the activation of the assistance on the pressures, the volumes and the flow rates in the different zones of the body.

Concerning the *pressure-volume* relationship of the DEA, the used model is the one developed in the appendix D. As a reminder, the variation of the internal radius of the tube is considered as uniform, and the model is based on the thin shells theory. The result consists in the following relationship:

$$\Delta P(\Delta V_{int}, U_{DEA}) = P_{elast}(\Delta V_{int}) - P_{electr}(\Delta V_{int}, U_{DEA}) \quad (5.1)$$

with U_{DEA} the voltage applied to the DEA which depends on the time and ΔV_{int} the variation of the internal volume ($\pi r_{int}^2 L_0 - \pi R_{int}^2 L_0$) given by the deformed internal radius r_{int} and the undeformed one R_{int} . With the analogy of the electrical domain, this variation corresponds to the one of electric charge. The main assumption for this model concerns the uniform radial expansion. In the real case, the tube should be attached to rigid frames and would deform to a geometry close to an ellipsoid.

5.3.3 Strategy of activation

In order to supply the DEA (U_{DEA}), a parametrised shape for the electrical activation is proposed (green line in Fig.5.8a). Its period corresponds to the one of the heart. The time

5.3. Integration of the DEA in the circulatory system

Parameter of evaluation	Values	Remarks
Mean flow rate (Cardiac output)	$\geq 5 [L \cdot min^{-1}]$	Objective of the heart in order to guaranty an healthy oxygenation of the organs
Radial stretch of elastomer	– []	Quantify the deformation of the DEA
Ejection fraction EF		Volumetric fraction
Energy LV	1.0 [J]	Energy provided by an healthy left ventricle
Energy DEA	– [J]	Energy provided by the DEA
Percent of energy provided by the LV and DEA to TPR	– [%]	

Valve Asc.1 + Asc.2
+ Desc.

E_{LV}
 E_{DEA}

$TPR + R_{arch}$

Table 5.2 – Parameters used to evaluate the results obtained through the activation of the DEA

during which the DEA is submitted to a voltage is defined through the *duty cycle* which is divided into three parts. The first one is defined by the time during the voltage is increased (*duty up*), the second one by the time during that the DEA is activated with a constant voltage (*duty const.*) and the last one is imposed by the two previous definitions and the duty cycle. The last parameter which could be varied is the phase shift between the cardiac cycle (systole and diastole) and the control of the DEA.

Parameters for evaluation

The parameters which allow determining if the assistance is helpful are challenging to define. According to the patient or the diseases, different parameters should be analysed. The proposed ones used for the evaluation are summarised in Table 5.2.

One of the most crucial parameters concerns the mean flow rate at the TPR^* . Indeed, one main objective of the heart is to provide a sufficient mean flow rate to this element, which represents the main beneficiary of oxygen. Moreover, the flow in the aortic arch which passes through the three vessels (R_{arch}) should also be guaranteed. The last studied flow is the one in the ascending aorta which defines the cardiac output.

Another indication which provides information about the state of the left ventricle is the ejection fraction. It interprets the volumetric fraction of blood ejected from the ventricle. Its definition is given by the ratio between the stroke volume (volume of blood ejected during the systole) and the end-diastolic volume (total volume in the ventricle).

The place around the ascending aorta is not infinite, and the size of the deformed DEA should be limited. Thus, the radial stretch of the cylinder is considered in this analysis. It may be noticed that the natural ascending aorta expands its radius of around 30%.

Another parameter concerns the energy provided by the left ventricle. According to the diseases, this energy is more or less critical compared to a healthy patient. Thus, this energy, provided by the *PV-loop*, should be analysed. However, the heart rate should be taken into account to define the power delivered by the left ventricle. Thus, the decreasing or increasing of the energy does not necessarily mean that the left ventricle tires more or less.

Then, another parameter which do not come from the medical domain is defined and is called: efficiency of the left ventricle. It represents the per cent of energy provided by it and consumed by the TPR ($TPR^* + R_{arch}$) and given by Eq.5.2. This parameter could be seen as a definition of the useful energy provided by the left ventricle compared to the lost one (through viscous losses).

$$\eta_{TPR \text{ from } LV} = \frac{E_{TPR}}{E_{LV}} \quad (5.2)$$

Finally, another parameter which is verified, concerns the maximum pressure in the aorta. Indeed, this pressure should be limited in order not to damage the natural tissues. Thus, the defined maximum acceptable pressure in this part is 180 mmHg .

5.3.4 Results and discussion

According to the variables for the supply voltage of the DEA, a lot of solution for the activation is possible. In this chapter, one specific shape is proposed through the parameters defined in Table 5.3.

This activation consists of the case where the duty cycle of the activated DEA is equivalent to the time during which the aortic valve is open. The slope of the increasing and the decreasing of the nominal electric field are similar. This variation is not too steep in order to avoid the considerable variation of pressure during the activation and the deactivation.

To perform such study, the used parameters of the model in Fig.5.7 are provided in the appendix E. For the geometry and the model of the DEA, the length of the tube is half of the one of the ascending aorta, i.e. 40 mm . The internal diameter is the same as the ascending aorta, i.e. 25 mm . Concerning the thickness, 1 mm has been chosen. It allows obtaining an

Parameter of activation	Value
Max. nominal electric field $E_{elec.DEA} = U_{DEA}/(R_{ext} - R_{int})$	$60 [V \cdot \mu m^{-1}]$
Duty cycle 1 & 2	50%
Duty Up 1 & 2	10%
Duty const. 1 & 2	30%

Table 5.3 – Parameters of the shape of activation

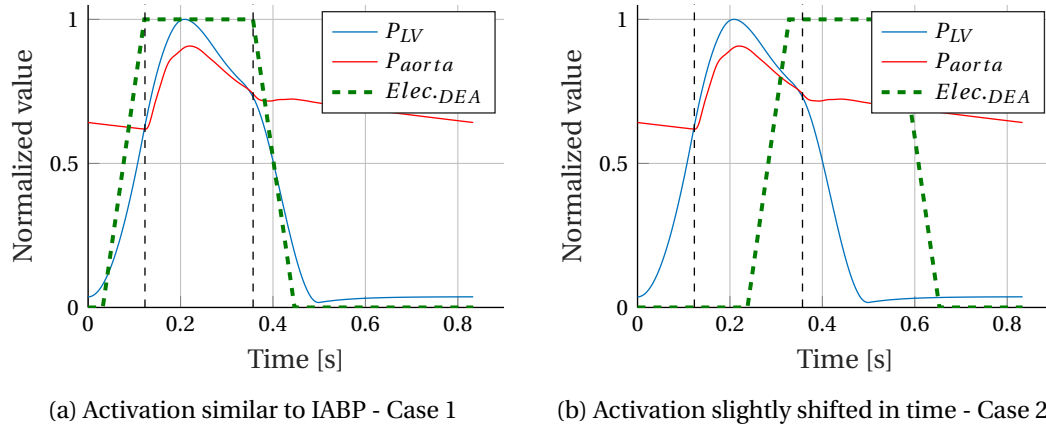


Figure 5.9 – Two examples of activation of the DEA

equivalent compliance characteristic similar to the natural ascending aorta.

The amplitude of the nominal electric field has been determined in order to ensure to not overpass the true electric field of $100 \text{ V} \cdot \mu\text{m}^{-1}$. It guarantees to stay below the maximum electric field which creates short-circuits through the dielectric (around $110 \text{ V} \cdot \mu\text{m}^{-1}$).

Influence of the phase shift

Too many solutions exist according to the variation of the different electronic parameters. For the previously proposed shape of activation, it has been shifted over one cycle with different delays. The results of the cardiac output, the energies, the ejection fraction as well as the efficiency of the left ventricle are provided in the appendix E. From the observations, it has been decided to develop two cases. The first one is the case when the DEA is activated right before the beginning of the opening of the aortic valve and decreased right after of its closing. This case corresponds to the intra-aortic balloon pump activation (Fig.5.8b). The second case is when the cardiac output has been increased and reached an optimum (see Fig.E.1a). It consists of the moment when the DEA is activated right before the end of the systole. The two cases are highlighted in Fig.5.9.

In Fig.5.10 and in the Table 5.4, the main results are provided and discussed in the next sections. In Fig.5.10a and in Fig.5.10b, respectively the healthy pressure in the left ventricle (blue) and the ascending aorta (red) and the flow rate in the aorta are provided. Concerning the flow rate, the one in the impedance $Z_{asc.1}$ (blue) and in $Z_{asc.2}$ (black) are given. For the flow rate in the compliance of the first and the second part of the ascending aorta (red - $C_{asc.1}$ and $C_{asc.2}$), the mean value is always null. However, according to the sign of the flow, it helps to understand if the two parts of the ascending aorta are filled or are emptied. In the next figures, only the one in the second region is provided.

Results: case 1

As mentioned earlier, the first case is similar to the one of the intra-aortic balloon pump. For the shape of the aortic pressure, the behaviour is similar to the one observed with IABP. When the voltage is increased (suction), the pressure before opening the aortic valve decreases, i.e. the afterload is reduced. Then, when the DEA is switched off (contraction), the pressure increases.

Concerning the variation of the flow rates, it seems that the main difference with the IABP concerns the one which comes from the descending aorta (black line in Fig.5.10d and through $Z_{asc.2}$ in Fig.5.7). When the DEA is activated, a flow comes back from the descending aorta in the DEA. However, no sources have been found in order to validate that with the IABP, this phenomenon does not appear.

When the actuator is switched off the blood is ejected from the DEA, and a portion of blood goes back in the direction to the left ventricle ($Z_{asc.1}$ in Fig.5.7). This back-flow is not a problem because it will supply the coronaries, allowing to irrigate the vessels of the heart with oxygen-rich blood. This phenomenon is beneficial according to surgeons and similar to the one observed with IABP. For all the studied flows and thus, the one in the TPR^* ($4.55 L \cdot min^{-1}$) and the R_{arch} ($0.47 L \cdot min^{-1}$), the mean values are always around the natural one, i.e. without activation. Even, if peak flows are lower than the natural one, the guaranty to keep a mean flow positive (in TPR^* and R_{arch}) and constant, which is very important for surgeons, is satisfied. The idea is to ensure to supply the capillaries with the blood during one cycle.

According to the performance presented in Table 5.4 (case 1), the main advantage concerns the decreasing of the energy provided by the left ventricle and the increasing of the equivalent efficiency. This effect could be assimilated to unload the left ventricle through the activation of the DEA. Through the consumption of the adenosine triphosphate (ATP), the left ventricle can contract and provides energy to the blood. The efficiency of conversion of the ATP into the energy provided by the left ventricle is very difficult to obtain. Thus, the decreasing of the energy provided by the left ventricle does not necessarily mean that this part of the heart is relieved. However, the proposed efficiency helps to understand the benefits, because the percentage of energy provided by the left ventricle compared to the one consumed by the TPR is higher. The rest consists of the energy dissipated in the other resistances (viscous losses). Because the cardiac output is kept constant, such a solution is helpful for the heart of a particular category of patient (e.g. people for which the left ventricle tired too much).

The radial stretch is important (64%), and according to space in the body, this value could be too large. Thus, according to the patient, the solution should be tuned to reach less deformation.

5.3. Integration of the DEA in the circulatory system

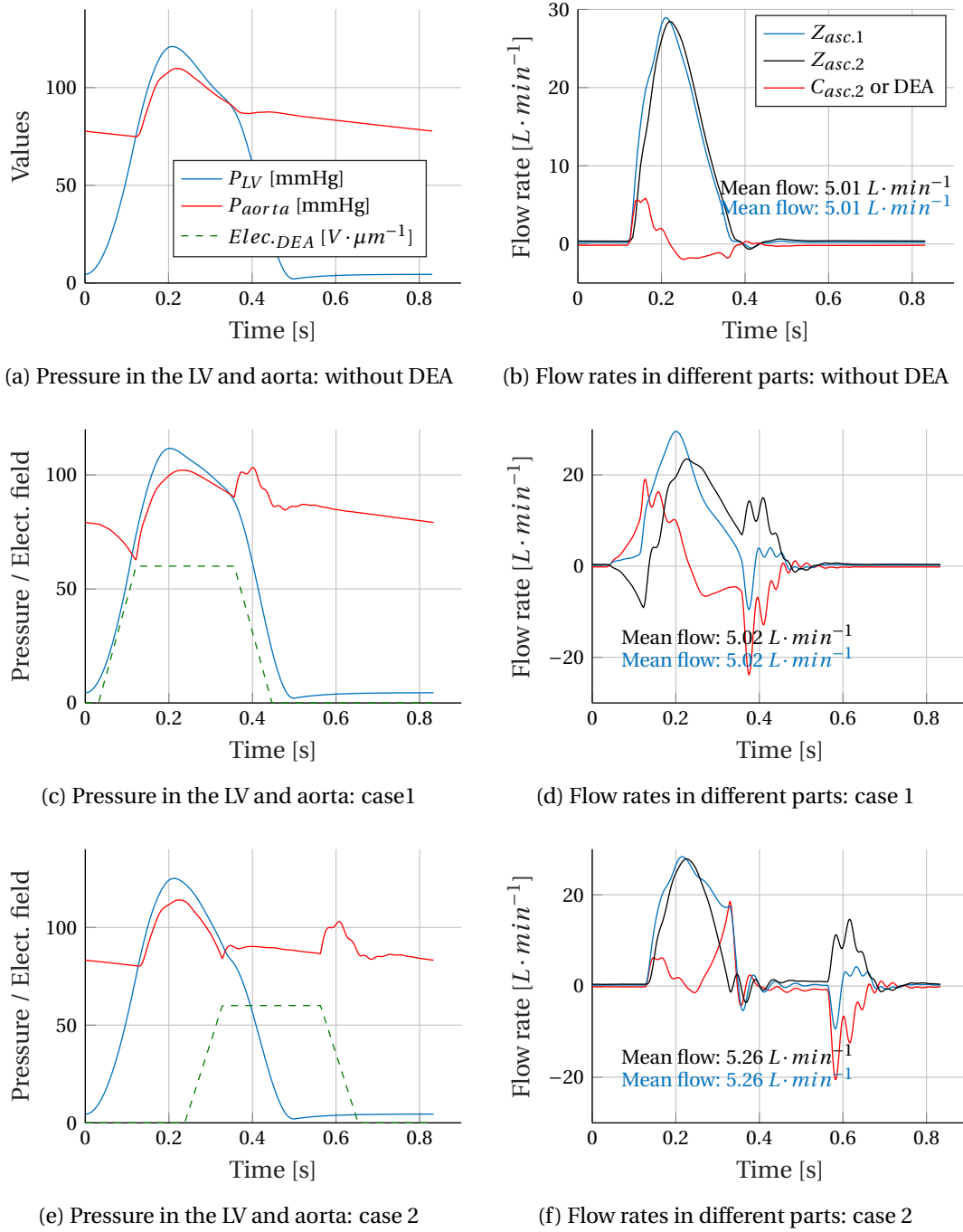


Figure 5.10 – Results from the models

Parameter of activation	Normal case	Case 1	Case 2
Cardiac output [$L \cdot min^{-1}$]	5.01	5.02 (=)	5.26 (✓)
Mean flow TPR^* [$L \cdot min^{-1}$]	4.54	4.55 (=)	4.77 (✓)
Max radial stretch []	1.25	1.64 (✓)	1.48 (✓)
Energy from LV [J]	1.0	0.92 (✓)	1.07 (✓)
Energy from DEA [J]	0	0.05 (✓)	0.007 (✓)
Energy to TPR ($TPR^* + R_{arch}$) [J]	0.77	0.77 (=)	0.84 (✓)
Efficiency LV [%] (Eq.5.2)	76.6	82.9 (✓)	78.5 (✓)
Eject. Frac [%]	62.3	62.4 (=)	65.4 (✓)

Table 5.4 – Hemodynamic values and efficiency for different cases

Results: case 2

The second case is treated because the cardiac output is increased with this solution (see Fig.E.1a). Because in several patients the main objective is to increase the cardiac output, this solution which allows such performance becomes interesting. Indeed, the IABP is sometimes used in such cases. By activating the system before that the aortic valve is closed (Fig.5.10e), the stroke volume is increased over one cycle (from 69 mL to 75 mL) which is equivalent to decrease the afterload. Through the softness of the membrane and the suction, more blood quits the left ventricle.

Another advantage with this solution concerns the back-flow of the descending aorta which is removed (Fig.5.10f). For the one present at the end of the systole, this phenomenon is also observed in a normal cardiac cycle. Thus, it should not be a problem.

As explained previously, the cardiac output is increased and also the energy provided by the left ventricle. The benefits are similar to the IABP even if the response of the aortic pressure is not comparable.

Concerning the ejection fraction, this parameter increases also.

With such a solution, the deformation (radial stretch) is lower (48% vs 64%) than the previous case. Thus, if the space in the body becomes a problem, this case could be more adequate than the first one.

5.3.5 Negative biasing through cardiac cycle

In chapter 3, negative biasing elements have been treated. It has been demonstrated that it is possible to obtain higher specific energy density with such element. In the studied application, it is also possible to use this phenomenon. Indeed, due to the variation of pressure because of the left ventricle, the adequate power supply allows for obtaining this biasing behaviour

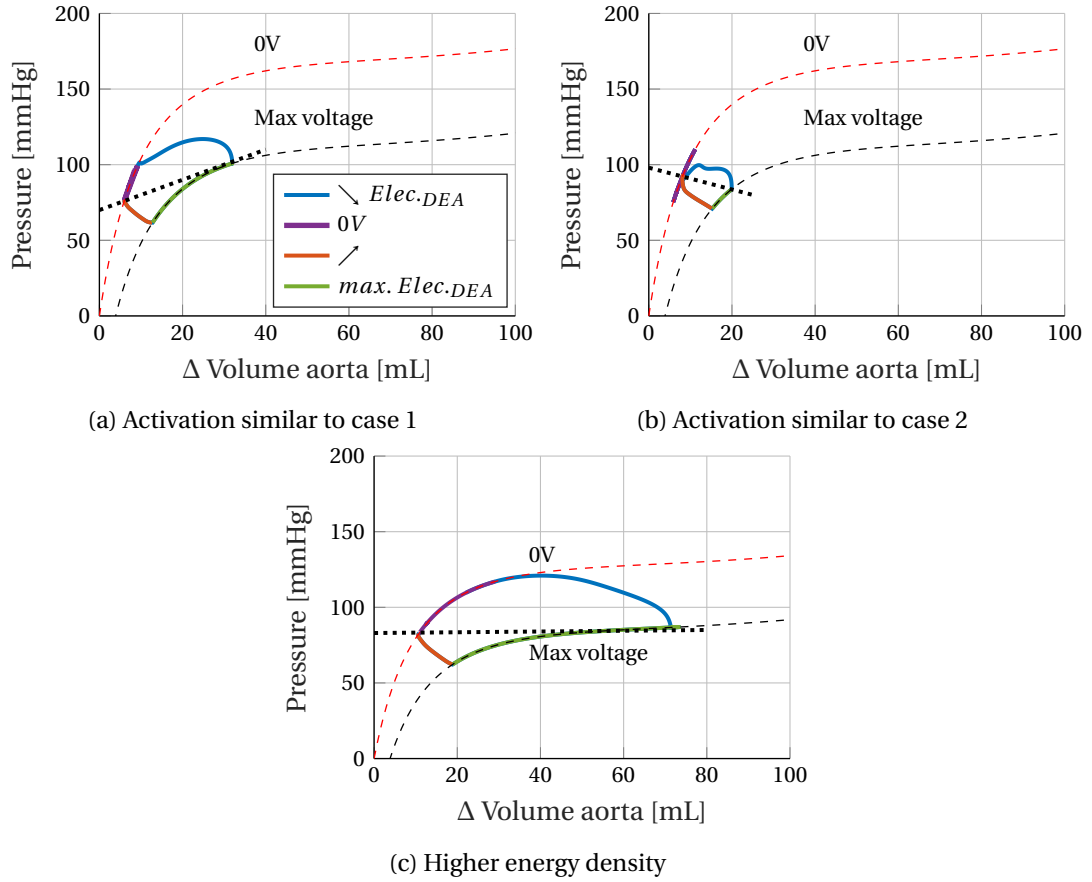


Figure 5.11 – Pressure vs volume variation in the aorta. Different case of cycle of activation

without any additional system.

The left ventricle acts such as a pump which ejects a quantity of blood in the ascending aorta such as previously described. When the DEA replaces this part of the aorta, it is submitted to this variation. By activating the actuator when the pressure is the smallest one and by deactivating when the pressure is the biggest one, the characteristic in Fig.5.11a is obtained. Even if in the figure the slope seems positive, this characteristic is called negative as seen in chapter 3, but without any additional spring. The advantage of the variation of pressure in the aorta is the possibility to use it such as negative biasing element. For such activation and design, an energy density of $27.5 \text{ mJ} \cdot \text{cm}^{-3}$ is reached (similar to the literature: $20 \text{ mJ} \cdot \text{cm}^{-3}$). In the previous study, case 1 works with such characteristic.

Without changing the geometry, but by varying the phase shift, the result in Fig.5.11b is obtained corresponding to case 2 of the previous section. It consists of an equivalent positive biasing element with an energy density of $9.2 \text{ mJ} \cdot \text{cm}^{-3}$.

Through such an application, the intrinsic variation of pressure coupled to the adequate activation allows using this negative biasing effect. However, another solution allows for increasing the energy density further. In Fig.5.11c, the stiffness of the DEA has been decreased.

It consists of the same geometry than previously studied with a strain energy density divided by a factor two. It allows to work in the smoother region of its characteristic, and an energy density of $107 \text{ mJ} \cdot \text{cm}^{-3}$ is reached. Even, if the negative biasing element helps increasing the energy density, the fact to work in the smoother region is more benefit. An ideal case would be to work in this smooth region with a negative biasing characteristic. However, in the case of the studied application, it is not possible to work in this smooth region due to the high variation of volume which is reached. No such space is available around the ascending aorta of humans.

The last proposed energy density is higher than the specific energy density presented in chapter 3. It could be explained by the fact that the proposed model does not consider the boundaries of the cylindrical tube (clamped at the extremities). Thus, intrinsic stability does not appear and does not limit the actuator. Moreover, the computed energy in this chapter is not exactly the specific energy density. Indeed, this energy density is computed as all the enclosed area such as in Fig.5.11. While in the chapter 3, only the area above the black dotted line was considered. The reason is that for the case in the previous chapter, the energy below the characteristic corresponds to kinetic energy and is lost through damping. Indeed, this zone is generally not usable in terms of useful energy.

5.4 Conclusion

The results mentioned above show some possibilities to use electroactive polymers such as cardiac assistance. The strategy of assistance where the tubular DEA is placed instead of a part of the ascending aorta was discussed. The cylindrical DEA has been designed in order to obtain similar stress characteristic than the natural aorta. The associated modified lumped parameters model which includes the DEA provides realistic results (similar to the one observed in literature) when the DEA is not activated. Through a simple shape of the electrical activation of the actuator, two cases have been highlighted. Both have provided interesting results in terms of decrease of the energy of the left ventricle or increase of the cardiac output. The negative biasing phenomenon due to the variation of the pressure seen by the DEA seems to play a role in order to increase the energy density and displacement of the actuator. The main potential problem is the induced back-flow when the DEA is deactivated. Such a phenomenon could create turbulence in the blood. However, the flow which returns in the coronaries to supply the heart is a positive result.

According to the disease, the activation is tunable, and the physiological parameters could be improved. However, the reaction of the patient is not considered, and it is challenging to predict such a phenomenon. For example and for a patient which is supported through the second case (Fig.5.9b), the body will probably decrease its heart rate in order to decrease the cardiac output ($5 \text{ L} \cdot \text{min}^{-1}$ being sufficient). Thus, the power provided by the left ventricle is reduced which could be an interesting solution. The real benefits of the proposed cardiac

assistance are difficult to discuss. Indeed, one effect or another could be positive but depends on the reaction of the patients themselves.

However, before concluding, all the results should be validated through in-vivo tests. The lumped model could also be improved to take into account ignored phenomenon that potentially could appear during animal experiments or real life. Moreover, the results obtained with the proposed solutions are for a given patient, and everybody is different. Thus, it is complicated to provide a more detailed conclusion.

The presented results in this section allow understanding the working principle and the effects of the actuator. Because the model of the cylindrical DEA is simplified, the results represent an ideal solution. By integrating a more accurate model which takes into account the boundaries and thus the intrinsic instabilities, more realistic solutions could be obtained.

Finally, an optimisation of the DEA could be proposed in order to provide more energy per cycle. The shape of activation could also be adapted in order to reach better performance.

6 Conclusions and Perspectives

The research proposed in this thesis is based on the technology of the dielectric elastomer. This domain allows developing soft actuators able to obtain large deformations. Generally, the actuators are proposed without providing any energy to an external load, the primary goal being to increase the stretch.

Thus, after a recall of DEA state of the art, the beginning of this research, inspired by the thermodynamic domain, was focused on the understanding of the technology. The development of a "0D" model of a planar uniaxial DE actuator is then developed. This model includes the variation of the stresses on the extremities according to the boundary conditions. The phase transition was studied in order to improve the definition found in the literature of the pull-in instability of DEAs.

A figure of merit (FOM) was proposed based on the study of the intrinsic stability of an ideal elastomer. This FOM includes electrical parameters, like the permittivity and the electrical breakdown limit, as well as the mechanical one (stiffness of the material). Moreover, the presence of an "elbow" in the stress characteristic was introduced, and its importance should be noted. This particularity helps the elastomer to stabilise and influences the energy density of such actuators.

An important topic of the development of actuators was then analysed in this thesis, i.e. the energy density. The introduced practical energy density, mainly used in the literature with quite significant values, is detailed. However, it seems that all the cycle could not be obtained when potential energy should be provided to a constant load.

From the "0D" model, another energy density was studied, i.e. the *specific energy density*. This definition seems to be more adequate when targeting a dielectric elastomer actuator. Through a case study (Elastosil®), it was shown that this energy density is ten times lower than the one usually mentioned in the literature.

The previous analysis has allowed studying another topic about energy density. Indeed, in the literature, the knowledge that the fact to increase the stretch allows to increase the energy density is discussed. From the "0D" model and the variation of parameters such as the constant load and the pre-stretch, it was observed to have similar behaviour. However, the

optima of the variation of stretch and energy density is not reached for the same parameters.

A solution to further improve the performance of a DEA was then introduced. A negative biasing element is used in order to increase the stretch and energy. From the "0D" model, it was also demonstrated that the optima of the performance are not coincident. However, with such an element, the energy density of the actuator was more than doubled compared to a constant load.

Due to the particular shape of the considered actuator, the design of a particular spring was proposed having a negative force characteristic over a certain range of deformation. Its particularity is to be cylindrical, free in its centre and can be deformed purely radially (no variation in the length direction). It allows obtaining a cylindrical actuator which can vary its internal volume in order to create actuators such as a pump.

A design of experiment has been proposed in order to understand the influence of the geometrical parameters on the force characteristic of the spring. It has also been demonstrated that the radial force of the spring could be analytically linked to the one obtained through an equivalent deformation of the beam in a particular direction dependent only on the number of modules. This solution has allowed to significantly decrease the computational time with FE analysis by reducing the number of geometrical parameters.

The working principle of the actuator has been validated through measurements. A cylindrical DEA has been rolled around the compressed spring and it has been demonstrated that the negative characteristic of the spring allows obtaining better performance than a constant load.

Finally, the cardiac assist device has been investigated due to the large similarity between the studied technology and this medical application. The proposed solution consists of replacing the natural ascending aorta with a tubular DEA. By activating the actuator according to the cardiac cycle, the actuator helps the left ventricle to work.

A modified lumped parameter model adapted to our case was proposed by integrating the model of the DEA instead of the one of the ascending aorta. Many possibilities of activation existed, but two major ones have been highlighted. The first one works such as the intra-aortic balloon pump, which is an existing invasive system already used by surgeons. Similar behaviour was confirmed, and it has been shown that the energy provided by the left ventricle was reduced through the proposed assistance. The second case consists of activating the DEA such that the cardiac output is increased, offering new perspectives in the domain of cardiac assistance.

6.1 Original contributions

In the proposed work, three main topics have been treated. Through a proposed "0D" model which considers the phase transition, a study of the energy density for the dielectric elastomer actuator was performed. Then, due to the cylindrical shape of the considered actuator and the well-known negative biasing load used to improve the performance, a special spring has been designed and analysed. With the aim of the cardiac assist device, a solution was proposed to

apply the DEA based technology in order to relieve the heart.

- *Understanding of linear uniaxial DEAs*

In this particular topic, three important phenomena have been putted forward.

- 1) The model and the study of the DEA through the thermodynamic domain was already performed. However, the analogy has been extended. The graphical representation of the phase transition and the use of tools like the Gibbs free energy, improve the understanding of this particular technology. Both have allowed providing a "0D" model able to simulate any linear uniaxial DE actuator.
- 2) The high energy density is often used in order to introduce the DEA. However, this aspect has been poorly investigated in the literature. Through the proposed definitions of the energy density which consider different boundary conditions, a better understanding of this assessment parameter was provided. According to the application, the adequate definition should be used in order to determine the potential of such technology. The *specific energy density* was introduced in order to represent the performance of a dielectric elastomer used such as an actuator. Indeed, this definition seems to reflect better the energy that the technology could provide to an external load compared to the one presented in the literature.
- 3) In order to improve the performance of the DEA, the main objective is often to increase the stretch. In this study, the constant biasing element, the negative one and the pre-stretch have been used in order to improve the stretch and the energy density of linear actuators. Through the "0D" model and the influence of the three aforementioned parameters, it is demonstrated that for some particular cases, the Elastosil® film reaches the bigger variation of stretch or the optimum specific energy density for different working conditions. Thus, the popular believes that the increase of stretch allows increasing the energy density, is validated for specific values (pre-stretches and biasing loads). However, it is not true for all of them. In all likelihood, this observation is valid for other material described through an hyperelastic model.

- *Original cylindrical actuator with radial deformation*

- 1) The negative biasing element is used in the literature in order to improve the stretch of DEA. The design of an original cylindrical spring with a radial displacement has been proposed. The use of arch-shaped beams allows reaching a negative characteristic of the radial force-displacement relationship without any additional external trigger.
- 2) By rolling an elastomer, composed of two electrodes, around this pre-compressed spring, a cylindrical actuator has been obtained. It consists in the first DEA which gathers the purely radial displacement of a cylindrical actuator and the negative stiffness spring.

- *Cylindrical DEA used as cardiac assist device*

Finally, a cardiac assist device has been proposed using the studied cylindrical DEA. A simple model which provides the pressure-volume characteristic is integrated into a lumped parameters model. This model allows simulating the circulatory system of a patient. According to the power supply, the cardiac output could be increased which is an essential objective for surgeons. Another interesting result is the possibility to decrease the energy provided by the left ventricle which allows to less solicit it. Through these observations, it is demonstrated that the technology of dielectric elastomer could be useful to assist the heart.

6.2 Outlook

Several improvements or other research fields could be proposed to complete this work. Five main directions have been identified and are developed here.

- *Further study of the cylindrical spring*

The proposed cylindrical spring with the negative stiffness characteristic has been studied, and its global behaviour has been proved. Regarding the design itself, one major problem was the unsymmetrical deformation of the actuator. In order to counter this problem, the design could be improved in order to remove the tangential component of the force which consists certainly in the main factor which induces the asymmetry. An head-to-tail design of the beams could maybe cancel such component. Then, a new spring could be manufactured in order to perfectly match the stress characteristic of the membrane and to obtain an actuator able of higher energy density.

- *Development of an ideal elastomer*

The study of an ideal elastomer with a linear stress-stretch characteristic has allowed determining a figure of merit dependent on both the electrical and mechanical properties of the material. With such FOM, available elastomer could be compared and classified in function of their energy density. Then, the conception of new material could be performed. According to the figure of merit, either Young's modulus could be decreased, or the permittivity increased. If possible, the viscosity should be kept as low as possible. It should be noticed that according to the FOM, Young's modulus could be increased (stiffer elastomer) if the ratio $\epsilon_0 \epsilon_r E B^2 / Y$ stays constant. This aspect constitutes a new objective in the domain of material science.

- *Analytical model of cylindrical DEA*

For the linear planar dielectric elastomer actuator, a "0D" model, which takes into special account phenomena such as the phase transition or the boundary conditions, has been provided. Because of the special cylindrical shaped actuator used in this study, an equivalent "0D" model more precise should be developed. Indeed, in the proposed *pressure-volume* relationship provided in the last chapter dealing with the cardiac assist

device, the deformation was supposed uniform. Specificity of the cylindrical geometry is that another mechanical instability appears by fixing the cylinder at the two extremities similar to the phase transition and should be considered in the model. However, it seems not realistic to target an analytical model. Numerical tools are certainly able to solve such phenomenon.

Through all these improvements of the model, the results obtained for the cardiac assist device will be more precise.

- *Validation of the lumped model including the influence of the DEA*

A DEA based cardiac assist device was proposed in order to relieve the heart. It has been demonstrated the feasibility of such assistance. However, the lumped parameter model which considers the DEA should be validated. Through a mock-up test bench which simulates the circulatory system, such validation could be performed. Then, because the reaction of the body is complicated to predict, the real possibility of assistance should be tested in-vivo. Indeed, several phenomena or adaptive reactions of the body are currently ignored and thus difficult to implement in a closed loop system.

- *Integration of the proposed system*

Once all the tests have been performed on the actuator, it should be tested in real condition. To perform such an experiment, the actuator will be integrated replacing part of the aorta through a surgical operation. A first problem is to define how the actuator will be fixed to the cut ascending aorta.

Moreover, the proposed solution consists of replacing existing aorta. This solution is not the most appropriate one in terms of invasive surgery and contact with the blood becomes a problem. It could be imagined to create a tubular actuator which is placed around the natural aorta. Because this actuator does not allow contraction, the cylindrical DEA could be rolled around the aorta by slightly compressing it. When the actuator is supplied, the system could expand up to the natural expansion of the aorta if the actuator is not physically glued to the aorta. This solution would allow reaching higher variation of volume because the original state being smaller than the natural aorta.

A Effective work of a DEA

A.1 Definition of the problem

In the literature, it seems that the proposed energy density is not adequate for an actuator but represents a theoretical maximum value. The specific energy density consists of an alternative definition and which can represent the effective energy density of an actuator done with this technology. In this appendix, the objective is to explain through an example, what could be a better representation of the energy density when the objective is to provide potential energy to a load.

To perform such an explanation, let us consider a planar dielectric elastomer actuator hold by an extremity and subjected to the gravity (Fig.A.1 - point 1). Two loads are in their initial position and supposed with the same mass. The first load (m_1) is located at λ_2 and the second one (m_2) at the position λ_3 . The main goal of this actuator is to provide potential energy to the load m_2 . Moreover, two electrodes are placed on the DEA to be able to activate it.

A.2 Effective work for a constant load

Definition of the cycle

The proposed cycle to provide potential energy to a load is represented in Fig.A.1 and the equivalent cycle on the nominal stress - stretch characteristic is given in Fig.A.2a. This stress characteristic allows representing the mechanical stress characteristic of the DEA when it is at rest(*OFF*) and when it is submitted to a constant voltage (*ON*)

Initially, the actuator states in position "0" which is equivalent to $\lambda = 1$ and when it is activated, the DEA reaches the position λ_2 (1). At this position, a load m_1 which is initially at this level is hanged to the actuator. Then, the system reaches the position λ_3 (2) where another load m_2 is hanged to the rest of the system. The DEA plus the two loads go down to the position λ_4 (3). At this height, the two loads have provided potential energy to the DEA. When the voltage

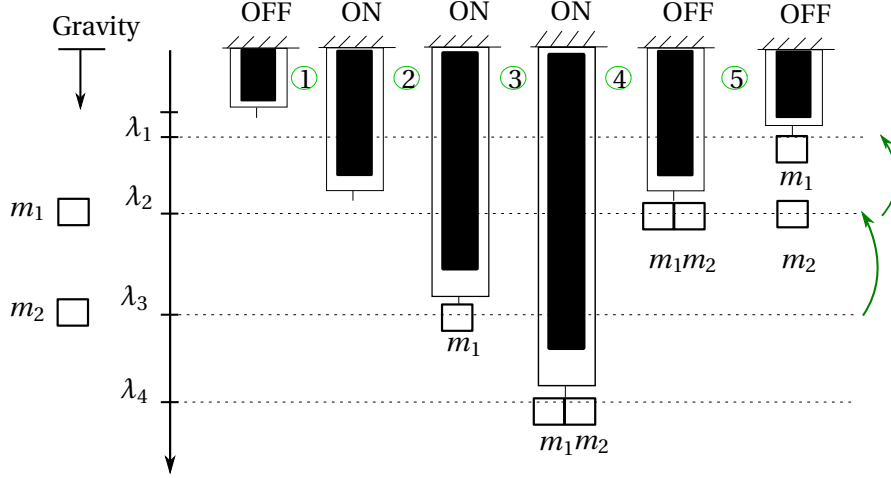


Figure A.1 – Example of DEA with two loads

is turned off, the complete system goes up to λ_2 (4). Therefore, the second load m_2 which is moved up from λ_3 to λ_4 wins potential energy. This load is left at this level, and the system of the DEA and the first load move up to λ_1 .

The first load m_1 is used as *pre-load*. In the chapter 2, this pre-load is used to increase the performance by adapting the area of the specific energy density.

Definition of the specific energy density

The specific energy density (blue area in the Fig.A.2b) highlights the energy density provided to the load m_2 . Indeed, the steps (3) and (4) could be done simultaneously which allows to obtain the path given by green dashed arrow. In the previous explanation, these two actions were done separately. The area enclosed by the two previously mentioned steps are not considered because, it represents always a kinetic energy lost during the cycle.

In the highlighted zone (blue area), the part *I* and *III* correspond to kinetic energy and the zone *II* is linked to the potential energy. It has been decided to consider these three zones to define the specific energy density.

In conclusion, m_1 allows to consider a pre-load, and the blue area allows to determine an energy density.

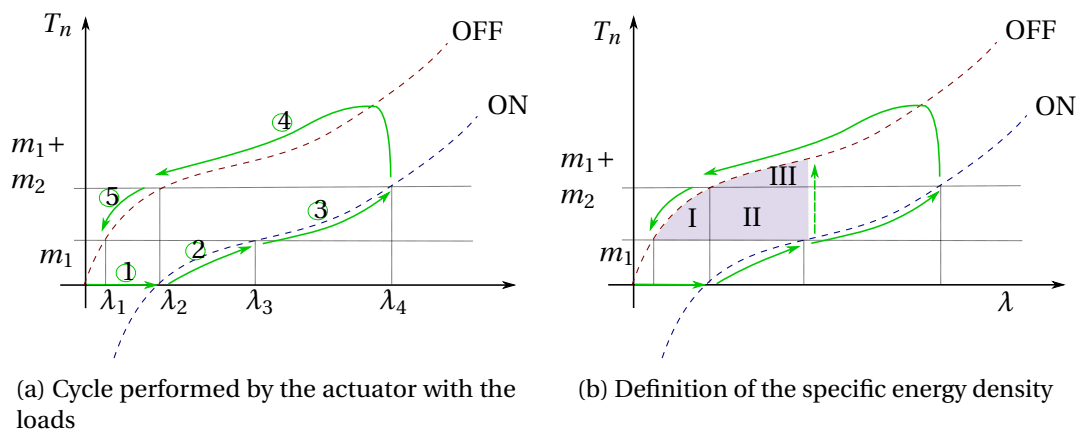


Figure A.2 – Schema of the nominal stress-strain characteristic to determine the specific energy density

B Design of experiment for the proposed spring

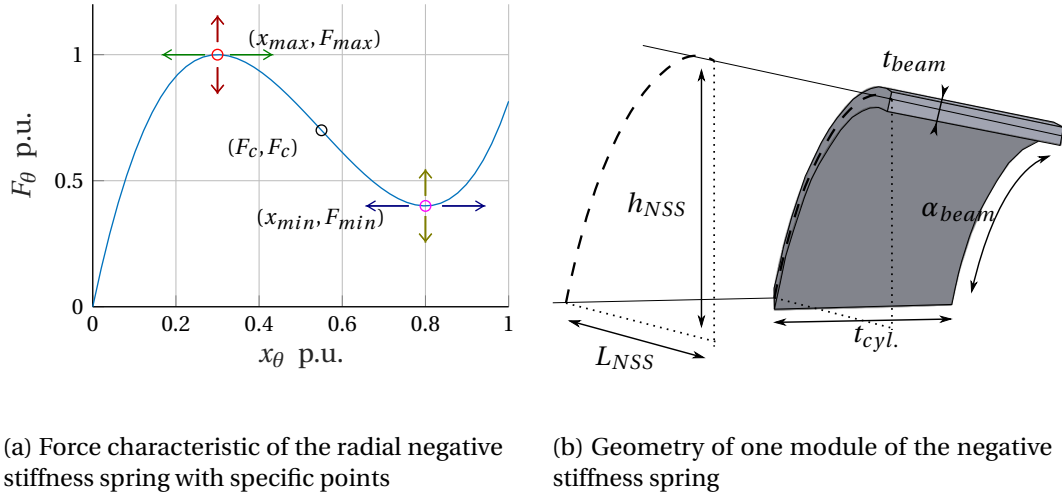


Figure B.1

The objective of the proposed design of experiment is to determine a model of the *force vs displacement* characteristic of the negative stiffness spring presented in chapter 3. The model does not consider all the geometry of the spring. Only the beam is studied according to its (F_θ, x_θ) characteristic. The radial components could be obtained through analytical post-processing.

The results in this appendix highlight that it seems very difficult through the proposed approach to provide an accurate model. Indeed, the errors of these models are too significant to consider them efficient. However, such study allows understanding the influence of the geometrical parameters on the force characteristic.

Four parameters have been highlighted in order to define the studied characteristic in function of the geometrical parameters (Fig.B.1b), i.e x_{max} , x_{min} , F_{max} , F_{min} (Fig.B.1a). As explained in the previous cited chapter, it has been shown that only one module defines the studied characteristic, if the beam of this module is deformed according to a specific path (given by

θ). Such a conclusion allows decreasing the computation time of the characteristic with FE analysis.

B.1 Methodology

To perform the design of experiment, the Doehlert model is chosen [105]. In order to determine the influence of input parameters on a studied one, the main objective is to define the boundaries for the input parameters and found a polynomial response which fit the answer of the model in these boundaries. It consists of an empirical model. In order to obtain the tested beams, FE analysis has been used.

The mind map of experiment is presented in Fig.B.2. As previously mentioned, the objective is to determine F_{max} , F_{min} , x_{max} and x_{min} of the force characteristic. The geometrical parameters are the arc length of the beam (α_{beam}), the thickness of the beam (t_{beam}), the length between the two feet of the beam (L_{NSS}), the thickness of the cylinder ($t_{cyl.}$) and finally the diameter of the cylinder (D_{int}).

B.2 Model of estimation

To perform the analysis, three polynomial models have been tested, i.e. linear, linear with interaction and quadratic model which are defined as:

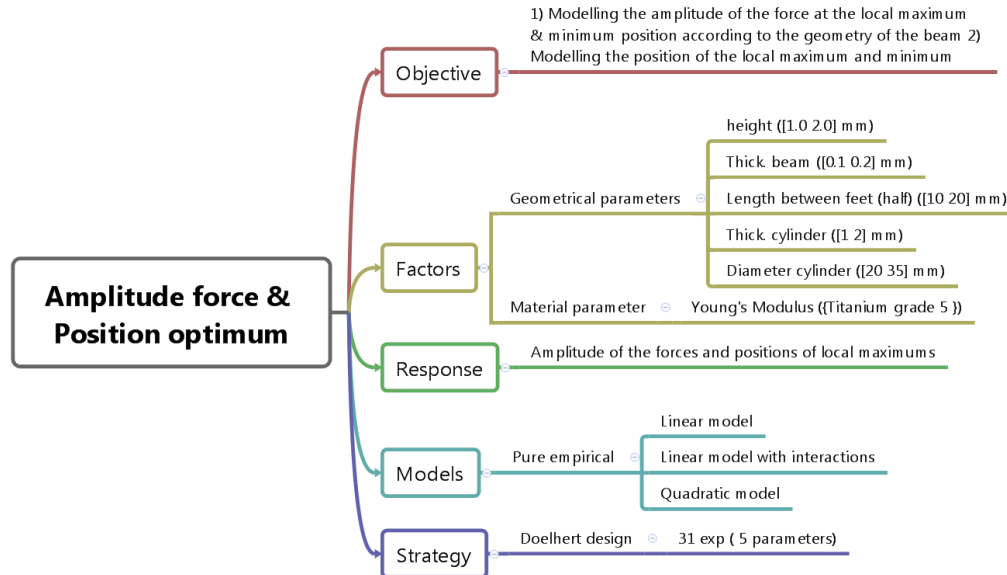


Figure B.2 – Mind map of experiment

- linear:

$$Y_{lin.} = a_0 + \sum_{i=0}^5 a_i X_i \quad (B.1)$$

- linear with interactions:

$$Y_{lin.withinter.} = a_0 + \sum_{i=0}^5 a_i X_i + \sum_{i<j}^{10} a_{ij} X_i X_j \quad (B.2)$$

- quadratic:

$$Y_{quad.} = a_0 + \sum_{i=0}^5 a_i X_i + \sum_{i<j}^{10} a_{ij} X_i X_j + \sum_{i=j}^5 a_{ij} X_i X_j \quad (B.3)$$

with:

- a_i : coefficient containing the main effect
- a_{ij} : coefficient containing the interaction effect
- Y : response
- X_i or X_j : inputs of the model

B.3 Results

The coefficients for the three models and for the two extrema (x_{max}, x_{min}) are provided in Fig.B.3. For the results of the forces (F_{max}, F_{min}), the coefficients are given in Fig.B.4.

Concerning the parameters of the linear with interaction model, the following coefficients are given, in this order: ($a_0, a_1, a_2, a_3, a_4, a_5, a_{12}, a_{13}, a_{14}, a_{15}, a_{21}, a_{23}, a_{24}, a_{25}, a_{34}, a_{35}, a_{45}$). For the quadratic model, the coefficients are: ($a_0, a_1, a_2, a_3, a_4, a_5, a_{12}, a_{13}, a_{14}, a_{15}, a_{21}, a_{23}, a_{24}, a_{25}, a_{34}, a_{35}, a_{45}, a_{11}, a_{22}, a_{33}, a_{44}, a_{55}$).

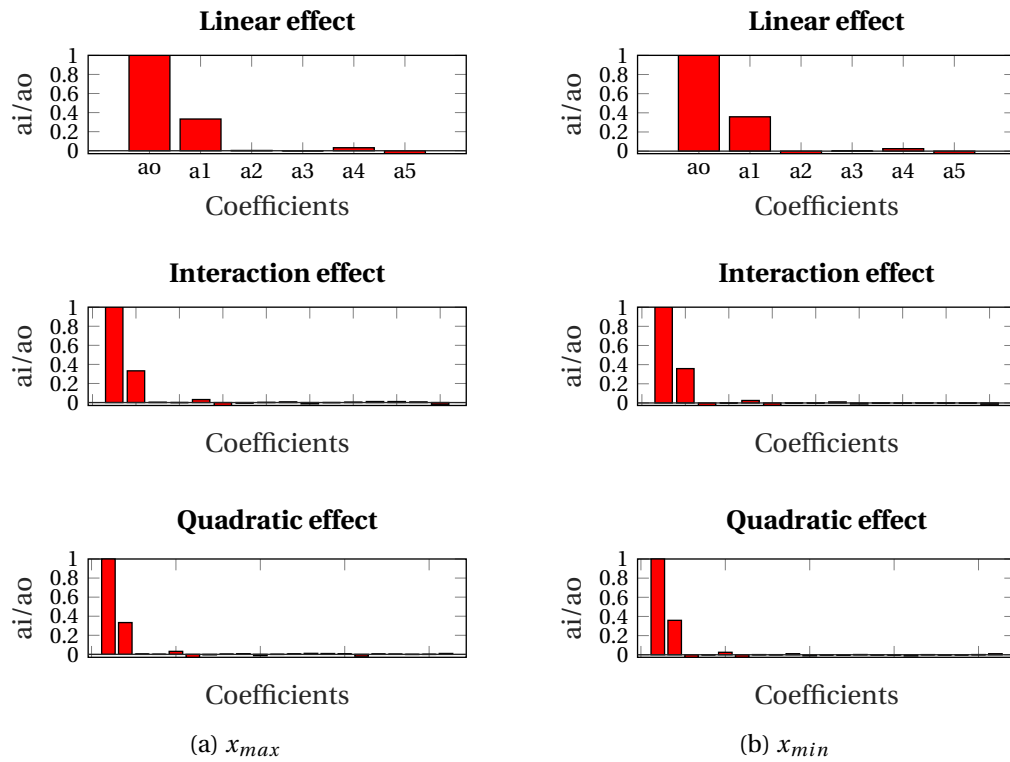
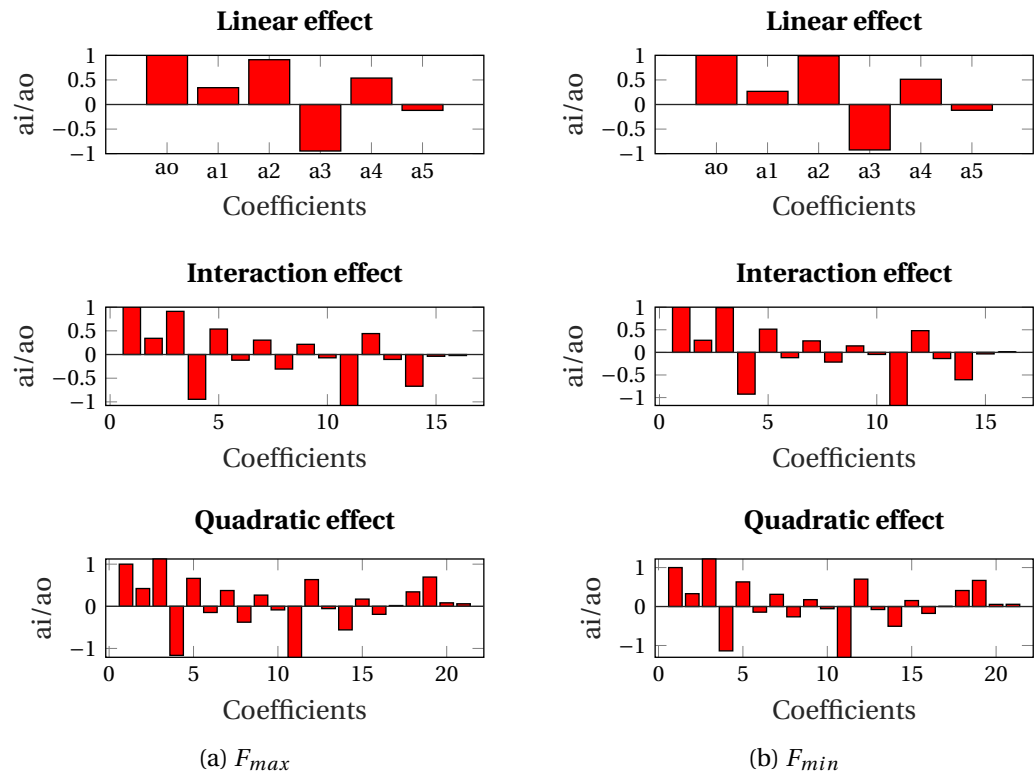


Figure B.3 – Results for linear , linear with interaction and quadratic model for x_{max} and x_{min} .

Figure B.4 – Results for linear, linear with interaction and quadratic model for F_{max} and F_{min} .

C Equivalent model of a radially stretched elastomer

C.1 Equivalent model

The analytical model to describe the deformation of a cylindrical elastomer with thin walls is well established. However, if for membranes with planar configuration the parameters of the strain energy density function are easily determined through pull-test, those of the cylindrical shape is more complicated to obtain. In this appendix, a solution is given in order to counter this problem based on the analysing of a circular segment. The main objective is to obtain the parameters of the model for the cylindrical elastomer where its length is kept constant. The geometrical parameters of the cylinder are defined in Tab.C.1.

For this analyse, a circular segment defined by its angle (α_m) is considered (left figure in Fig.C.1). The segment is deformed radially by its two extremities (Δr), and each of them induces the force $F_{rad.}$ in the previously mentioned direction. By deforming the segment in such configuration, its shape tends to be similar to a planar membrane such as represented in the right part of Fig.C.1. In such deformation, the length of the membrane is equal to s . The force in the radial direction is composed of the force of the considered membrane (i^{th}) and

Geometrical parameters	Definition
Initial internal radius	R_{int}
Initial external radius	R_{ext}
Deformed internal radius	r_{int}
Deformed external radius	r_{ext}
Initial thickness	t_0
Deformed thickness	t
Length of the cylinder	L_0
Angle of circular segment	α_m

Table C.1 – Definition of the geometrical parameters of the cylinder

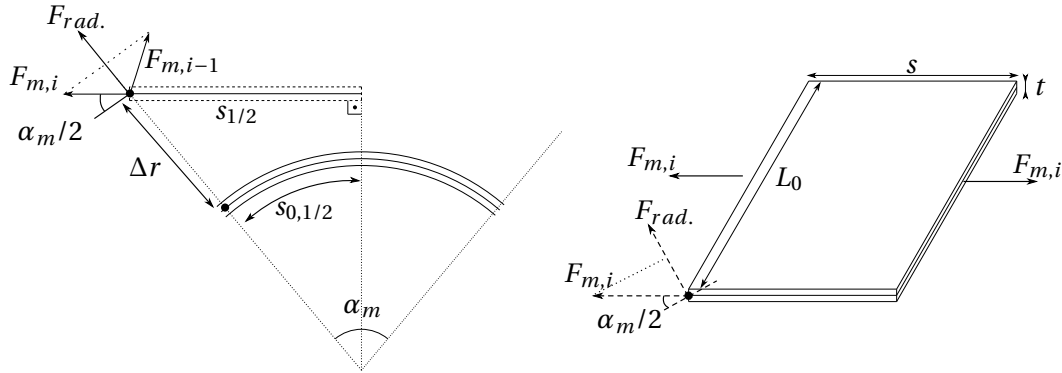


Figure C.1 – Circular segment of cylinder and its equivalent deformation in the pure-shear configuration

the previous one $((i-1)^{th})$ located at its left. Their relation is given by:

$$F_{rad.} = F_{m,i} + F_{m,i-1} = F_{m,i} \cdot 2 \sin\left(\frac{\alpha_m}{2}\right) \quad (C.1)$$

where $F_{m,i}$ is the force perpendicular to the edge of the planar representation of the segment. Because the length of the cylinder is kept constant, the conservation of volume of the elastomer induces:

$$\lambda_t \cdot \lambda_s \cdot 1 = 1 \quad (C.2)$$

where λ_t and λ_s represent the stretch in the thickness and the width direction respectively. The ratio between the length of the tube (L_0) and the initial length of the arc (s_0) is big enough in order to consider the membrane in the pure-shear configuration, i.e. the stress in the axial direction is non-null. The force to deform the membrane by a stretch equivalent to λ_s is then:

$$F_{m,i}(\lambda_s) = \frac{L_0 t_0}{\lambda_s} \left(\lambda_s \frac{\delta W}{\delta \lambda_s} - \lambda_t \frac{\delta W}{\delta \lambda_t} \right) \quad (C.3)$$

The second term of Eq.C.3 represents the stress in the width direction of the elastomer. Through the definition of the strain energy density function and the Yeoh model, Eq.C.3 becomes:

$$F_{m,i}(\lambda_s) = \frac{L_0 t_0}{\lambda_s} (2\lambda_s^2 - 2\lambda_s^{-2})(C_{10} + 2C_{20}(\lambda_s^2 + \lambda_s^{-2} - 2) + 3C_{30}(\lambda_s^2 + \lambda_s^{-2} - 2)^2) \quad (C.4)$$

Then, the variable change is performed in order to obtain the force in function of the radial deformation. In order to achieve this, the definition of the length of the undeformed segment

C.2. Link between the radial force and the equivalent pressure

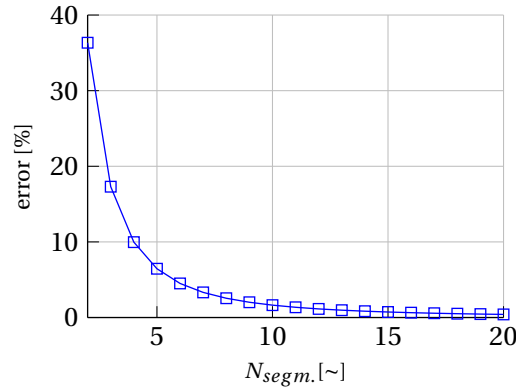


Figure C.2 – Influence of the number of modules on the hypothesis between λ_s and λ_r

(circular geometry) and the deformed one (planar geometry) are used and λ_s becomes:

$$\lambda_s = \frac{s}{s_0} = \frac{2\sin(\alpha_m/2)\lambda_r R_{int}}{\alpha_m R_{int}} = \frac{2\sin(\alpha_m/2)}{\alpha_m} \lambda_r \quad (C.5)$$

From this definition and by considering α_m equivalent to the number of segment divided by the circumference of the cylinder, the limit when the number of segment tends to infinite becomes:

$$\lim_{N_{segm.} \rightarrow \infty} \frac{2\sin(\alpha_m/2)}{\alpha_m} = \frac{2}{2\pi} \lim_{N_{segm.} \rightarrow \infty} \sin\left(\frac{\pi}{N_{segm.}}\right) N_{segm.} = 1 \quad (C.6)$$

Thus, by considering the number of segment sufficiently high, the stretch λ_s becomes equivalent to the radial stretch (λ_r). Fig.C.2 shows the error of this consideration in function of the number of circular segments. Above $N_{segm.} > 4$, the error is less than 10%, and for a number of segments superior to 6, this error is below 4.5%.

From Eq.C.4, Eq.C.5 and the hypothesis about the radial stretch, Eq.C.1 becomes:

$$F_{rad.} = \frac{L_0 t_0}{\lambda_r} \alpha_m \left[(2\lambda_r^2 - 2\lambda_r^{-2})(C_{10} + 2C_{20}(\lambda_r^2 + \lambda_r^{-2} - 2) + 3C_{30}(\lambda_r^2 + \lambda_r^{-2} - 2)^2) \right] \quad (C.7)$$

C.2 Link between the radial force and the equivalent pressure

Let's now consider the theory of thin shell for a cylinder which puts forward that the pressure in the tube is given by:

$$P_{cylind.} = \sigma_h \frac{t}{r} = \sigma_h \frac{\lambda_t t_0}{\lambda_r R_{int}} \quad (C.8)$$

where σ_h is the hoop stress in the cylinder and r is the equivalent radius which could be

Appendix C. Equivalent model of a radially stretched elastomer

approximated by the internal radius if the thickness is considered as small enough.

From Fig.C.3a and by considering the cylindrical coordinate system of the circular segment, the force balance provides the reaction force $F_{press.}$ which represents an equivalent force in the radial direction.

$$F_{press.} = 2F_{hoop} \sin(\alpha_m/2) = 2 \sin(\alpha_m/2) \cdot \sigma_h t L_0 \quad (C.9)$$

From the Eq.C.6, $2 \sin(\alpha_m/2)$ is equivalent to α_m if the number of segment is big enough. Thus, from Eq.C.8 and by highlighting the internal radius (r_{int}), the cylindrical equivalent force (Eq.C.9) which could be linked to an equivalent pressure applied on the surface of the segment, becomes:

$$F_{press.} = \frac{\sigma_h t}{r_{int}} (r_{int} \alpha_m L_0) = P_{cylind.} \cdot S_{int} \quad (C.10)$$

where S_{int} is the internal surface of the circular segment which is dependent on the internal radius. In Fig.C.3b, the error between the pressure determined through Eq.C.10 and the real pressure is given and obtained through FE analysis. For the different angle of the segment, the membrane is deformed by its two extremities like in Fig.C.1, and the results are used to compute the equivalent pressure given by Eq.C.10. This analyse is performed for different radial stretches.

Eq.C.10 is reasonable (lower than 12% for deformation bigger than 5%) for a number of segment sufficiently high (greater than 12).

Then, the assumption that the elastomer is incompressible is taken which induces the following equality:

$$\pi(R_{ext}^2 - R_{int}^2)L_0 = \pi(r_{ext}^2 - r_{int}^2)L_0 \quad (C.11)$$

with the definition of the undeformed and deformed thickness, the previous equation is written as:

$$1 = \frac{t_0^2 - 2R_{int}t_0}{t^2 - 2r_{int}t} \quad (C.12)$$

Due to the hypothesis that the thickness is much smaller than the radius, the Eq.C.12 highlights that $\lambda_t \equiv 1/\lambda_r$. Through this consideration and Eq.C.10, the equivalent force in the radial direction becomes:

$$F_{press.} = \frac{L_0 t_0}{\lambda_r} \alpha_m \cdot \sigma_h(\lambda_{r_{int}}) \quad (C.13)$$

This last equality shows that Eq.C.7 and Eq.C.13 are similar. Thus, the equivalent pressure

C.2. Link between the radial force and the equivalent pressure

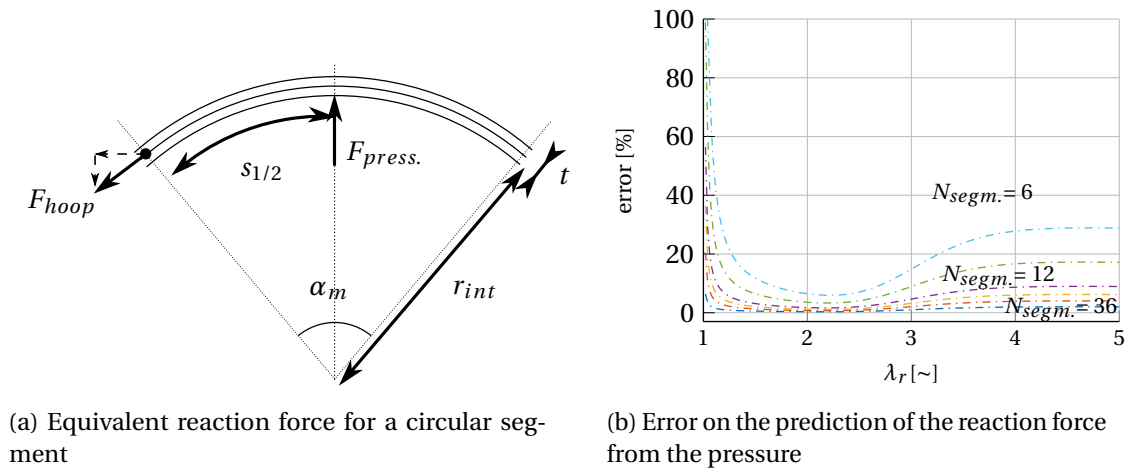


Figure C.3 – Equivalent pressure from the radial force

$(P_{cylind.})$ is linked to the radial force applied at the extremities of the segment ($F_{rad.}$) if the number of modules is sufficiently high.

D Model of a uniformly deformed cylindrical DEA

In order to describe the behaviour of a cylindrical DEA submitted to internal pressure, a model is proposed with several assumptions. The main one is that the length of the tube is constant when the cylinder is submitted to an external difference of pressure or voltage. Moreover, the pressure in the cylinder induces a uniform deformation along the length of the DEA. However, an initial pre-stretch in the axial direction could be applied to the DEA.

The electrodes are located on the inner and outer surface of the tube, and the electric field tends to decrease the thickness of the elastomer. Finally, the conservation of the volume of the highly deformable elastomer is considered. Through the previous hypothesis and the thin-shell theory, the characteristic of the variation of the internal volume of the tube according to the variation of the inner pressure is provided.

D.1 Pressure characteristic of cylindrical DEA

The studied cylindrical DEA consists in a tube defined by its internal (r_{int}) and external (r_{ext}) radii (Fig.D.1) and given by:

$$r_{int} = \lambda_{rint} \cdot R_{int} \quad (D.1) \quad r_{ext} = \lambda_{ext} \cdot R_{ext} \quad (D.2)$$

where λ_{rint} and λ_{ext} are respectively the internal and external stretch of the initial internal (R_{int}) and external (R_{ext}) radii. As previously explained, the studied actuator has an axial length which is kept constant ($l = \lambda_z L$). The axial stretch consists only in a pre-stretch deformation. Thus, the relation between the two radii is known:

$$\lambda_{ext} = \sqrt{\lambda_z^{-1} - \left(\frac{R_{int}}{R_{ext}}\right)^2 (\lambda_z^{-1} - \lambda_{rint}^2)} \quad (D.3)$$

The radial equilibrium equation [106] obtained through the divergence of the stress tensor in the cylindrical coordinate system could be used in order to determine the difference between the internal ($\sigma_{r,int}$) and the external ($\sigma_{r,ext}$) radial stress which corresponds to the difference

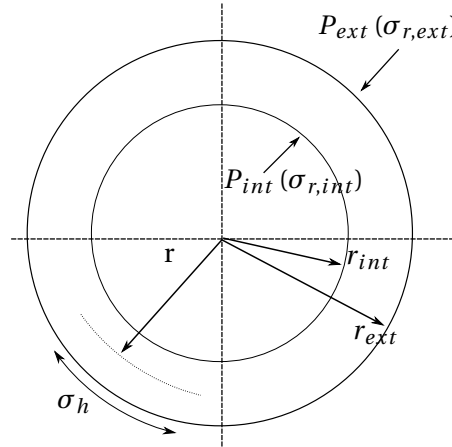


Figure D.1 – 2D model of cylindrical DEA

of pressure applied between the wall of the cylinder.

$$\frac{\delta \sigma_r}{\delta r} + \frac{\sigma_r - \sigma_h}{r} + \frac{1}{r} \frac{\delta \sigma_{rh}}{\delta \sigma_h} + \frac{\delta \sigma_{rz}}{\delta z} = 0 \quad (\text{D.4})$$

where the term σ_r represents the radial stress, σ_h the hoop stress (also called circumferential stress and often denoted θ), σ_{rh} and σ_{rz} are the shear stresses and considered null. r is the deformed radius of the cylinder along the thickness (Fig.D.1).

As previously explained, the elastomer is not defined through a constant Young's modulus but through a hyperelastic model. In this thesis, the same model is used for all the studied cases, i.e. the Yeoh model. In the cylindrical coordinate system, and according to the derivative of W , each i^{th} component of the stress in the principal directions are defined as [38]:

$$\sigma_i = \lambda_i \frac{dW(\lambda_r, \lambda_h, \lambda_z)}{d\lambda_i} - p \quad (\text{D.5})$$

where $\lambda_r (= dr/dR)$, $\lambda_h (= r/R)$ and $\lambda_z (= l/L)$ are respectively the radial, the hoop and the axial strain and p is an unknown hydrostatic pressure. Assuming incompressibility of the polymer and a constant axial length during the deformation ($\lambda_z = \text{const}$), the radial stretch becomes $\lambda_r = (\lambda_h \lambda_z)^{-1}$.

According to Zhu [107] and the definition of the stress in the principal directions, the difference between the radial and the hoop stress becomes:

$$\begin{aligned} \sigma_r - \sigma_h &= -\lambda_h \frac{\delta W(\lambda_h, \lambda_z)}{\delta \lambda_h} + \epsilon_0 \epsilon_r E(\lambda_h, \lambda_z, q)^2 \\ &= (2\lambda_h^{-2} \lambda_z^{-2} - 2\lambda_h^2) \cdot (C_{10} + 2C_{20}(\lambda_h^{-2} \lambda_z^{-2} + \lambda_h^2 + \lambda_z^2 - 3) + 3C_{30}(\lambda_h^{-2} \lambda_z^{-2} + \lambda_h^2 + \lambda_z^2 - 3)^2 \\ &\quad + \epsilon_0 \epsilon_r E(\lambda_h, \lambda_z, q)^2 \end{aligned} \quad (\text{D.6})$$

where the last term corresponds to the Maxwell pressure. In the case of a cylindrical actuator, the electric field is given by:

$$E(\lambda_h, \lambda_z, Q) = \frac{Q}{2\pi\epsilon_0\epsilon_r LR} \frac{1}{\lambda_h \lambda_z} \quad (D.7)$$

with q the electrical charges and $\epsilon_0\epsilon_r$ the permittivity of the elastomer. Through the appropriate change of parameter (λ_h), by replacing Eq.D.6 in Eq.D.4 and by splitting the integral in two distinguished parts, the integral becomes:

$$\begin{aligned} \Delta P(\lambda_{rint}, \lambda_z, q) &= \sigma_r(\lambda_{ext}, \lambda_z, q) - \sigma_r(\lambda_{rint}, \lambda_z, q) \\ &= \int_{\lambda_{rint}}^{\lambda_{ext}} \frac{1}{(1 - \lambda_h^2 \lambda_z)} \cdot \frac{\delta W(\lambda_h, \lambda_z)}{\delta \lambda_h} d\lambda_h \\ &\quad + \int_{\lambda_{rint}}^{\lambda_{ext}} \frac{-1}{\lambda_h (1 - \lambda_h^2 \lambda_z)} \cdot \epsilon_0 er E^2(\lambda_h, \lambda_z, q) d\lambda_h \end{aligned} \quad (D.8)$$

The first term of Eq.D.8 is equivalent to the elastic component of the pressure, P_{elast} , where another part is subtracted which depends on the electrical activation, P_{electr} . The difference of pressure to apply to the inner surface of the cylinder to reach the strain λ_{rint} is therefore given by:

$$\Delta P(\lambda_{rint}, \lambda_z, q) = P_{elast}(\lambda_{rint}, \lambda_z) - P_{electr}(\lambda_{rint}, \lambda_z, q) \quad (D.9)$$

The elastic term of Eq.D.8 is dependent on a hyperelastic model, with the Yeoh one, this integral could be solved. However, the integral is no more solvable, if the Gent model is chosen.

Concerning the variation due to the electrical part, the definition of the electric field (Eq.D.7) and the fact that the difference of voltage between each electrodes is linked to the electric field through $E(\lambda_h) = -du/d\lambda_h$ [107], P_{electr} becomes:

$$P_{electr}(\lambda_{rint}, \lambda_z, u) = \frac{1}{2}\epsilon_0\epsilon_r u^2 \frac{1}{\log(r_{ext}/r_{int})^2} \left(\frac{1}{r_{int}^2} - \frac{1}{r_{ext}^2} \right) \quad (D.10)$$

where the external stretch is directly dependent on the internal one (Eq.D.3). Through a limited development of Eq.D.10, P_{electr} becomes:

$$P_{electr} = 2\epsilon_0\epsilon_r u^2 \frac{\lambda_z}{R_{ext}^2 - R_{int}^2} \quad (D.11)$$

Appendix D. Model of a uniformly deformed cylindrical DEA

Thus, the difference of pressure due to the electric term is constant for a given voltage and pre-stretch. The error with the model which does not consider the constant electric term for the pressure (P_{electr}) is between 0.01% and 0.5% for respectively no pre-stretch and $\lambda_z = 3.0$.

E Data of the lumped model

E.1 Parameters of the models

The values of the parameters of the different models used in chapter 5 are given here.

Equivalent lumped parameters model

The parameters of Table E.1 are the ones of a healthy human and are found in the literature. The objective is to determine how reacts the cardiac cycle to the activation of the DEA. Concerning the compliance of the different part and the inertance, the following equations have been used in order to validate the values found in literature:

$$L = \rho \frac{l}{(d^2/4)\pi} \quad (\text{E.1}) \quad C = \frac{2\pi(d/2)^3 t^2 E^2}{(tE - P_0(d/2))^3} \quad (\text{E.2})$$

with L the inertance of the different tube, ρ the density of the fluid, l and d , respectively the length and the diameter of the corresponding tube. The previous equations allow determining the value for the different part of the model according to their geometry. Indeed, the objective is to consider a more precise model around the aorta, and such parameters are not necessarily defined in the literature. However, the diameter d , the thickness of the walls t and the Young's modulus of the aorta are found in the literature. This model of compliance is linearised around the initial pressure P_0 . Here the value of 80 mmHg is chosen to be the minimum pressure in the aorta for a healthy human.

The heart is represented through a constant pressure in the atrium and the elastance of the left ventricle which is patient dependent. For the studied case, the value comes from the literature. Concerning the values of the aorta (ascending and descending), the compliance and inertance come from Eq.E.2 and Eq.E.1. Concerning the resistance, the values found in the literature have been used. Indeed, the equivalent equation able to compute this parameter is for laminar flow, and no more in-depth study of the fluid has been performed to obtain a good prediction model for the resistance. The compliance and resistance of the rest of the body comes in the

Appendix E. Data of the lumped model

Parameter	Value
Atrium pressure: P_{atr}	4.5 [mmHg]
Mitral valve resistance: D_{mi}	0.05 $\left[\frac{mmHg \cdot min}{L} \right]$
Aortic valve resistance: D_{ao}	0.05 $\left[\frac{mmHg \cdot min}{L} \right]$
Max. left ventricle elastance	2200 $\left[\frac{mmHg}{L} \right]$
Min. left ventricle elastance	40 $\left[\frac{mmHg}{L} \right]$
Compli. asc. 1: $C_{asc.1}$	0.00015 $\left[\frac{L}{mmHg} \right]$
Imped. acs. 1: $Z_{asc.1}$	0.35 $\left[\frac{mmHg \cdot min}{L} \right]$ and $1.3e-4 \left[\frac{mmHg \cdot min^2}{L} \right]$
Compli. asc. 2: $C_{asc.2}$	0.00015 $\left[\frac{L}{mmHg} \right]$
Imped. acs. 2: $Z_{asc.2}$	0.35 $\left[\frac{mmHg \cdot min}{L} \right]$ and $1.3e-4 \left[\frac{mmHg \cdot min^2}{L} \right]$
Compli. desc.: $C_{desc.}$	0.00015 $\left[\frac{L}{mmHg} \right]$
Imped. desc.: $Z_{desc.}$	0.7 $\left[\frac{mmHg \cdot min}{L} \right]$ and $0.00025 \left[\frac{mmHg \cdot min^2}{L} \right]$
Resist. aortic arch: R_{arch}	180 $\left[\frac{mmHg \cdot min}{L} \right]$
Distal compliance: C_{dist}	0.003 $\left[\frac{L}{mmHg} \right]$
TPR^*	18 $\left[\frac{mmHg \cdot min}{L} \right]$
Heart rate: HR	72 $\left[\frac{beat}{min} \right]$

Table E.1 – Definition of the parameters of the model proposed in Fig.5.7 ([108], [109], [102])

literature (Windkessel model) as well.

One parameter has been tuned, i.e. R_{arch} . Several researches have demonstrated that the mean flow which passes through this element for a healthy patient is around 0.5 L/min. Thus, the resistance has been tuned in order to obtain a similar value.

Hyperelastic parameter

In order to simulate the DEA (Elastosil film), the Yeoh model has been chosen. Through a uniaxial pull-test and a fitting process, the unknown parameters of the model are obtained and given in Tab.E.2. The dielectric constant is provided by the manufacturer.

Parameter of the DEA	Value
Yeoh parameter: C_{10}, C_{20}, C_{30}	281200, -8087.4, 976.6 [Pa]
dielectric permittivity: ϵ_r	2.8
Internal radius of the tube: R_{int}	12.5 [mm]
Initial thickness of the tube: $R_{ext} - R_{int}$	1.0 [mm]
Length of the tube: L_0	40 [mm]

Table E.2 – Definition of the parameters of the DEA tube

E.2 Main results

In this section, several results are provided which come from the proposed lumped model with the DEA. The power supply signal, presented in chapter 5, is used and it has been shifted over one cycle.

The mean flow in the ascending aorta (cardiac output) and the one which reaches the TPR are presented. Then, the energy provided by the left ventricle, obtained via the PV-loop, the energy provided by the DEA and the one consumed by the TPR ($TPR^* + R_{arch}$) are given. Finally, the ejection fraction (stroke volume divided by end-diastolic volume) and the efficiency of the left ventricle are given. This efficiency consists in the per cent of energy from the left ventricle which supplies the TPR. For several values, the one obtained when the DEA is not activated is given (green dashed lines).

E.2.1 Influence of the phase shift

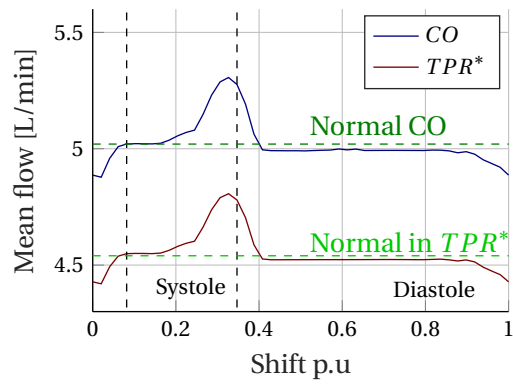
The following results (Fig.E.1) are obtained with the parameters which provide the equivalent compliance than a natural aorta in considering thus a wall thickness of the tubular DEA of 1 mm.

For each interesting parameters, the *normal* value is provided which represents the value for a healthy patient.

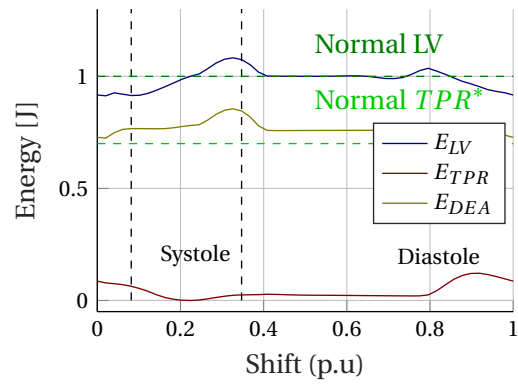
According to the phase shift between the activation and the heartbeat, two main cases are highlighted and studied in the thesis. The first one is when the energy provided by the left ventricle is low and its efficiency high (shift around 0.1). The second studied case is when the mean flow is increased (shift around 0.4).

All the cases could be analysed deeper according to the objective for the patient. However only these two specific cases have been analysed in this research.

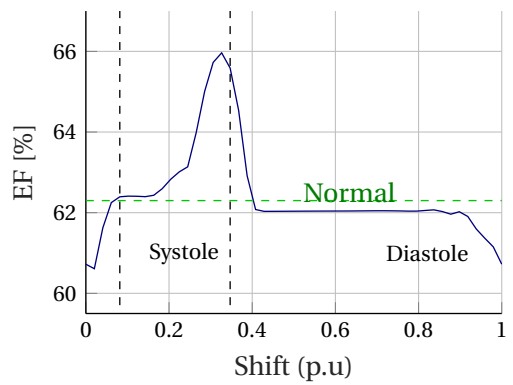
Appendix E. Data of the lumped model



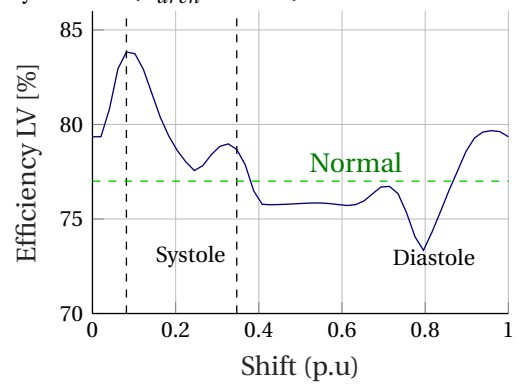
(a) Mean flow rate in the aorta and TPR^*



(b) Energy from the LV, the DEA and received by the TPR ($R_{arch} + TPR^*$)



(c) Ejection fraction



(d) Efficiency of the left ventricle

Figure E.1 – Results for different shift of the actuation voltage

Nomenclature

Acronyms

<i>Symbol</i>	<i>Description</i>
DEAP	Dielectric electroactive polymer
DEA	Dielectric elastomer actuator
IPMC	Ionic polymer metal composite
PDMS	Polydimethylsiloxane
EB	Electrical breakdown
EMI	Electromechanical instability
LT	Loss of tension
FE (analysis)	Finite element (analysis)
FOM	Figure of merit
(i) VAD	(implantable) Ventricular assist device
TET	Transcutaneous energy transfer
IABP	Intra aortic balloon pump
PV	Pressure-volume
LV	Left ventricle
TPR	Total peripheral resistance
ESPVR	End systolic pressure volume relationship
EDPVR	End diastolic pressure volume relationship
EF	Ejection fraction
ECG	Electrocardiogram
ATP	Adenosine triphosphate

Nomenclature

List of symbols

<i>Symbol</i>	<i>Unit</i>	<i>Description</i>
α_m	rad	Angle of one module
α_{beam}	rad	Angle of the curved beam
$\alpha_{supp.,low}$	rad	Angle of the lower and upper part of the support of the module
$\alpha_{supp.,up}$		
C	$L \cdot mmHg$	Compliance
C_{LV}	$mmHg \cdot L$	Compliance of the left ventricle
C_{i0}	-	Coefficient of the Yeoh model
ν	-	Poisson's ratio
D	$C \cdot m^{-2}$	Electrical displacement
\tilde{D}	$C \cdot m^{-2}$	Nominal electrical displacement
ΔT_n	Pa	Difference of nominal stress
$\Delta x,y,z$	m	Variation of distance
Δr	m	Variation of the radial displacement
$\eta_{TPR \text{ from } LV}$	%	Percent of energy provided by the LV to the TPR
$\eta_{TPR \text{ from } DEA}$	%	Percent of energy provided by the DEA to the TPR
$\eta_{Eff.,LV}$	%	Efficiency of the LV
E_{LV}	J	Energy provided by the left ventricle
E_{DEA}	J	Energy of the DEA
E_{TPR}	J	Energy provided to the TPR ($TPR^* + R_{arch}$)
$E_{lec.DEA}$	$V \cdot \mu m^{-1}$	Nominal electric field applied to the DEA
ϵ_0	-	vacuum permittivity
ϵ_r	-	dielectric constant / permittivity of the material
E	$V \cdot m^{-1}$	Electric field
\tilde{E}	$V \cdot m^{-1}$	Nominal electric field
F_i	N	Force in the direction i
\vec{F}_γ	N	Reaction force on the beams
$\vec{F}_{support}$	N	Reaction force of the support
F_{radial}	N	Radial component of the force of the support

Nomenclature

$F_{tang.}$	N	Tangential component of the force of the support
F_{θ}	N	Reaction force of the displacement along the equivalent straight line (θ)
F_{max}, F_{min}	N	Amplitude of the force of the local maximum and minimum of the radial force characteristic of the spring
$F_{rad, misalign.}$	N	Radial force measured on the support misaligned
$F_{rad.}$	N	Equivalent force in the radial direction
$F_{m,i}$	N	Reaction force of the stretch of the membrane in pure-shear configuration
$F_{neg.,2}, F_{neg.,1}$	N	Random negative stiffness force characteristic
g	-	Gibbs free energy
γ	rad	Phase of the reaction force on the beams
k	$N \cdot m^{-1}$	Stiffness of equivalent spring
κ	$Pa \cdot V \cdot m^{-1}$	Ratio of the FOM
λ_i	m/m	Stretch in the direction i
$\lambda_{pre,i}$	m/m	Pre-stretch in the direction i
λ_{max}	m/m	Maximal stretch
λ_s	m/m	Stretch of the membrane in pure-shear configuration
L	$mmHg \cdot min^2 \cdot L^{-1}$	Inertance
L_0	m	Initial width of the membrane in pure-shear configuration
L_i	m	Undeformed geometry in the direction i
l_i	m	Deformed geometry in the direction i
L_{NSS}	m	Length between the feet of the beam
$N_{segm.}$	-	Number of module which composed the cylindrical spring
p	Pa	Unknown hydrostatic pressure
P	Pa	Pressure
P_i	Pa	Pressure in the direction i
P_{LV}	mmHg	Pressure in the left ventricle
P_{aorta}	mmHg	Pressure in the ascending aorta
P_{elast}	Pa	Elastic component of the pressure in cylinder
P_{electr}	Pa	Electric component of the pressure in cylinder

Nomenclature

P_{atr}	Pa	Pressure in left atrium
ϕ	rad	Angle of the reaction force of the beam
$p_{Maxwell}$	Pa	Maxwell's pressure
q	C	Electrical charges
Q	$L \cdot min^{-1}$	Flow rate
R_{int}	m	Undeformed internal radius of the cylinder
R_{ext}	m	Undeformed external radius of the cylinder
r_{int}	m	Deformed internal radius of the cylinder
R	$mmHg \cdot min \cdot L^{-1}$	Resistance (fluid or electric)
TPR^*	$mmHg \cdot min \cdot L^{-1}$	Special total peripheral resistance (without resistance aortic-arch)
S	-	Slope of the line of the criteria of stability
σ_i	Pa	Characteristic of the line criteria for stability
σ_1^*	Pa	Stress in the direction i
$\tilde{\sigma}_1$	Pa	Nominal stress of ideal elastomer
s_i	m/m	Strain in the direction i
s_0	m	Initial length of the membrane in pure-shear configuration
T_n	Pa	Nominal stress
$T_{n,trans}$	Pa	Nominal stress at the transition
T_{max}	Pa	Maximal nominal stress
T_{const}	Pa	Constant nominal stress
T	$^{\circ}C$	Temperature
$t_{cyl.}$	m	Thickness of the cylinder of the spring
t_{beam}	m	Thickness of the beam
θ	rad	Angle of the equivalent straight line
u	V	Voltage
U_{DEA}	V	Activation voltage of the DEA

Nomenclature

V_{int}	L	Internal volume
W	-	Strain energy density function
$W_{\bar{D}}$	-	Strain energy density function according to the nominal electrical displacement
$W_{\bar{E}}$	-	Strain energy density function according to the nominal electric field
W_s	-	Strain energy density function (elastic term)
W_q	-	Strain energy density function according to the electrical charges
W_{ideal}	J	Energy defining the figure of merit
$W_{pract.}$	$J \cdot m^{-3}$	Practical energy density
$W_{specific}$	$J \cdot m^{-3}$	Specific energy density
x, y, z	m	Cartesian dimension
x_{Θ}	m	Equivalent position of the upper part of the beam compared to the lower one
x_{max}, x_{min}	m	Position of the local maximum and minimum of the radial force characteristic of the spring
$X_{\theta, xmax},$ $X_{\theta, xmin}$	m	Model to determine x_{max} and x_{min}
Y	Pa	Young's modulus
y_B	m	Position of the upper part of the beam in the coordinate (e_{x*}, e_{y*})
Z	$mmHg \cdot min \cdot L^{-1}$	Impedance

Bibliography

- [1] Y. Bar-Cohen, *Electroactive Polymer (EAP) Actuators as Artificial Muscles: Reality, Potential, and Challenges*, Press Monographs, SPIE Press, 2001.
- [2] M. Shahinpoor and K. J. Kim, “Ionic polymer–metal composites: Iv. industrial and medical applications,” *Smart Materials and Structures* **14**(1), p. 197, 2005.
- [3] L. Soon-Gie, P. Hoon-Cheol, P. Surya, and Y. Youngtai, “Performance improvement of ipmc (ionic polymer metal composites) for a flapping actuator,” *International Journal of Control Automation and systems* **4**(6), pp. 748–755, 2006.
- [4] R. Pelrine, R. Kornbluh, J. Joseph, R. Heydt, Q. Pei, and S. Chiba, “High-field deformation of elastomeric dielectrics for actuators,” *Materials Science and Engineering: C* **11**(2), pp. 89 – 100, 2000.
- [5] T. Lu, J. Huang, C. Jordi, G. Kovacs, R. Huang, D. R. Clarke, and Z. Suo, “Dielectric elastomer actuators under equal-biaxial forces, uniaxial forces, and uniaxial constraint of stiff fibers,” *Soft Matter* **8**, pp. 6167–6173, 2012.
- [6] R. Pelrine, R. Kornbluh, Q. Pei, and J. Joseph, “High-speed electrically actuated elastomers with strain greater than 100%,” *Science* **287**(5454), pp. 836–839, 2000.
- [7] M. Kolloosche, J. Zhu, Z. Suo, and G. Kofod, “Complex interplay of nonlinear processes in dielectric elastomers,” *Phys. Rev. E* **85**, p. 051801, May 2012.
- [8] J. Huang, T. Li, C. C. Foo, J. Zhu, D. R. Clarke, and Z. Suo, “Giant, voltage-actuated deformation of a dielectric elastomer under dead load,” *Applied Physics Letters* **100**(4), p. 041911, 2012.
- [9] S. Akbari, S. Rosset, and H. R. Shea, “Improved electromechanical behavior in castable dielectric elastomer actuators,” *Applied Physics Letters* **102**(7), p. 071906, 2013.
- [10] S. Rosset, S. Araromi, S. Schlatter, and H. Shea, “Fabrication process of silicone-based dielectric elastomer actuators,” *Journal of Visualized Experiments (JoVE)* (108), p. 13. e53423, 2016.
- [11] EPFL-LMTS, “Peta-pico-voltron project, petapicovoltron.com,” 2016.

- [12] D. K. Biswal and B. Nayak, "Analysis of time dependent bending response of ag-ipmc actuator," *Procedia Engineering* **144**, pp. 600 – 606, 2016. International Conference on Vibration Problems 2015.
- [13] K. Jia, T. Lu, and T. Wang, "Response time and dynamic range for a dielectric elastomer actuator," *Sensors and Actuators A: Physical* **239**, pp. 8 – 17, 2016.
- [14] L. Maffli, S. Rosset, M. Ghilardi, F. Carpi, and H. Shea, "Ultrafast all-polymer electrically tunable silicone lenses," *Advanced Functional Materials* **25**(11), pp. 1656–1665, 2015.
- [15] T. Rashid and M. Shahinpoor, "Force optimization of ionic polymeric platinum composite artificial muscles by means of an orthogonal array manufacturing method," *Proc. SPIE* **3669**, pp. 289–298, 1999.
- [16] R. Zhang, X. Huang, T. Li, P. Irvani, and P. Keogh, "Novel arrangements for high performance and durable dielectric elastomer actuation," *Actuators* **5**(3), 2016.
- [17] M. Siripong, S. Fredholm, Q. A. Nguyen, B. Shih, J. Itescu, and J. Stolk, "A cost-effective fabrication method for ionic polymer-metal composites," *MRS Proceedings* **889**, 2005.
- [18] C. Chung, P. Fung, Y. Hong, M. Ju, C. Lin, and T. Wu, "A novel fabrication of ionic polymer-metal composites (ipmc) actuator with silver nano-powders," *Sensors and Actuators B: Chemical* **117**(2), pp. 367 – 375, 2006.
- [19] R. C. Richardson, M. C. Levesley, M. D. Brown, J. A. Hawkes, K. Watterson, and P. G. Walker, "Control of ionic polymer metal composites," *IEEE/ASME Transactions on Mechatronics* **8**, pp. 245–253, June 2003.
- [20] X. Ye, Y. Su, and S. Guo, "A centimeter-scale autonomous robotic fish actuated by ipmc actuator," *2007 IEEE International Conference on Robotics and Biomimetics (ROBIO)*, pp. 262–267, 2007.
- [21] J. Shintake, S. Rosset, B. Schubert, D. Floreano, and H. Shea, "Versatile soft grippers with intrinsic electroadhesion based on multifunctional polymer actuators," *Advanced Materials* **28**(2), pp. 231–238, 2016.
- [22] O. A. Araromi, S. Rosset, and H. R. Shea, "Versatile fabrication of pdms-carbon electrodes for silicone dielectric elastomer transducers," *2015 Transducers - 2015 18th International Conference on Solid-State Sensors, Actuators and Microsystems (TRANSDUCERS)*, pp. 1905–1908, June 2015.
- [23] D. Xu, T. G. McKay, S. Michel, and I. A. Anderson, "Enabling large scale capacitive sensing for dielectric elastomers," *Proc. SPIE* **9056**, pp. 90561A–90561A–8, 2014.
- [24] R. Pelrine, R. D. Kornbluh, J. Eckerle, P. Jeuck, S. Oh, Q. Pei, and S. Stanford, "Dielectric elastomers: generator mode fundamentals and applications," *Proc. SPIE* **4329**, pp. 148–156, 2001.

- [25] J. Maas and C. Graf, "Dielectric elastomers for hydro power harvesting," *Smart Materials and Structures* **21**(6), p. 064006, 2012.
- [26] S. Chiba, M. Waki, T. Wada, Y. Hirakawa, K. Masuda, and T. Ikoma, "Consistent ocean wave energy harvesting using electroactive polymer (dielectric elastomer) artificial muscle generators," *Applied Energy* **104**, pp. 497 – 502, 2013.
- [27] J. Loverich, I. Kanno, and H. Kotera, "Concepts for a new class of all-polymer micropumps," *The Royal Society of Chemistry 2006* **6**, pp. 1147–54, 10 2006.
- [28] L. Maffli, S. Rosset, and H. R. Shea, "Zipping dielectric elastomer actuators: characterization, design and modeling," *Smart Materials and Structures* **22**(10), p. 104013, 2013.
- [29] N. Goulbourne, M. I. Frecker, E. M. Mockensturm, and A. J. Snyder, "Modeling of a dielectric elastomer diaphragm for a prosthetic blood pump," *Proc.SPIE* **5051**, pp. 5051 – 5051 – 13, 2003.
- [30] F. Carpi, C. Menon, and D. E. D. Rossi, "Electroactive elastomeric actuator for all-polymer linear peristaltic pumps," *IEEE/ASME Transactions on Mechatronics* **15**, pp. 460–470, 2010.
- [31] G. Mao, X. Huang, J. Liu, T. Li, S. Qu, and W. Yang, "Dielectric elastomer peristaltic pump module with finite deformation," *Smart Materials and Structures* **24**(7), p. 075026, 2015.
- [32] G. Kofod, P. Sommer-Larsen, R. Kornbluh, and R. Pelrine, "Actuation response of polyacrylate dielectric elastomers," *Journal of Intelligent Material Systems and Structures* **14**(12), pp. 787–793, 2003.
- [33] S. Risse, B. Kussmaul, H. Kruger, and G. Kofod, "A versatile method for enhancement of electromechanical sensitivity of silicone elastomers," *RSC Adv.* **2**, pp. 9029–9035, 2012.
- [34] L. D. Lillo, A. Schmidt, D. A. Carnelli, P. Ermanni, G. Kovacs, E. Mazza, and A. Bergamini, "Measurement of insulating and dielectric properties of acrylic elastomer membranes at high electric fields," *Journal of Applied Physics* **111**(2), p. 024904, 2012.
- [35] M. Wissler and E. Mazza, "Electromechanical coupling in dielectric elastomer actuators," *Sensors and Actuators A: Physical* **138**(2), pp. 384 – 393, 2007.
- [36] J. Sheng, H. Chen, B. Li, and Y. Wang, "Influence of the temperature and deformation-dependent dielectric constant on the stability of dielectric elastomers," *Journal of Applied Polymer Science* **128**(4), pp. 2402–2407, 2012.
- [37] J. D. Nam, H. R. Choi, J. C. Koo, Y. K. Lee, and K. J. Kim, *Dielectric Elastomers for Artificial Muscles*, pp. 37–48. Springer London, London, 2007.

- [38] R. W. Ogden, "Large deformation isotropic elasticity - on the correlation of theory and experiment for incompressible rubberlike solids," *Proceedings of the Royal Society of London A: Mathematical, Physical and Engineering Sciences* **326**(1567), pp. 565–584, 1972.
- [39] M. Mooney, "A theory of large elastic deformation," *Journal of Applied Physics* **11**(9), pp. 582–592, 1940.
- [40] O. H. Yeoh, "Some forms of the strain energy function for rubber," *Rubber Chemistry and Technology* **66**(5), pp. 754–771, 1993.
- [41] E. M. Arruda and M. C. Boyce, "A three-dimensional constitutive model for the large stretch behavior of rubber elastic materials," *Journal of the Mechanics and Physics of Solids* **41**(2), pp. 389 – 412, 1993.
- [42] A. N. Gent, "Engineering with rubber," in *Engineering with Rubber (Third Edition)*, A. N. Gent, ed., pp. I – XVIII, Hanser, third edition ed., 2012.
- [43] R. Ogden, *Non-Linear Elastic Deformations*, Dover Civil and Mechanical Engineering, Dover Publications, 1997.
- [44] L. Mullins, "Effect of stretching on the properties of rubber," *Rubber Chemistry and Technology* **21**(2), pp. 281–300, 1948.
- [45] M. Wissler and E. Mazza, "Modeling and simulation of dielectric elastomer actuators," *Smart Materials and Structures* **14**(6), p. 1396, 2005.
- [46] H. Wang, M. Lei, and S. Cai, "Viscoelastic deformation of a dielectric elastomer membrane subject to electromechanical loads," *Journal of Applied Physics* **113**(21), p. 213508, 2013.
- [47] M. H. R. Ghoreishy, "Determination of the parameters of the prony series in hyper-viscoelastic material models using the finite element method," *Materials & Design* **35**, pp. 791 – 797, 2012.
- [48] S. Michel, X. Q. Zhang, M. Wissler, C. Löwe, and G. Kovacs, "A comparison between silicone and acrylic elastomers as dielectric materials in electroactive polymer actuators," *Polymer International* **59**(3), pp. 391–399, 2010.
- [49] I. D. Johnston, D. K. McCluskey, C. K. L. Tan, and M. C. Tracey, "Mechanical characterization of bulk sylgard 184 for microfluidics and microengineering," *Journal of Micromechanics and Microengineering* **24**(3), p. 035017, 2014.
- [50] A. Schmidt, P. Rothmund, and E. Mazza, "Multiaxial deformation and failure of acrylic elastomer membranes," *Sensors and Actuators A: Physical* **174**, pp. 133 – 138, 2012.

- [51] J. Huang, S. Shian, R. M. Diebold, Z. Suo, and D. R. Clarke, "The thickness and stretch dependence of the electrical breakdown strength of an acrylic dielectric elastomer," *Applied Physics Letters* **101**(12), p. 122905, 2012.
- [52] D. Gatti, H. Haus, M. Matysek, B. Frohnapfel, C. Tropea, and H. F. Schlaak, "The dielectric breakdown limit of silicone dielectric elastomer actuators," *Applied Physics Letters* **104**(5), p. 052905, 2014.
- [53] J.-S. Plante and S. Dubowsky, "Large-scale failure modes of dielectric elastomer actuators," *International Journal of Solids and Structures* **43**(25), pp. 7727 – 7751, 2006.
- [54] X. Zhao and Z. Suo, "Theory of dielectric elastomers capable of giant deformation of actuation," *Phys. Rev. Lett.* **104**, p. 178302, Apr 2010.
- [55] B. Li and Z. Zhao, "Electromechanical deformation of dielectric elastomer in two types of pre-stretch," *EPL (Europhysics Letters)* **106**(6), p. 67009, 2014.
- [56] R. Huang and Z. Suo, "Electromechanical phase transition in dielectric elastomers," *Proceedings of the Royal Society of London A: Mathematical, Physical and Engineering Sciences* **468**(2140), pp. 1014–1040, 2012.
- [57] X. Zhao, W. Hong, and Z. Suo, "Electromechanical hysteresis and coexistent states in dielectric elastomers," *Physical Review B* **76**, pp. 134113–, 10 2007.
- [58] S. Rosset, L. Maffli, S. Houis, and H. R. Shea, "An instrument to obtain the correct biaxial hyperelastic parameters of silicones for accurate dea modelling," *Proc.SPIE* **9056**, pp. 9056 – 9056 – 12, 2014.
- [59] R. Zhang, P. Lochmatter, A. Kunz, and G. M. Kovacs, "Spring roll dielectric elastomer actuators for a portable force feedback glove," *Proc.SPIE* **6168**, pp. 6168 – 6168 – 12, 2006.
- [60] G. Scirè Mammano, G. Berselli, and E. Dragoni, "Design of a dielectric elastomer cylindrical actuator with quasi-constant available thrust: Modeling procedure and experimental validation," *Journal of Mechanical Design* **136**, 12 2013.
- [61] F. Carpi and D. D. Rossi, "Dielectric elastomer cylindrical actuators: electromechanical modelling and experimental evaluation," *Materials Science and Engineering: C* **24**(4), pp. 555 – 562, 2004.
- [62] J. Zhou, L. Jiang, and R. E. Khayat, "Electromechanical response and failure modes of a dielectric elastomer tube actuator with boundary constraints," *Smart Materials and Structures* **23**(4), p. 045028, 2014.
- [63] P. Chakraborti, H. K. Toprakci, P. Yang, N. D. Spigna, P. Franzon, and T. Ghosh, "A compact dielectric elastomer tubular actuator for refreshable braille displays," *Sensors and Actuators A: Physical* **179**, pp. 151 – 157, 2012.

- [64] R. Jones and R. Sarban, "Model validation and feedback controller design for a dielectric elastomer actuator," *Journal of Intelligent Material Systems and Structures* **27**, 12 2015.
- [65] D. McCoul and Q. Pei, "Tubular dielectric elastomer actuator for active fluidic control," *Smart Materials and Structures* **24**(10), p. 105016, 2015.
- [66] S. Che, T. Lu, and T. Wang, "Electromechanical phase transition of a dielectric elastomer tube under internal pressure of constant mass," *Theoretical and Applied Mechanics Letters* **7**(3), pp. 121 – 125, 2017.
- [67] Z. Suo, "Theory of dielectric elastomers," *Acta Mechanica Solida Sinica* **23**(6), pp. 549 – 578, 2010.
- [68] H. Callen, *Thermodynamics and an Introduction to Thermostatistics*, Wiley, 1985.
- [69] J. Zhu, M. Kolloosche, T. Lu, G. Kofod, and Z. Suo, "Two types of transitions to wrinkles in dielectric elastomers," *Soft Matter* **8**, pp. 8840–8846, 2012.
- [70] M. Kolloosche, G. Kofod, Z. Suo, and J. Zhu, "Temporal evolution and instability in a viscoelastic dielectric elastomer," *Journal of the Mechanics and Physics of Solids* **76**, pp. 47 – 64, 2015.
- [71] S. J. A. Koh, C. Keplinger, R. Kaltseis, C.-C. Foo, R. Baumgartner, S. Bauer, and Z. Suo, "High-performance electromechanical transduction using laterally-constrained dielectric elastomers part i: Actuation processes," *Journal of the Mechanics and Physics of Solids* **105**, pp. 81 – 94, 2017.
- [72] L. Mullins, "Softening of rubber by deformation," *Rubber Chemistry and Technology* **42**(1), pp. 339–362, 1969.
- [73] R. D. Kornbluh, R. Pelrine, H. Prahlaad, B. M. Annjoe Wong-Foy, S. Kim, J. Eckerle, and T. Low, "From boots to buoys: promises and challenges of dielectric elastomer energy harvesting," 2011.
- [74] G. K. Lau, T. G. La, and D. D.-T. Tan, "High-stress dielectric elastomer actuators with oil encapsulation," in *2014 11th International Conference on Ubiquitous Robots and Ambient Intelligence (URAI)*, pp. 196–197, Nov 2014.
- [75] Q. Pei, "Artificial muscles based on synthetic dielectric elastomers," in *2009 Annual International Conference of the IEEE Engineering in Medicine and Biology Society*, pp. 6826–6829, Sept 2009.
- [76] G. Berselli, R. Vertechy, G. Vassura, and V. Castelli, "Design of a single-acting constant-force actuator based on dielectric elastomers," *ASME. J. Mechanisms Robotics*. **1**(3), 2009.
- [77] S. Zakaria, "Electrical breakdown and mechanical ageing in dielectric elastomers," *Danmarks Tekniske Universitet (DTU), Phd Thesis*, 2016.

- [78] A. Wingert, M. D. Lichter, and S. Dubowsky, "On the design of large degree-of-freedom digital mechatronic devices based on bistable dielectric elastomer actuators," *IEEE/ASME Transactions on Mechatronics* **11**, pp. 448–456, Aug 2006.
- [79] M. Hodgins, A. York, and S. Seelecke, "Experimental comparison of bias elements for out-of-plane deap actuator system," *Smart Materials and Structures* **22**(9), p. 094016, 2013.
- [80] J. Qiu, J. H. Lang, and A. H. Slocum, "A curved-beam bistable mechanism," *Journal of Microelectromechanical Systems* **13**, pp. 137–146, April 2004.
- [81] M. A. Bradford, B. Uy, and Y.-L. Pi, "In-plane elastic stability of arches under a central concentrated load," *Journal of Engineering Mechanics* **128**(7), pp. 710–719, 2002.
- [82] B. Camescasse, A. Fernandes, and J. Pouget, "Bistable buckled beam and force actuation: Experimental validations," *International Journal of Solids and Structures* **51**(9), pp. 1750 – 1757, 2014.
- [83] J. Beharic, "Analysis of a compressed bistable buckled beam on a flexible support," *Journal of Applied Mechanics* **81**, p. 081011, 2014.
- [84] J. Chavanne, Y. Civet, and Y. Perriard, "Design of an innovative cylindrical spring with a negative stiffness," in *2018 IEEE/ASME International Conference on Advanced Intelligent Mechatronics (AIM)*, pp. 557–562, July 2018.
- [85] C. N. Elias, J. H. C. Lima, R. Valiev, and M. A. Meyers, "Biomedical applications of titanium and its alloys," *JOM* **60**, pp. 46–49, Mar 2008.
- [86] D. Ginat, H. Massey, S. Bhatt, and V. Dogra, "Imaging of Mechanical Cardiac Assist Devices," *Journal of Clinical Imaging Science* **1**(1), p. 21, 2011.
- [87] Carmat, "carmatsa.com."
- [88] W. fundation ETHZ, "wysszurich.com."
- [89] M. Takagaki, D. Rottenberg, P. McCarthy, N. Smedira, R. Dessoify, M. Al-Ahamadi, D. Shoshani, and K. Fukamachi, "A novel miniature ventricular assist device for hemodynamic support," *ASAIO Journal* **47**(4), pp. 412 – 416, 2001.
- [90] R. Dowling, L. A. Gray, S. W. Etoch, H. Laks, D. Marelli, L. E. Samuels, J. W. C. Entwistle, G. Couper, G. J. Vlahakes, and O. H. Frazier, "The abiocor implantable replacement heart.," *The Annals of thoracic surgery* **75** **6 Suppl**, pp. S93–9, 2003.
- [91] O. Frazier, T. Myers, S. Westby, and I. Gregoric, "Use of the jarvik 2000 left ventricular assist system as a bridge to heart transplantation or as destination therapy for patients with chronic heart failure," *Ann. Surg* **237**(5), pp. 631–636, 2003.

- [92] L. Arusoglu, N. Reiss, M. Morshuis, M. Schönbrodt, K. Hakim-Meibodi, and J. Gummert, "The thoratec system implanted as a modified total artificial heart: the bad oeynhausien technique," **13**, pp. E391–3, 12 2010.
- [93] S. Heart, "Sunshine c-pulse, www.sunshineheart.com."
- [94] E. M. Nakhiah C. Goulbourne, Mary I. Frecker, "Electro-elastic modeling of a dielectric elastomer diaphragm for a prosthetic blood pump," *Proc.SPIE* **5385**, pp. 5385 – 5385 – 12, 2004.
- [95] C. Ioannou, N. Stergiopulos, A. Katsamouris, I. Startchik, A. Kalangos, M. Licker, N. Westerhof, and D. Morel, "Hemodynamics induced after acute reduction of proximal thoracic aorta compliance," *European Journal of Vascular and Endovascular Surgery* **26**(2), pp. 195 – 204, 2003.
- [96] K. R. Walley, "Left ventricular function: time-varying elastance and left ventricular aortic coupling," *Critical Care* **20**, p. 270, Sep 2016.
- [97] O. Frank, "The basic shape of the arterial pulse. first treatise: Mathematical analysis," *Journal of Molecular and Cellular Cardiology* **22**(3), pp. 255 – 277, 1990.
- [98] N. Westerhof, G. Elzinga, and P. Sipkema, "An artificial arterial system for pumping hearts.," *Journal of Applied Physiology* **31**(5), pp. 776–781, 1971. PMID: 5117196.
- [99] M. Vuk and Q. Alfio, "Analysis of lumped parameter models for blood flow simulations and their relation with 1d models," *ESAIM: M2AN* **38**(4), pp. 613–632, 2004.
- [100] W. Borutzky, "Bond graph methodology: Development and analysis of multidisciplinary dynamic system models," *New York, Springer* , 2010.
- [101] M. Pillon, "Du modèle du coeur naturel au réglage du coeur artificiel," p. 356, 1990.
- [102] F. M. Colacino, F. Moscato, F. Piedimonte, M. Arabia, and G. Danieli, "Left ventricle load impedance control by apical vad can help heart recovery and patient perfusion: A numerical study," **53**, pp. 263–77, 05 2007.
- [103] M. Capoccia, "Development and characterization of the arterial windkessel and its role during left ventricular assist device assistance," *Artificial Organs* **39**(8), pp. E138–E153.
- [104] K. Her, J. Y. Kim, K. M. Lim, and S. W. Choi, "Windkessel model of hemodynamic state supported by a pulsatile ventricular assist device in premature ventricle contraction," in *Biomedical engineering online*, 2018.
- [105] J. Goupy and L. Creighton, *Introduction aux plans d'expériences - 3ème édition*, Technique et ingénierie, Dunod, 2006.
- [106] W. M. Lai, D. Rubin, and E. Krempl, "Chapter 3 - kinematics of a continuum," in *Introduction to Continuum Mechanics (Fourth Edition)*, pp. 69 – 153, Butterworth-Heinemann, Boston, 2010.

- [107] G. K. Jian Zhu, Hristiyan Stoyanov and Z. Suo, “Large deformation and electromechanical instability of a dielectric elastomer tube actuator,” *Journal of Applied Physics* **108**, 2010.
- [108] B. Casas, J. Lantz, F. Viola, G. Cedersund, A. F. Bolger, C.-J. Carlhäll, M. Karlsson, and T. Ebbers, “Bridging the gap between measurements and modelling: a cardiovascular functional avatar,” in *Scientific Reports*, 2017.
- [109] J. Alastruey, A. W. Khir, K. S. Matthys, P. Segers, S. J. Sherwin, P. R. Verdonck, K. H. Parker, and J. Peiró, “Pulse wave propagation in a model human arterial network: Assessment of 1-d visco-elastic simulations against in vitro measurements,” *Journal of Biomechanics* **44**(12), pp. 2250 – 2258, 2011.

Curriculum Vitae

Jonathan CHAVANNE

Born November 3, 1990

Swiss Citizen

jonathan.chavanne@alumni.epfl.ch

Studies and professional experience

- | | |
|-------------|--|
| 2014 - 2019 | Teaching assistant and PhD student at the Integrated Actuators Laboratory (LAI), École polytechnique fédérale de Lausanne, Switzerland |
| 2013 - 2014 | Master project, IREQ, Montréal, Canada |
| 2012 - 2013 | Master of Science in Microengineering, École polytechnique fédérale de Lausanne, Switzerland |
| 2009 - 2012 | Bachelor of Science in Microengineering, École polytechnique fédérale de Lausanne, Switzerland |
| 2006 - 2009 | Scientific High School, Lycée Cantonal de Porrentruy, Switzerland |

Patent

- Jonathan Chavanne, Yoan Civet and Yves Perriard *Spring with a plurality of elements, and actuator including such a spring*, CH Patent CH20170001440, filed Nov. 27th, 2017., International Patent WO2018IB59267, submitted Nov. 23rd, 2018

Publications

- Jonathan Chavanne, Bachir Kedjar, Arezki Merkhoul, Kamal Al-Haddad and Yves Perriard. Numerical Computation of Hydro Electrical Generators Field Form Coefficients. In 20th International Conference on the Computation of Electromagnetic Fields (Com-pumag), July 2015.

- Daniel Grivon, Jonathan Chavanne and Yves Perriard. Comparison of Two Different Eddy Currents Based Levitation Techniques. In *International Symposium on Linear Drives for Industry Applications (LDIA)*, July 2015.
- Jonathan Chavanne, Paolo Germano, Yoan Civet and Yves Perriard. Measurement of the mechanical power of an EAP based pump. In *International Conference on Advanced Intelligent Mechatronics (AIM)*, July 2015.
- Paolo Germano, Jonathan Chavanne and Yves Perriard. Inductive supply for a highly insulated device. In *18th International Conference on Electrical Machines and Systems (ICEMS 2015)*, October 2015.
- Cecile Cuchet, Jonathan Chavanne, Yoan Civet, and Yves Perriard. Mechanical modeling of a magnetic membrane for a soft actuator. In *19th International Conference on Electrical Machines and Systems (ICEMS 2016)*, October 2016.
- Jonathan Chavanne, Yoan Civet and Yves Perriard. Modelling of a dielectric electroactive polymer tubular shape sensor for pressure measurements. In *International Conference on Advanced Intelligent Mechatronics (AIM)*, July 2016.
- Jonathan Chavanne, Yoan Civet and Yves Perriard. Energy analysis of a DEAP based cylindrical actuator coupled with a radial negative stiffness spring. In *Electroactive Polymer Actuators and Devices (EAPAD)*, March 2017.
- Jonathan Chavanne, Yoan Civet and Yves Perriard. Design of an Innovative Cylindrical Spring with a Negative Stiffness. In *International Conference on Advanced Intelligent Mechatronics (AIM)*, July 2018.
- Raphael Mottet, Jonathan Chavanne, Alexis Boegli and Yves Perriard. Electric Charge Transfer Between Cascading Dielectric Electroactive Polymer Actuators. In *21th International Conference on Electrical Machines and Systems (ICEMS 2018)*, October 2018.

